microwave JOURNAL®

contents

VOLUME 25, NUMBER 10
USPS 396-250
OCTOBER 1982

ON THE COVER: Three companies, California Eastern Labs, Hewlett-Packard and Maury Microwave, worked together in a unique team effort to design the universal microwave transistor test system pictured. Artwork courtesy of Hewlett-Packard. Cover story begins on p. 95.

*Euro-Global Edition Only.

Press run for this issue is 44,952 copies.

EXECUTIVE EDITORIAL OFFICE
610 Washington Street, Dedham, MA 02026
Tel: 617 326-8220 710 348-0481
TELEX: 951-659
MICROSOL DEDM

EUROPEAN EDITORIAL OFFICE
25 Victoria Street London SW1H OEH England
Tel: 01-222-0466 **TELEX:** 885744

Microwave Journal is issued without charge upon written request to qualified persons working in that portion of the electronics industry including governmental and university installation that deal with VHF through light frequencies. Other subscriptions; domestic, $36 per year, two year subscriptions $65; foreign, $48 per year, two year subscriptions $85: back issues (if available) and single copies $5.00.

 Microfilm copies of Microwave Journal 300 N. Zeeb Rd., Ann Arbor, MI 48106 are available from University Microfilms.

POSTMASTER: send address corrections to Microwave Journal, 610 Washington Street, Dedham MA 02026.

BPA

Horizon House also publishes Telecommunications and Journal of Electronic Defense

Solid State, 95 GHZ Tracking Radar System

J. A. Scheer and P. P. Britt
Georgia Institute of Technology, Engineering Experiment Station, Atlanta, GA

Introduction

Millimeter wave radar technology is maturing to the point that 95 GHz systems are being considered for operational tactical applications, in particular for air-to-ground seeker and reconnaissance applications.

Optimum system design requires a full understanding of the reflectivity characteristics of the targets and clutter as they apply to potential signal processing techniques. An instrumentation sensor has been developed to provide the capability to evaluate various signal processing techniques applicable to 95 GHz air-to-ground radar systems. This paper describes the 95 GHz terminal homing studies sensor.

Georgia Institute of Technology, Engineering Experiment Station (GIT/EES) has designed and developed a state-of-the-art millimeter wave tracking radar system under subcontract from the General Electric Company Aircraft Equipment Division. The system is being used by Massachusetts Institute of Technology, Lincoln Laboratory (MIT/LL) in the Lincoln Laboratory Millimeter Terminal Homing Program as an instrument to help evaluate various millimeter wave system concepts.

Objective

The objective of the program was to develop a sensor which

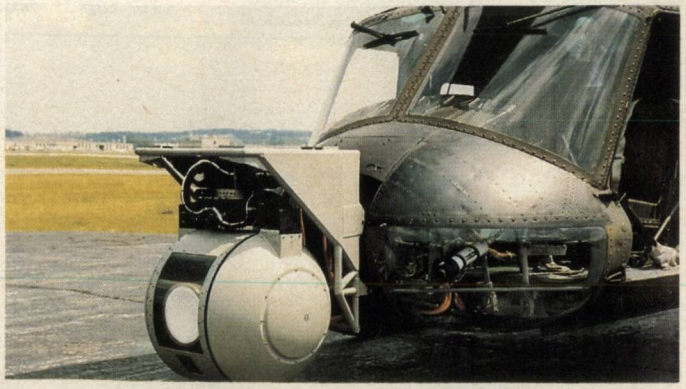

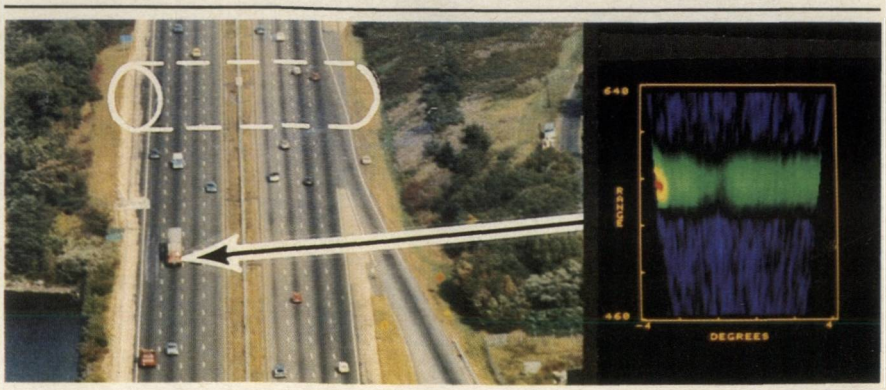

Route 128 Radar Scan
A narrow field-of-view TV camera co-located with a radar scan antenna on pod gimbals (upper right), photographs the highway segment being mapped (lower right). The radar scan to the right of the picture shows a typical reflection obtained from a moving truck. Scan geometry is shown by the dotted white outline. The radar mapped with an antenna depression angle of 20° and a slant range to the ground of approximately 500 m. This produced a beam footprint about 10 m in cross range and 30 m in range. Azimuthal scan angle was set to 8° (about 80 m in cross-range) and the scan rate was set at 6° per second. The scan shows receiver thermal noise in blue, vegetation in green, and strong reflections in red.

could be used to investigate techniques associated with millimeter wave terminal homing system development. Lincoln Laboratory is using the tracking radar system in a closed looped mode on a helicopter platform to evaluate various tracking and signal processing techniques. The helicopter flies a flight profile approaching a target and the radar, mounted in the chin of the helicopter, in conjunction with the General Electric data acquisition system, provides detection and tracking data for later evaluation.

TABLE I

RADAR PARAMETERS

Transmitter	
Type:	Pulsed Impatt
Frequency:	94 to 95 GHz
Pulse Length:	100 ns (nanoseconds)
Chirp Bandwidth:	250 MHz nominal
Power:	5 watts peak
PRF:	20 kHz (max.)
Antenna	
Type:	4 horn monopulse lens
Aperture:	10 inch diameter
Beamwidth:	1° to 3°
Gain:	42 dB (including monopulse comparator losses
Receiver	
Type:	Integrated mixer/preamp Linear
Dynamic Range:	40 dB instantaneous
AGC:	120 dB gain control
Bandwidth:	500 MHz (IF) 5 MHz (video)
Noise Figure:	8 dB (SSB)
Input Losses:	3 dB (waveguide losses)

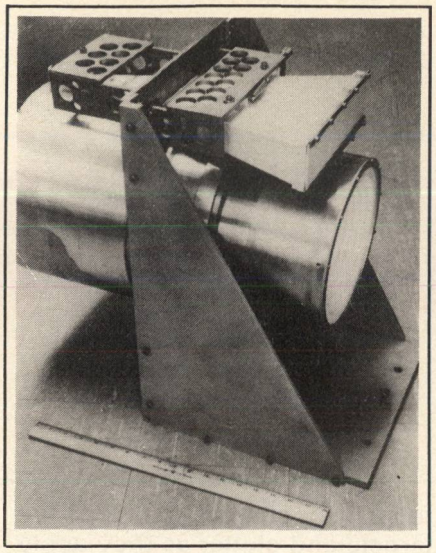

Fig. 1 Radar RF unit in test fixture.

Radar Parameters

The radar is described as an instrumentation system with the following salient features:

- Solid State
- Chirped Transmitter
- Four Horn Monopulse Tracking
- Simultaneous Lobing Tracking
- Variable Beamwidth
- Range Tracker
- Automatic Gain Control
- Digital Interface

Table 1 is a list of the radar parameters.

The radar is comprised of two assemblies — an RF unit contain-

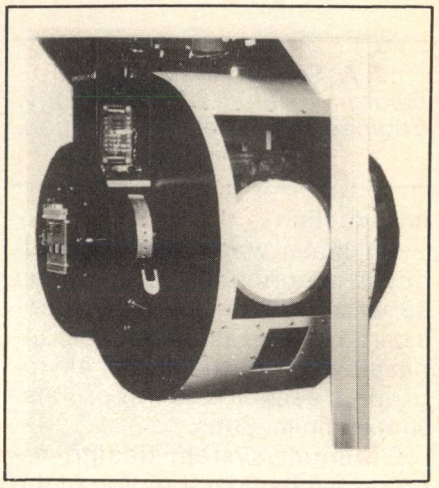

Fig. 2 RF unit mounted in gimballed pedestal.

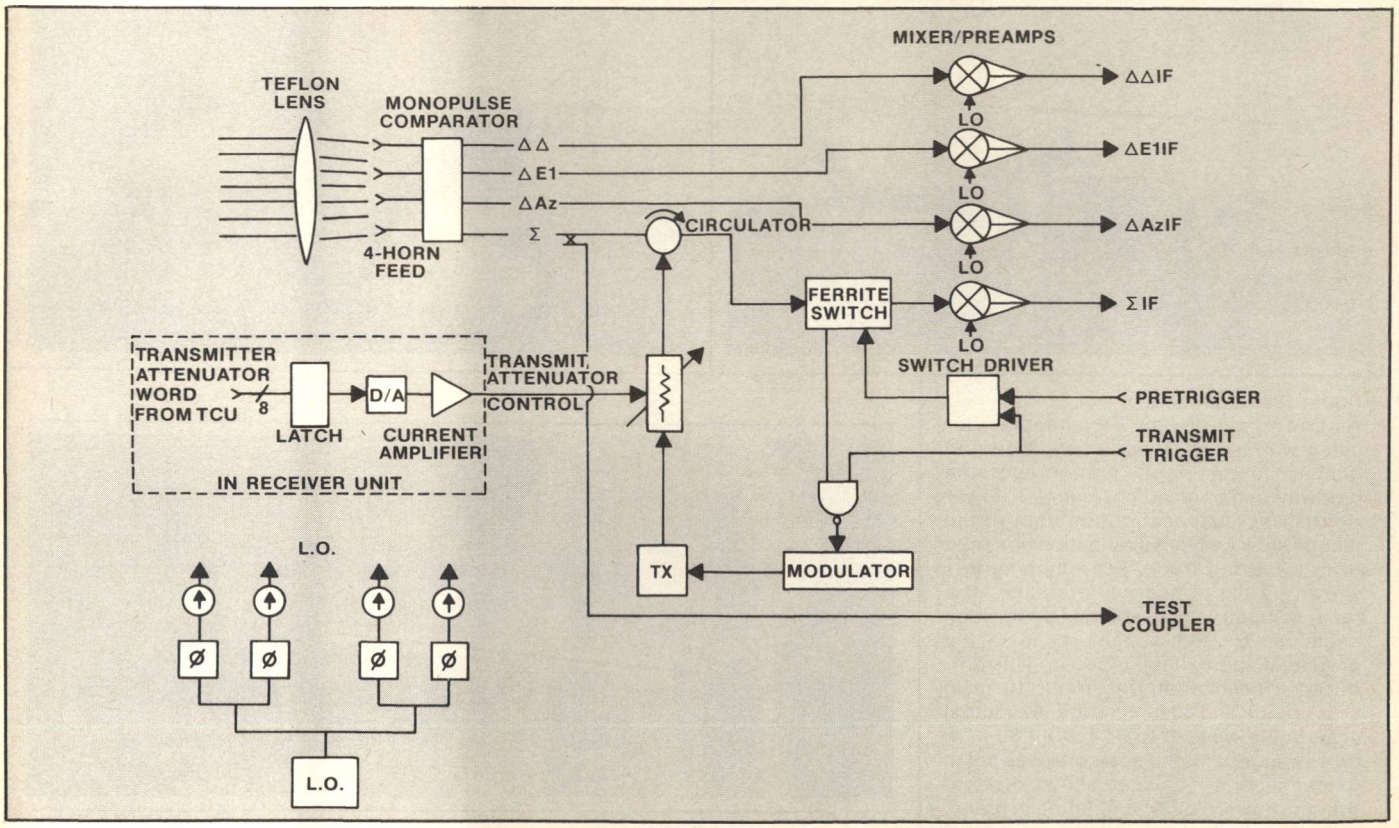

Fig. 3 RF unit block diagram.

ing all millimeter wave components, and the receiver unit containing IF processing circuitry, signal conditioning circuits and power supplies. Figure 1 shows the RF unit mounted in a test fixture with a separate 1° x 3° fan beam antenna. All the control signals for the radar system are supplied via the serial data buss from the General Electric timing and control uint (TCU). All radar data, i.e., digitized sampled video and tracking signals are supplied to the TCU on a 12 bit data buss.

RF Unit

The RF portion of the system is mounted in a gimballed pedestal as shown in Figure 2 on the chin of the helicopter. It includes the antenna, transmitter and receiver components up to and including, the mixer/preamplifiers and the local oscillator. Figure 3 is a block diagram of the RF portion of the system.

The antenna is a lens which is illuminated with a 4 horn feed. The lens, shown in Figure 4, is made of Teflon. The inside surface is hyperbolically shaped, and the outside surface consists of stepped parallel surfaces. The 10-inch diameter provides a beamwidth of 1° when focused. The beam can be defocused by "screwing" the lens in or out relative to the feed, providing a beamwidth of up to 3°. Figure 5 shows the 4 horn feed and the monopulse comparator.

The signals associated with the four received lobes are processed in a conventional monopulse comparator (hybrid array) to provide the sum (Σ), delta azimuth (ΔAz), delta elevation (ΔEl) and delta delta (ΔΔ) channels. The ΔΔ channel is not terminated, rather the ΔΔ signal is preserved and processed at IF in a manner similar to that of the other channels. The reason for preserving the signal in this channel will be made clear later.

Comparator output signals for each of the three delta channels are fed directly to integrated wide band mixer/preamplifiers in which the RF signals are mixed with the local oscillator signal to generate the intermediate frequency (IF) signal, nominally at 750 MHz. The

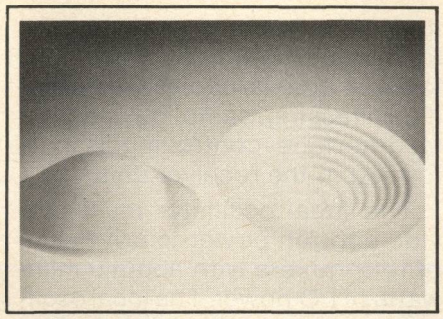

Fig. 4 Teflon lens.

sum channel has a similar mixer/preamplifier, but between the mixer and the monopulse comparator are a coupler (to provide a sample of the RF for transmitter measurements or to inject a signal for receiver tests), a circulator and a ferrite switch (used as a receiver protector).

The ferrite switch, which is in the high attenuation state during the transmit pulse, switches to the low attenuation mode in approximately 0.5 μs, providing a minimum range capability of about 80 meters. The IF signals out of the

four mixer/preamplifiers are sent to the receiver unit by way of four low loss coaxial cables. All further IF processing, sampling and digital interface controlling is performed in the receiver unit.

The local oscillator must provide enough power to drive each of four mixers with about 5 milliwatts of LO power. The local oscillator output is divided into four channels; each channel contains a phase shifter and an isolator leading to a mixer input port. The losses associated with the splitters, phase shifters and isolators require that the local oscillator output be about 30 milliwatts. Since at the time of development, this much power was not available in a tunable Gunn local oscillator (a Gunn was desired for low noise characteristics and tuning is required to match the transmitter frequency) at 95 GHz, a 47 GHz Gunn source is used with a frequency doubler.

The balanced mixer/preamplifiers use beam-lead Gallium Arsenide diodes for reliability. The SSB noise figure is 8 dB, and the RF to IF gain is approximately 35 dB. The bandwidth at the preamplifier output is about 2 GHz. The high gain of the preamplifier stage allows for the use of all the required signal tailoring elements (i.e., filters, attenuators, couplers) before another stage of gain is required.

The transmitter, shown in Figure 6, is a pulsed Hughes Impatt diode oscillator providing about 5 watts peak power for a pulse length of about 100 nanoseconds. The modulator provides a pulsed current ramp which creates a chirped RF output signal when combined with the heating effects in the diode junction. The chirp bandwidth is approximately 250 MHz.

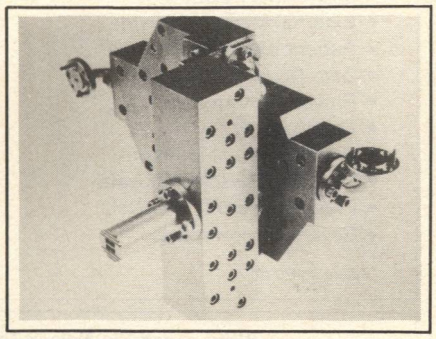

Fig. 5 TRG 4-horn feed and monopulse comparator.

This chirped RF output signal is processed through a current controlled ferrite attenuator [controlled by the radar timing and control unit (TCU)] that provides up to 30 dB of transmitter attenuation to avoid receiver saturation due to large targets at close range. The transmitter/attenuator output is then processed through a three port circulator (duplexer) to the sum channel.

Receiver Unit

The receiver unit consists of the IF processing circuits, detectors, integrating sample-and-hold circuits, video amplifiers, tracking phase detectors, analog-to-digital (A/D) converters, signal conditioning circuits and power supplies. Figure 7 is a block diagram of the receiver unit showing the IF processing. Figure 8 shows the detection, sampling and digital signal conditioning functions.

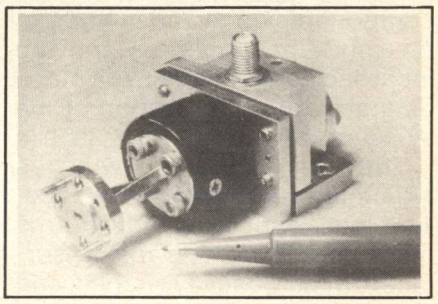

Fig. 6 Hughes IMPATT pulsed oscillator.

The four IF signals from the RF unit are supplied to the receiver unit by way of four low loss coaxial cables. Each signal goes through a channel consisting of:

- coupler
- low pass filter (LPF)
- two voltage controlled attenuators
- high pass filter (HPF)
- two way splitter

The coupler allows injection of a built-in-test signal which is generated by gating a 750 MHz oscillator. The test signal is controlled by the radar TCU, to confirm proper operation of the receiver, sampling, analog-to-digital converting and digital interface functions.

The high pass filter passes signals above 500 MHz, and the low pass filter cuts off at 1,000 MHz.

These two filters define the IF bandpass and limit the noise bandwidth to 500 MHz.

Two voltage controlled attenuators, each providing up to 60 dB of attenuation, are used to control the IF gain. Although normal operation seldom requires a total attenuation of more than 40 dB, two attenuators are used because the phase characteristics are well matched over the lower attenuation ranges. The resulting phase match (between channels) is better for two 20 dB attenuators than for one 40 dB attenuator.

Each channel has a two way splitter, allowing each channel to have an input to the IF hybrid array as well as allowing the sum channel and the ΔAz and ΔEl channels to be applied to the angle and range tracking and detection circuits. The four IF channels are applied to the hybrid array which is an image of the RF monopulse comparator array. This array reconstructs the four original receive lobes so that the simultaneous lobing technique can be used for angle tracking. Although the information contained in the ΔΔ channel is not useful for conventional monopulse tracking, it is required for reconstruction of the four original receive beams. IF amplifiers are used between the two way splitters and the hybrid array to provide adequate signal level for reliable detection. The four channels are named A, B, C and D.

The sum channel, beside being applied to the hybrid array, goes to a four way splitter to provide a sum signal for range tracking, detection and references for the azimuth and elevation error detectors. The four way splitter is preceded by an amplifier and followed by amplifiers as appropriate for setting the signal levels for the various functions.

The ΔAz and ΔEl channels, in addition to being applied to the hybrid array, are amplified and applied to the azimuth and elevation phase detectors and amplifier circuits which use the sum channel as a reference to determine the azimuth and elevation tracking errors.

The A, B, C, D and sum chan-

[Continued on page 64]

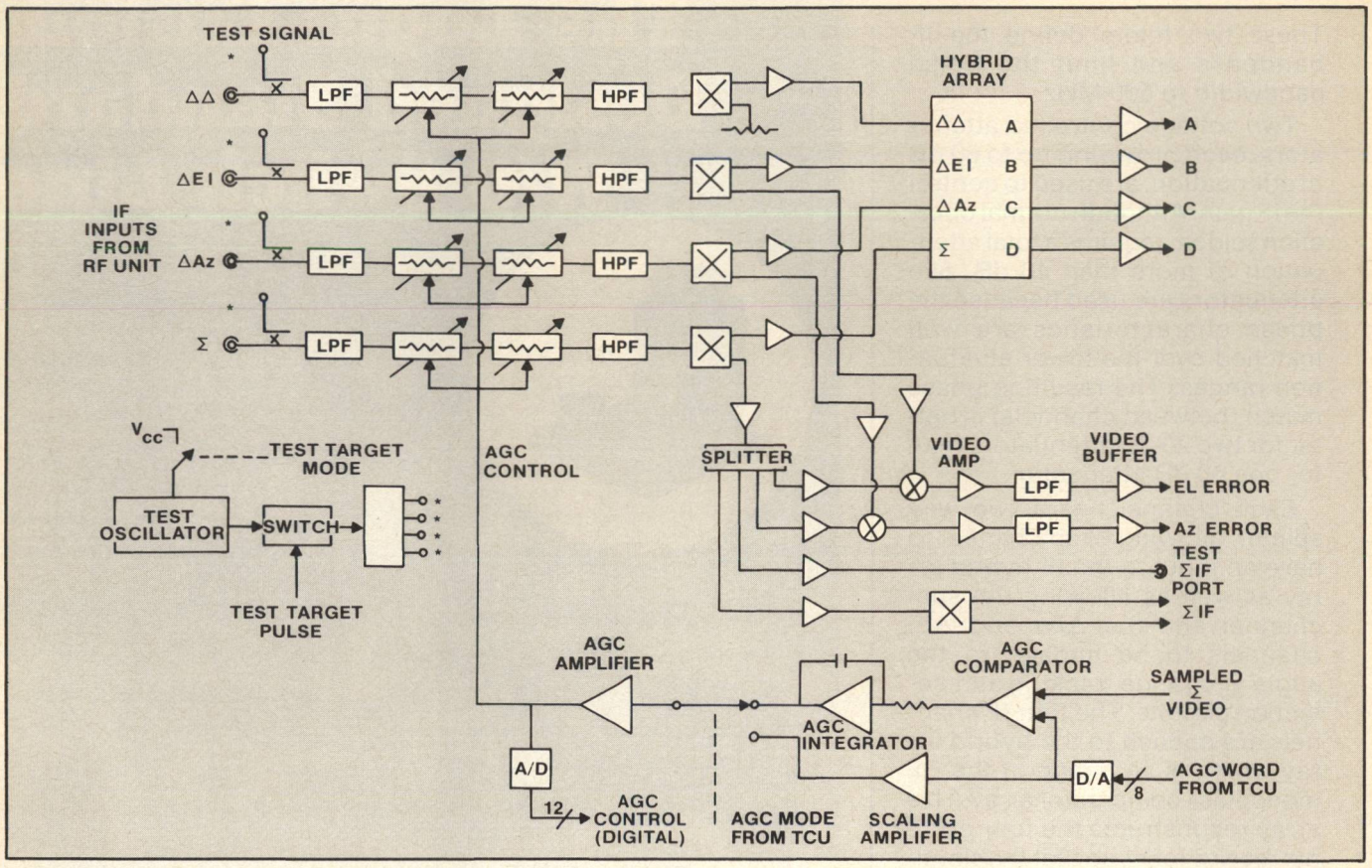

Fig. 7 IF processing block diagram.

nels all go the integration sample and hold circuits; the sample time is determined by the TCU. The sum channel actually goes to two such circuits; one samples the total return from the designated range cell, and the other uses an early gate and late gate to provide range tracking signals. The azimuth and elevation tracking error signals are applied to conventional sample and hold circuits.

The outputs from all the sampling circuits are applied to 12 bit A/D converters. The sampled signals are converted to digital words and multiplexed over the serial data buss to the radar TCU. The early gate/late gate signals are used for range tracking and the ΔAz and ΔEl signals are used for angle tracking. The sampled sum signal is used in the AGC loop to maintain relatively constant sum channel amplitude for consistent angle tracking loop gain. All of the tracking loops are closed through the radar TCU. The AGC loop may be closed through the TCU or in the radar receiver unit itself; the mode being determined by a command on the serial data buss to the radar from the TCU.

The following commands and signals are supplied to the radar from the TCU:

- Transmit command
- Test target injection command
- AGC mode
- AGC offset/AGC control
- Transmitter attenuator
- Pretrigger (pulse)
- Transmit trigger (pulse)
- Early gate (pulse)
- Late gate (pulse)
- Angle gate (pulse)

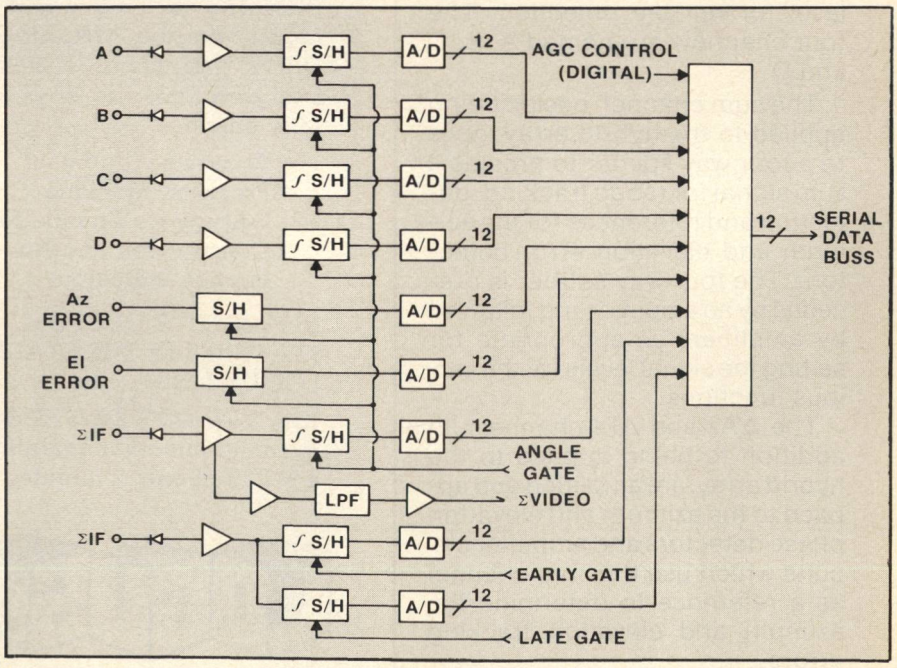

Fig. 8 Detector, sampling and A/D converter circuits.

- Test Target (pulse)
- Various operating commands and signals

The block diagrams in Figures 3, 7 and 8 show where these signals are used.

Except for the 6 pulse signals, the command and control words are all received on the serial data buss. The transmit trigger pulse is gated or "anded" with the transmit command before being applied to the transmitter modulator. Pretrigger is used to switch the receiver protector into the high attenuation mode. Early gate, late gate and angle gate control the sample circuits. The test target is generated at the test target pulse time if the test target injection command is on. The transmitter attenuator word is converted to a current and applied to the ferrite attenuator.

The AGC function has two modes; TCU control and radar control. When the AGC is controlled by the TCU, the digital AGC word from the TCU is converted to an analog signal, scaled and applied to the voltage controlled attenuators. When the AGC is in the radar mode, the circuits in the receiver unit control the attenuators. In this case, the reference for the AGC loop is supplied by the TCU and a digital representation of the attenuator control voltage is sent back to the TCU via the serial data buss.

Summary

The radar described above is a state-of-the-art, versatile instrumentation sensor which demonstrates the fact of tracking system capability at 95 GHz. The system is used to evaluate tracking performance limitations with such a system. The airborne platform allows evaluation of tracking performance for actual targets in a realistic clutter environment at realistic depression angles. The adaptation of the system permits evaluation of a variety of signal processing techniques over a wide dynamic range of conditions.

Acknowledgements

Development of the radar described was performed on a subcontract from the General Electric Company under project monitorship and with the valuable guidance of Mr. Richard Thompson.

Mr. Donald Temme and Mr. Thomas Bryant of MIT/LL also contributed greatly to the system developed.

Pope P. Britt *received his BSME degree from the University of Alabama in 1960.*

As an engineer with General Electric, Utica, New York (1961-1973), with Martin Marietta, Orlando, FL (1973-1978) and with the Experiment Station of Georgia Tech, Atlanta, GA (78 to present) his work in technology development has been primarily: radar system concepts, antennas, planar and conformal arrays, seekers and applications of millimeter wave technology.

Jim Scheer *received a BSEE degree from Clarkson College in 1966 and an MSEE from Syracuse University in 1973.*

As an engineer he has worked on a wide variety of radar development programs while working at General Electric Company in Utica, New York from 1966 to 1975 and the Georgia Institute of Technology, Engineering Experiment Station since 1975. He is currently involved in development of a variety of millimeter wave systems. ■

Frequency Agile Microstrip Antennas

P. Bhartia and I. J. Bahl*

Abstract

Microstrip antennas suffer from having a very low bandwidth characteristic. This paper describes a novel technique for increasing the operational frequency range of microstrip patch antennas using varactor diodes at the radiating edges of the stucture. Theoretical and experimental results confirm that bandwidths of the order of 30% are achievable with this method compared to the 1-2% bandwidth of the unloaded patch.

Introduction

Narrow bandwidth has been one of the limitations of microstrip antennas[1]. Bandwidth of microstrip patch radiators may be improved by coupling parasitic $\lambda/4$ resonators to the radiating edges[2] or parasitic elements to the non-radiating edges[3], of rectangular shaped antennas. Using this method it is not difficult to double the bandwidth of rectangular microstrip patch antennas. Another technique of improving the bandwidth is by using the log-periodic arrangement of rectangular patches[4 5]. Using a 9-element log-periodic structure, 30% bandwidth in terms of good input VSWR, radiation control and efficiency better than 70% has been obtained[4].

In all the above reported techniques, the size of the antenna structures becomes prohibitively large and such methods are not very suitable in realizing large arrays where good control over sidelobe and other radiation characteristics is required. In addition, these techniques cannot be used for other geometries of microstrip antennas. In this paper, a new approach for obtaining wide-bandwidth operation of microstrip patch antennas is described. The method can be used with any patch configuration and also does not increase the size of the antenna element.

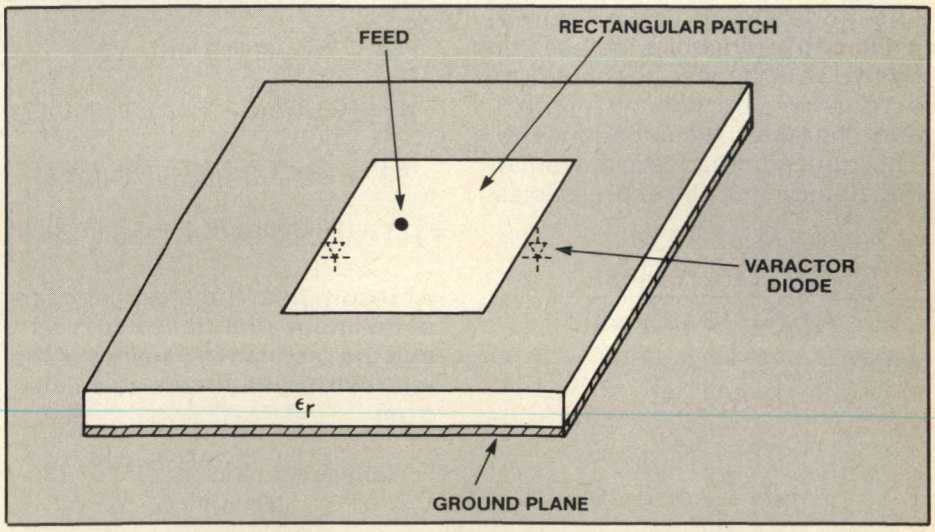

Fig. 1 Broadband rectangular patch microstrip antenna.

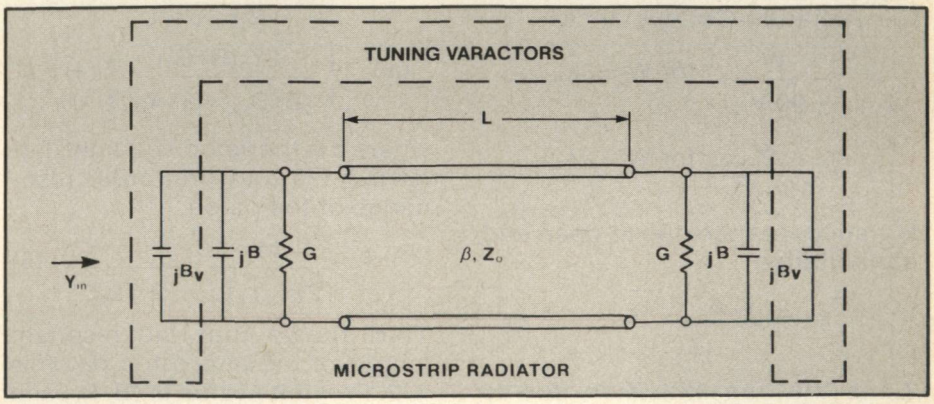

Fig. 2 Equivalent circuit for a microstrip antenna with tuning varactors.

*Dr. P. Bhartia is with the Defence Electronics Division, Defence Research Establishment, Ottawa, Ottawa K1A 0Z4, Canada.
Dr. I. J. Bahl is with the Electro-Optical Products Division, ITT, Roanoke, Va.

Analysis

It is a well known fact that the electrical length of a transmission line loaded periodically with reactive components can be increased or decreased depending upon the type of reactance used. For example, if voltage controlled tuning varactors are connected across the open ends (radiating edges) of a rectangular patch antenna as shown in Figure 1, the electrical length is increased and thus the resonant frequency is decreased. Thus by varying electrically the capacitance of the varactors, the resonant frequency of the patch can be adjusted (within the specified limits). This increases the operational frequency range for the structure, making it suitable for frequency diversity operation, multifrequency transmitting antennas etc.

The rectangular microstrip antenna of width W and length L having tuning varactors at the radiating edges may be analyzed by using the equivalent transmission line model. As shown in Figure 2, a microstrip radiator is represented by two admittances connected by a transmission line of length L and characteristic impedance Z_o. The input admittance of the radiating element may be expressed as:

$$Y_{in} = G + j(B + B_v) + Y_o \times \frac{G+j\,(B+B_v+Y_o\tan\beta L)}{Y_o+j\,(G+JB+jB_v)\tan\beta L}$$

where

$$Y_o = \frac{1}{Z_o}$$

$$\beta = \frac{2\pi}{\lambda_o}\sqrt{\varepsilon_e}\ ,\ \varepsilon_e$$

is the effective dielectric constant[6]

G = radiation Conductance

$$= \frac{W^2}{90\lambda^2_o} \quad \text{for } W << \lambda_o$$

$$= \frac{w}{120\lambda^2_o} \quad \text{for } W >> \lambda_o$$

B = susceptance due to open end capacitance

$$= \frac{k_o \Delta l\ \sqrt{\varepsilon_e}}{Z_o},$$

Δl is the line extension due to fringing field[6]

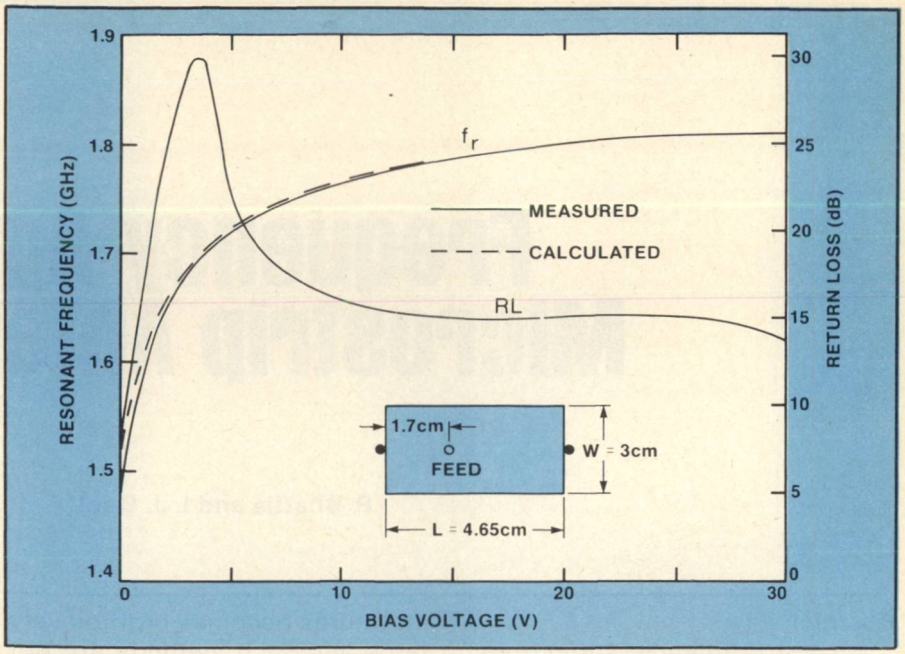

Fig. 3 Resonant frequency and return loss for the varactor loaded rectangular patch microstrip antenna.

$B_v = \omega C_v$, C_v is the varactor capacitance

Equation (1) may be rewritten as

$$Y_{in} = G+j(B+B_v)+ Y_o \times \Big[\Big\{[G+j(B+B_v+Y_o\tan\beta L)] \times [Y_o-(B+B_v)\tan\beta L-jG\tan\beta L]\Big\} \div \Big\{[Y_o-(B+B_v)\tan\beta L]^2 + G^2\tan^2\beta L\Big\}\Big] \quad (2)$$

At resonance, the imaginary part of the input admittance Y_{in} is zero and the resonant frequency of the microstrip antenna is calculated from

$$\tan\beta L = \frac{2Y_o(B+B_v)}{(B+B_v)^2+G^2-Y_o^2} \quad (3)$$

$$\text{or } f_r = \frac{c}{2\pi\ \sqrt{\varepsilon_e}L} \times \tan^{-1}\left\{\frac{2Y_o(B+B_v)}{(B+B_v)^2+G-Y_o^2}\right\} \quad (4)$$

where c is the velocity of light. For $(B+B_v) = 0$ and first order resonance of the patch,

$$f_r = \frac{c\pi}{2\pi\sqrt{\varepsilon_e}L} = \frac{c}{2\sqrt{\varepsilon_e}L} \quad (5)$$

This shows that the resonant length of the microstrip patch is $\lambda/2$. For finite value of $(B+B_v)$ and first order resonance,

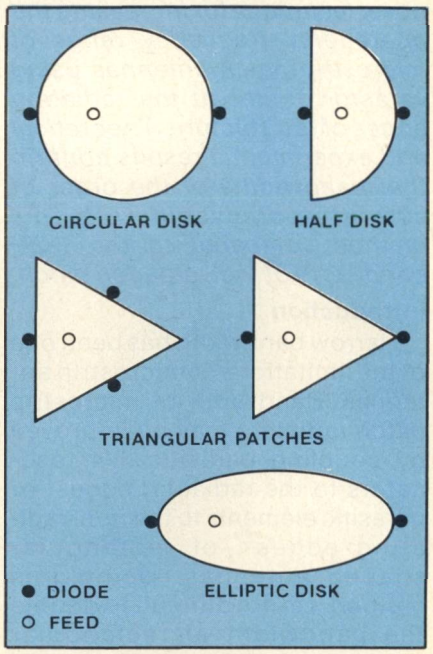

Fig. 4 Other broadband configurations.

$$f_r = \frac{c\,\delta\,\pi}{2\pi\sqrt{\varepsilon_e}L} = \delta\,\frac{c}{2\sqrt{\varepsilon_e}L} \quad (6)$$

where δ is a fraction. This shows that for a given length of the patch, the resonant frequency is decreased by connecting a capacitive susceptance to the radiating ends. Hence by varying the varactor's capacitance, the resonant frequency of the microstrip patch antenna can be changed.

Experimental Results

In order to verify the theoretical

results for the resonant frequency, some experiments were carried out. A matched rectangular patch microstrip antenna was designed and fabricated using duroid substrate (ε_r = 2.32 and h=0.159cm). The matching was obtained by selecting a suitable feed position along the length of the patch. The dimensions of the rectangular patch were W = 3.0 cm and L = 4.65cm. At the center frequency the measured value of the VSWR was less than 1.2 and the bandwidth (VSWR $\leq$ 2.0) value was about 2%.

The two identical varactor diodes (Model Alpha DVH-6733-168-001) were mounted as shown in Figure 1. These diodes have a tuning range of 2.4-0.4 pF when reversed biased between 0 and 30V. The measured values of the resonant frequency and the return loss as a function of bias voltage are shown in Figure 3. The theoretical values of the resonant frequency calculated from (4) are also shown. These calculations include the additional connecting line lengths due to diodes. There is good agreement between the measured and calculated results. The measured values of the bandwidth (the fractional frequency range over which the VSWR $\leq$ 2) obtained with these diodes was 22%.

To verify this technique with other configurations (shown in Figure 4), the commonly used circular disk was designed and tested on duroid substrate having h = 0.159cm. The radius of the circular disk was 2.0 cm. The antenna was fed at one third of the radius from the center of the disk. At the center frequency the measured VSWR was less than 1.2 and the bandwidth of this configuration was about 2%.

The measured resonant frequency and return loss as a function of bias voltage for the circular disk antenna are shown in Figure 5. The measured bandwidth in this case was found to be about 30%.

Radiation characteristics were also investigated over the bandwidth range. In general, no significant changes occurred in either the radiation characteristics, beamwidths or cross polarization. In the broadside direction, the axial ratio was generally 35dB down with its being a maximum of about 20dB around 45°. Although E plane characteristics do not change, the H plane beamwidth decreases with increasing frequency as shown in Figure 6, which is as expected. Finally, no significant variations were found in the measured gain values, which were measured at 5±.5dB.

Conclusions

A new technique to improve the operational bandwidth of microstrip patch antennas has been described. The technique does not improve the instantaneous bandwidth and work is currently under-

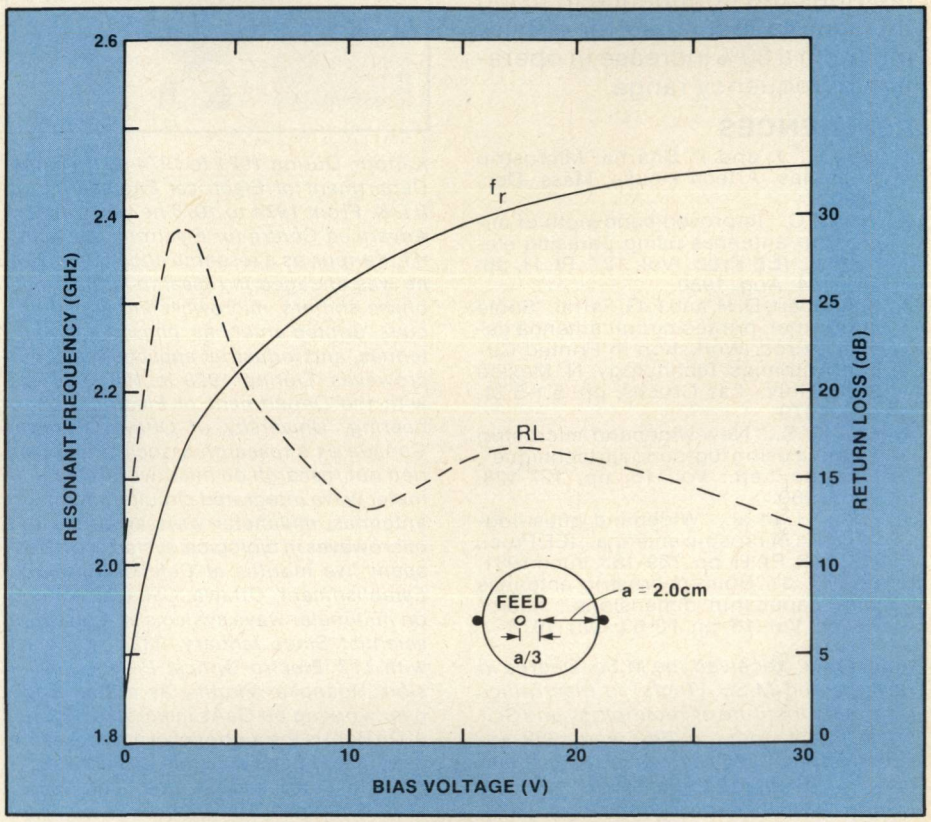

Fig. 5 Resonance frequency and return loss for the varactor loaded circular disk microstrip antenna.

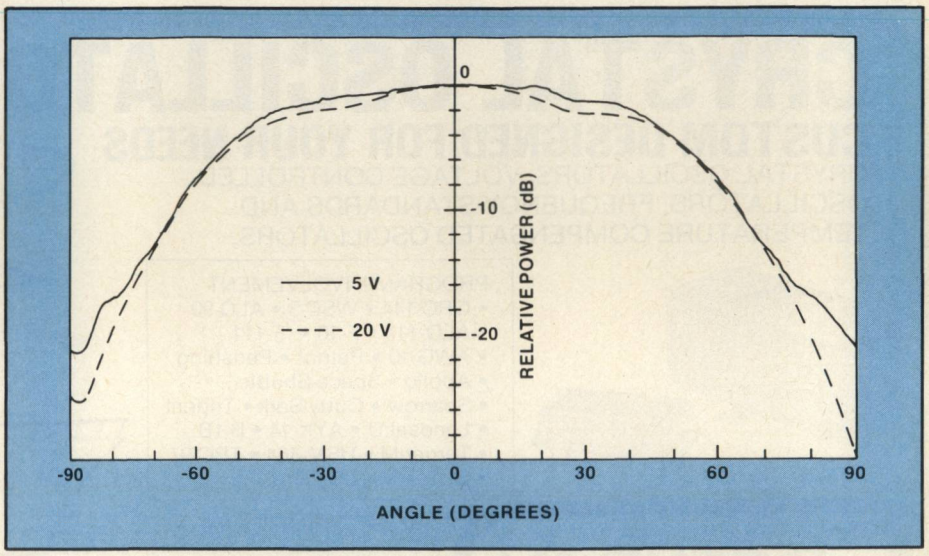

Fig. 6 H-plane patterns at 5V and 20V biases for the circular patch antenna.

way to investigate the possibility of applying ramp voltages to the varactors to overcome this problem. However, this method of increasing frequency range for microstrip patch configurations is useful even in its present form for a large number of applications. Good agreement between the theoretical and experimental results provides the confidence in using this simple technique for obtaining up to a 30% increase in operational frequency range.

REFERENCES

1. Bahl, I. J. and P. Bhartia, Microstrip Antennas, Artech House, Mass. Dec. 1980.
2. Wood, C. "Improved bandwidth of microstrip antennas using parasitic elements", IEE Proc., Vol. 127, Pt. H, pp. 231-234, Aug. 1980.
3. Schaubert, D. H. and F. G. Farrar, "Some conformal, printed circuit antenna design", Proc. Workshop in Printed Circuit Antennas Technology, N. Mexico State Univ., Las Cruces, pp. 5.1-5.21. Oct. 1979.
4. Hall, P. S., "New wideband microstrip antenna using log-periodic technique", Electron Lett., Vol. 16, pp. 127-128, Feb. 1980.
5. Pues, H. et al., "Wideband quasi-log-periodic microstrip antenna", IEE Proc., Vol. 128, Pt. H, pp. 159-163, June 1981.
6. Bahl, I. J. "Build microstrip antennas with paper-thin dimensions", Microwaves, Vol. 18, pp. 50-63, Oct. 1979.

Inder Bahl, *received the M.Sc. Degree in Physics and M.Sc. [Tech.] in Electronics from Birla Institute of Technology and Science, Pilani, India in 1967 and 1969, respectively. In 1975 he received a Ph.D. Degree in Electrical Engineering from the Indian Institute of Technology [IIT], Kanpur.*

From 1969 to 1970 he worked in Troposcatter Communication Project at IIT, Kanpur. During 1971 to 1974 he ws in the Department of Electrical Engineering at IIT/K. From 1974 to 1978 he was with the Advanced Centre for Electronic Systems, IIT, Kanpur, as a research engineer, where he was engaged in research in pin diode phase shifters, microwave integrated circuits, printed antennas, phased-array antennas, and industrial applications of microwaves. During 1979 to 1981, he was with the Department of Electrical Engineering, University of Ottawa, Ottawa, Canada as a research associate and carried out research on microwave and millimeter wave integrated circuits, microstrip antennas, millimeter wave antennas and microwaves in biological systems. Dr. Bahl spent five months at Defense Research Establishment, Ottawa, Canada, working on millimeter wave systems as a research scientist. Since January 1982 he has been with ITT Electro-Optical Products Division, Roanoke, Virginia as a Staff Engineer working on GaAs integrated circuits.

Dr. Bahl is the author of over 50 research papers and has published two books: *Microstrip Lines and Slotlines* and *Microstrip Antennas.* His third book on *Millimeter Wave Techniques and Applications* is to be published. Dr. Bahl is a senior member of IEEE.

Prakash Bhartia, *obtained the B. Tech [Hons] degree in Electrical Engineering from the Indian Institute of Technology, Bombay in 1966 and the M.Sc and Ph.D degrees from the University of Manitoba, Winnipeg, Canada in 1968 and 1971 respectively.*

From 1971 to 1973 he was a Research Associate at the University of Manitoba and joined the faculty of Engineering at the University of Regina in 1973 where he served as Assistant Dean. In 1977 he joined the Defence Research Establishment, Ottawa and was simultaneously appointed an Adjunct Professor at the Universtiy of Ottawa. He has conducted research in both theoretical and applied electromagnetics, scattering, diffraction, radio, satellite and inertial navigation etc. He is currently Head of Electromagnetics at DREO with responsibility for programs in Navigation, Electromagnetic Compatibility and Electromagnetic Pulse Effects. He has authored or coauthored over 100 technical papers and a book 'Microstrip Antennas' [Dedham, Artech House 1980] and also holds patents.

Dr. Bhartia is a Senior Member of IEEE, an Associate Editor of the Journal of Microwave Power and serves on the Editorial Review Boards of MTT and AP. ■

A Microprocessor Controlled Variable Phase and Amplitude Antenna Feed Network Unit

J. P. Starski, B. Ingemannsen and A. Olausson
Chalmers University of Technology Gothenburg, Sweden

Introduction

During the period of 1976 to 1980 the Division of Network Theory at Chalmers University of Technology worked on a special antenna feed network unit (AFNU). The goal of the project was to design and build a 16 channel antenna feed network unit with variable phase and amplitude in each channel separately. The antenna feed network unit utilizes a corporate feed technique and subsequently it consists of 1 input and 16 outputs. The specification allowed a narrow band design. The AFNU operates at X-band (8.9-9.1 GHz). Every channel can be set in phase from 0° to 360° in steps by 5° and in attenuation from 0 dB to 20 dB in steps by 1 dB. Phase and attenuation settings are independent of each other.

The project was partly supported by the National Defense Research Institute in Sweden.

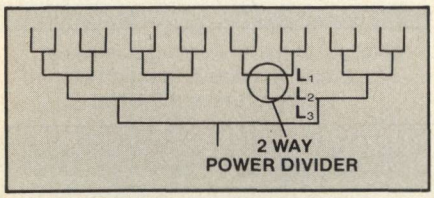

Fig. 1 A 16-way power divider.

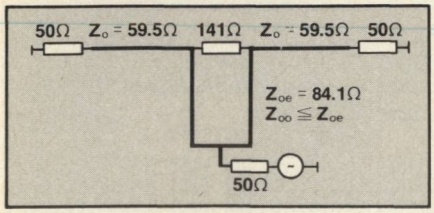

Fig. 2 A 2-way power divider with 2-section maximally flat matching of the input port.

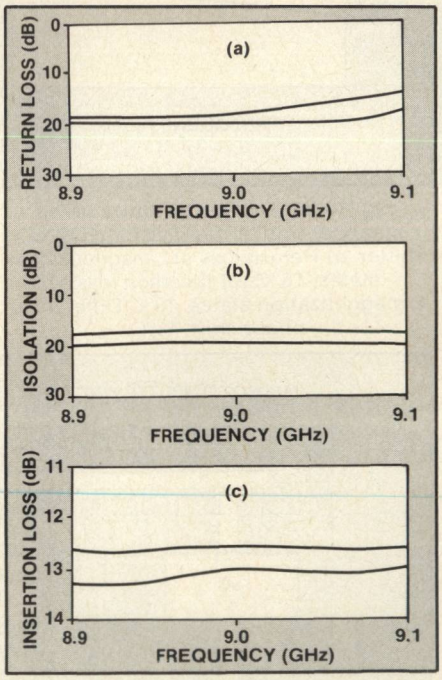

Fig. 3 Performance of the 16-way power divider module: a) Return loss, b) Isolation, c) Insertion loss.

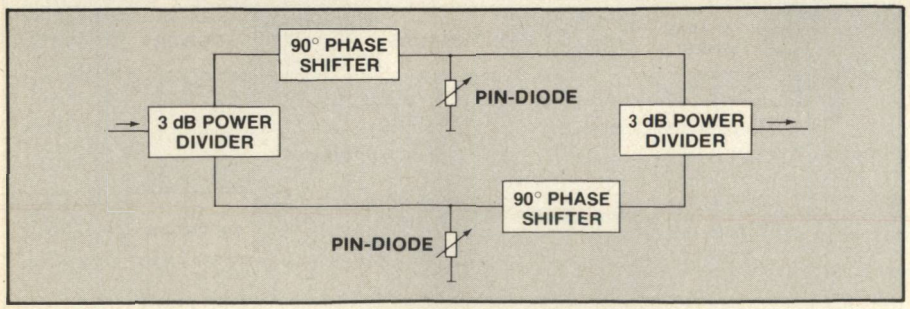

Fig. 4 Variable attenuator consisting of 2 PIN diodes, 2 matched power dividers and 2 90 degrees phase shifters.

Power Divider

The power divider[1] is designed as a 1:16 module, Figure 1. The incoming power is equally split between the outports. The power divider is built in stripline with the dielectric Rexolite 2700 and with a ground plane spacing of 3.18 mm (1/8″). The power divider consists of 2-way power dividers of Wilkinson type, Figure 2. The electric length between the 2-way power dividers L_1, L_2 and L_3 are chosen to give a maximum bandwidth. The resistive film is used as an isolating resistance.

The power divider module has the following performance (frequency range 8-10 GHz).

Insertion loss, max	13.5 dB
Power loss due to power split	12 dB
Net insertion loss, max	1.5 dB
Net insertion loss, average	0.9 dB
Return loss, input port	20 dB
Return loss, output ports	13 dB
Isolation between adjacent ports	15 dB

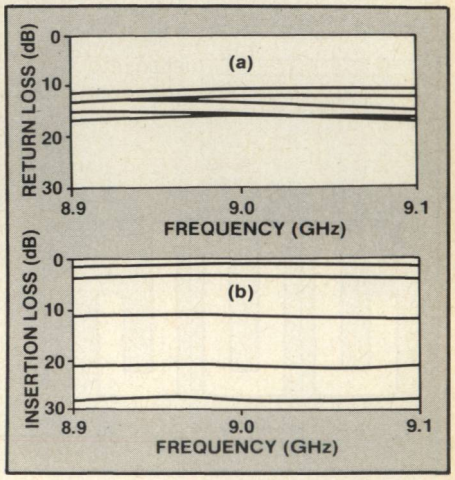

Fig. 5 Typical performance of the variable attenuator: a) Return loss at different attenuation levels, b) Insertion loss.

In Figure 3 an overall performance of the power divider module is shown for a frequency range 8.9-9.1 GHz.

Attenuator

The attenuator[2] consists of two 3 dB power dividers, 90° phase shifters and PIN diodes, Figure 4.

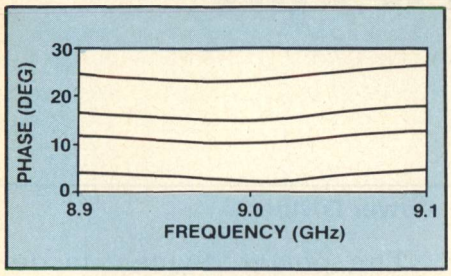

Fig. 6 Phase variation versus attenuation for the variable attenuator.

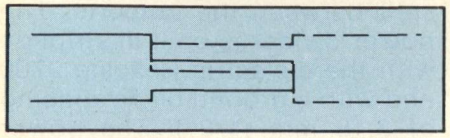

Fig. 7 A schematic of the DC block.

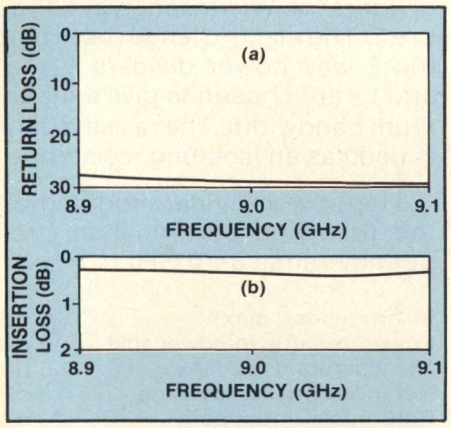

Fig. 8 Typical performance of the DC block: a) Return loss, b) Insertion loss.

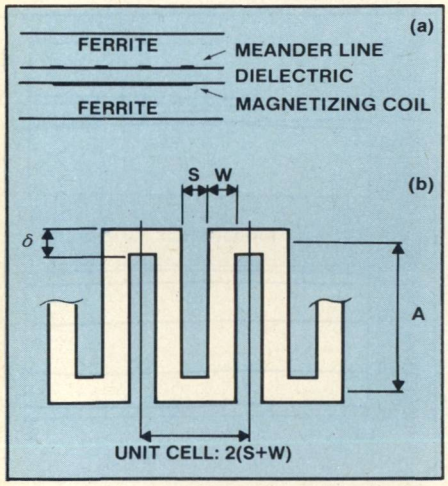

Fig. 9 a) A cross section of the meander-line ferrite-dielectric phase shifter, b) A meander line pattern used in the phase shifter.

The principle of operation can be most easily explained with even and odd modes. The even mode is the transmission one. The diodes are biased simultaneously and create reflections which are absorbed in the isolation resistors (odd mode). Usually the function of the power divider and the 90° phase shift is achieved by a quadrature coupler. This design uses, however, a Wilkinson power divider and transmission lines as 90° phase shifters.

The performance of the attenuator is shown in Figure 5. Figure 6 shows the measured phase variation for different diode driving currents.

DC Blocks

The design of the attenuator with Wilkinson hybrids creates a problem in DC blocking the biasing current. Since a stripline realization was used the 3-dimensional components as capacitors are difficult to use and were subsequently

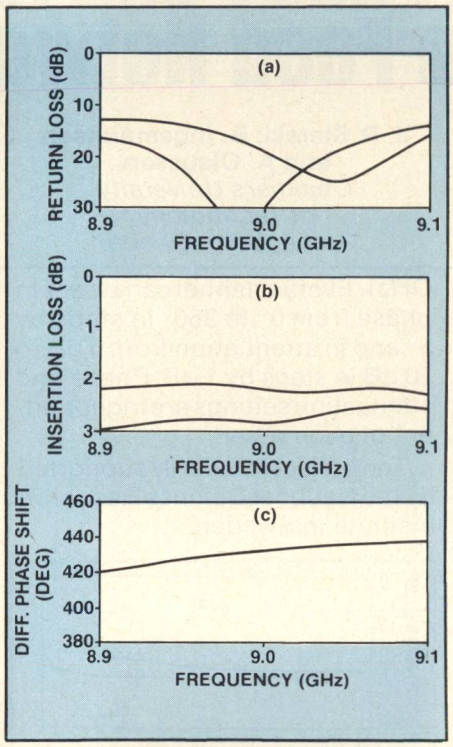

Fig. 10 Typical performance of the meander-line ferrite-dielectric phase shifter: a) Return loss at 2 magnetization states, 18°C, b) Insertion loss at 2 magnetization states, 18°C Differential phase shift, 18°C.

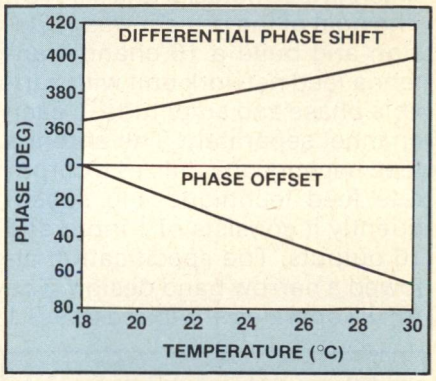

Fig. 11 Differential phase shift and phase offset as a function of temperature, f=9.0 GHz.

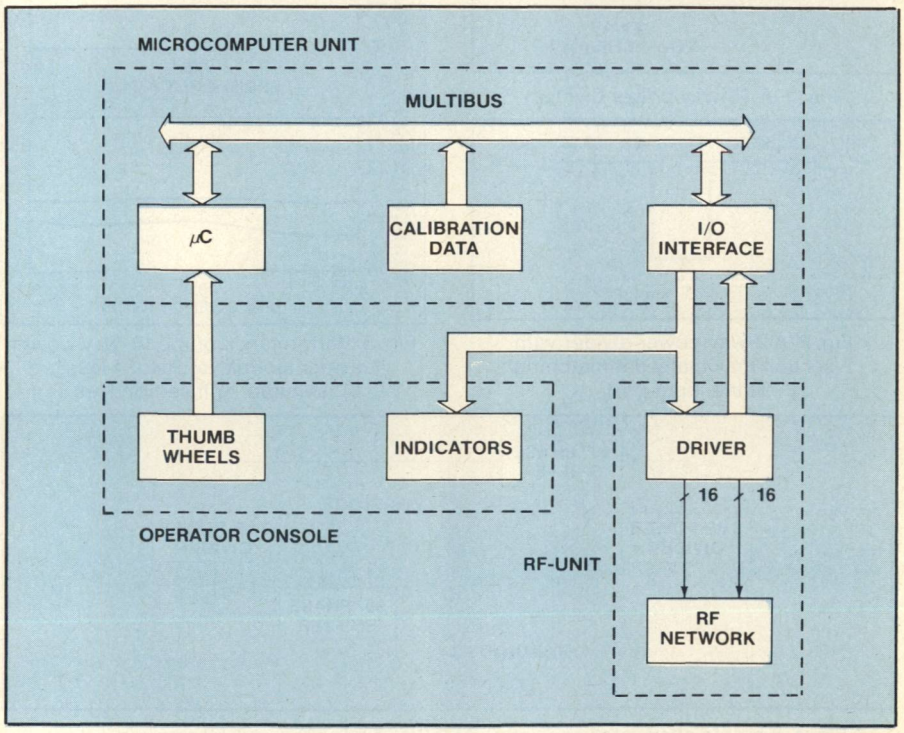

Fig. 12 AFNU — Block diagram.

avoided. A 3 dB CTL coupler with no output arms was used instead, Figure 7.

The performance of the DC block is shown in Figure 8. Two DC blocks were used, one on each side of the attenuator.

Phase Shifter

A meander line phase shifter with multi-layer, ferrite-dielectric structure was used, Figure 9a. The phase shifter is constructed with 0.125 mm (0.005″) thick RT-Duroid as a dielectric. A 50Ω meander line pattern is etched on a dielectric sheet as shown in Figure 9b. The magnetic circuit consists of 1.6 mm thick ferrite pieces and thin rectangular steel pieces accurately machined to a thickness of 0.25 mm. The steel pieces are tightly fitted in the slots made in the dielectric. The 4-piece toroid is latched to various magnetizations with the help of a magnetizing coil printed on the dielectric piece itself. Trans-Tech ferrite is used in the phase shifter.

Figure 10 shows the maximum differential phase shift along with insertion loss and return loss. In the vicinity of the design frequency the matching and insertion loss figure are good, while at higher frequencies the reflections increase sharply due to the approaching stop-band of the meander circuit. The same phenomenon occurs at lower frequencies due to the rapid change in the impedance of the lines arising from the frequency dependence of the permeability. All measurements are done at a constant temperature.

Figure 11 shows the variation of the phase shift and offset phase with temperature. A significant temperature dependence can be observed.

Steering and Control System

The steering equipment[3] was designed to take care of the correct setting of the phase and the attenuation. Studying the previously described attenuator and phase shifter circuits it is obvious that none is perfect. There is a considerable phase change due to the increase of the attenuation in the attenuator, Figure 6, and the attenuation in the phase shifter is

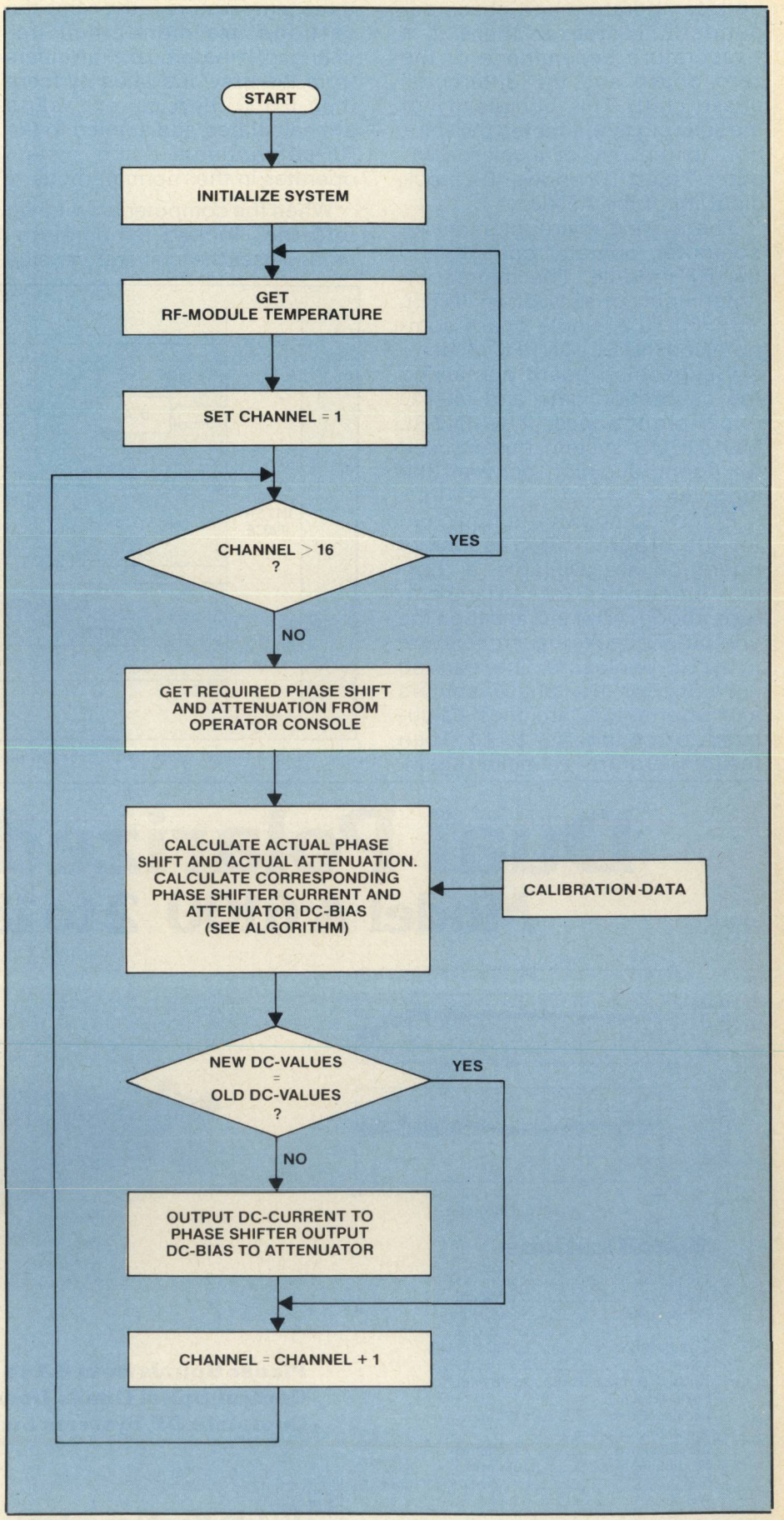

Fig. 13 The flowchart of the AFNU steering program.

both temperature and phase dependent. Moreover there is a temperature dependence of the zero phase and the differential phase shift. This complexity of the steering task directed the solution to the use of a microcomputer. Figure 12 shows the block diagram of the AFNU.

There are 3 main units: microcomputer, operator console and the RF-module. The microcomputer unit consists of an INTEL SBC 80/10 A single board computer, an INTEL 16K PROM memory expansion board containing the calibration data and an I/O expansion board. The INTEL MULTIBUS system bus is used for communication between the modules.

Figure 13 shows the flowchart for the program. Two modes of operation are available, a "normal" mode and a "locked temperature" mode. After initialization the computer checks the temperature in the RF-enclosure. The required currents for the phase shifters and attenuators are then calculated for channels 1 to 16. Then the temperature is checked again. If the temperature is the same the settings are maintained unchanged. If the temperature differs from the previous value by more than 0.5°C, new current values are calculated and applied to the RF-components if the system operates in the "normal" mode.

When the computer is switched into the "locked temperature" mode it uses the temperature value present at the switching moment (locked temperature), and any change in actual temperature is neglected by the system. This gives a possibility to avoid RF-transients during a measurement cycle if the feed network is incorporated in a test setup. Both the locked temperature and the actual temperature are displayed on the console panel.

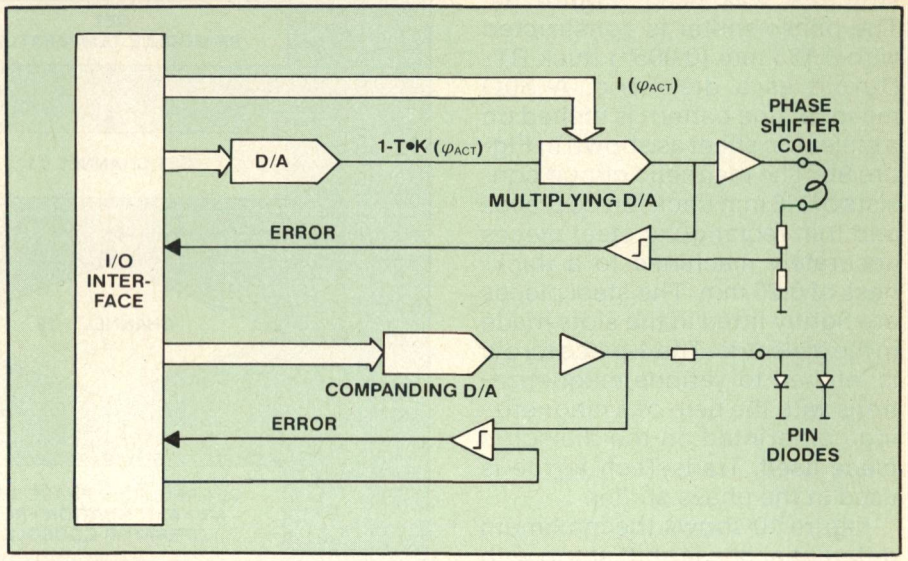

Fig. 14 The simplified driver circuits for the phase shifter and attenuator.

[Continued on page 80]

[From page 78] **NETWORK UNIT**

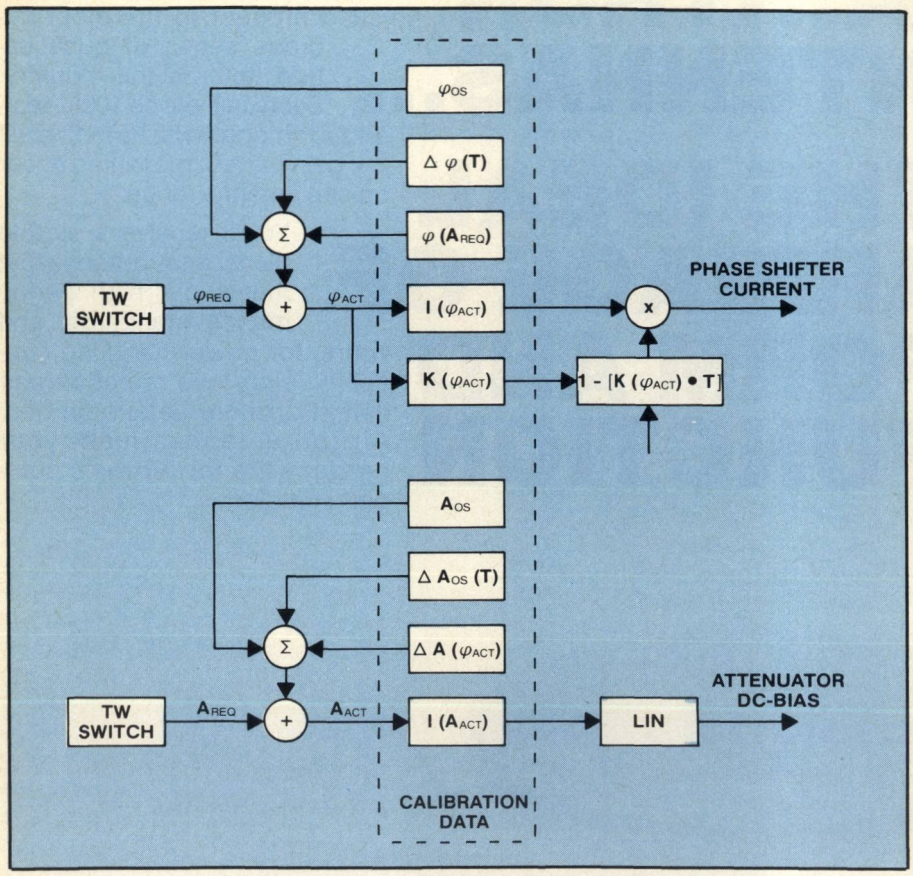

Fig. 15 The calculation procedure of the current value for the phase shifter (upper part) and attenuator (lower part).

Figure 14 shows the simplified schematic of the driver circuits. The companding DAC performs the linearization of the PIN diode characteristics. The error detectors check the current drivers, phase shifter coils and PIN diodes for proper operation. If a continuous error is detected, the corresponding front panel error indicator is activated. The average power to each driver output stage is limited to avoid burnout of the coils or diodes in case of computer or driver malfunction.

The calculation procedure of the current value for the phase shifters is shown in the upper part of Figure 15. The lower part of this figure explains the calculations for the attenuators. The calibration data are obtained by a special calibration procedure for each channel.

A_{OS} = Attenuation offset at 18°C

ΔA_{OS} (T) = Variation in A_{OS} as a function of temperature

ΔA (φ_{ACT}) = Attenuation variation as a function of φ_{ACT}

[Continued on page 82]

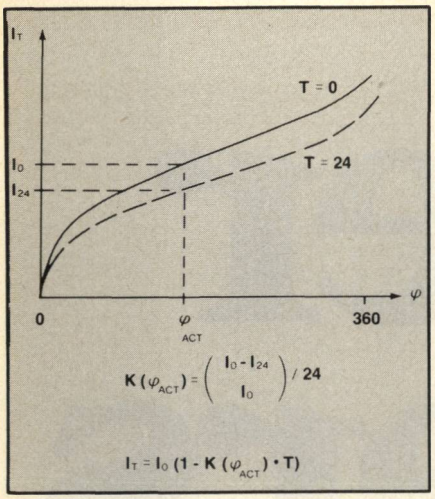

Fig. 16 Temperature constant as a function of the actual phase shift.

$I(A_{REQ})$ = Attenuator DC-bias giving A_{REQ}

φ_{OS} = Phase offset at 18°C

$\Delta\varphi_{OS}(T)$ = Variation in φ_{OS} as a function of temperature

$\Delta\varphi(A_{REQ})$ = Phase variation as a function of A_{REQ}

$I(\varphi_{ACT})$ = Phase shifter current giving φ_{ACT} at 18°C

T = Normalized operating temperature

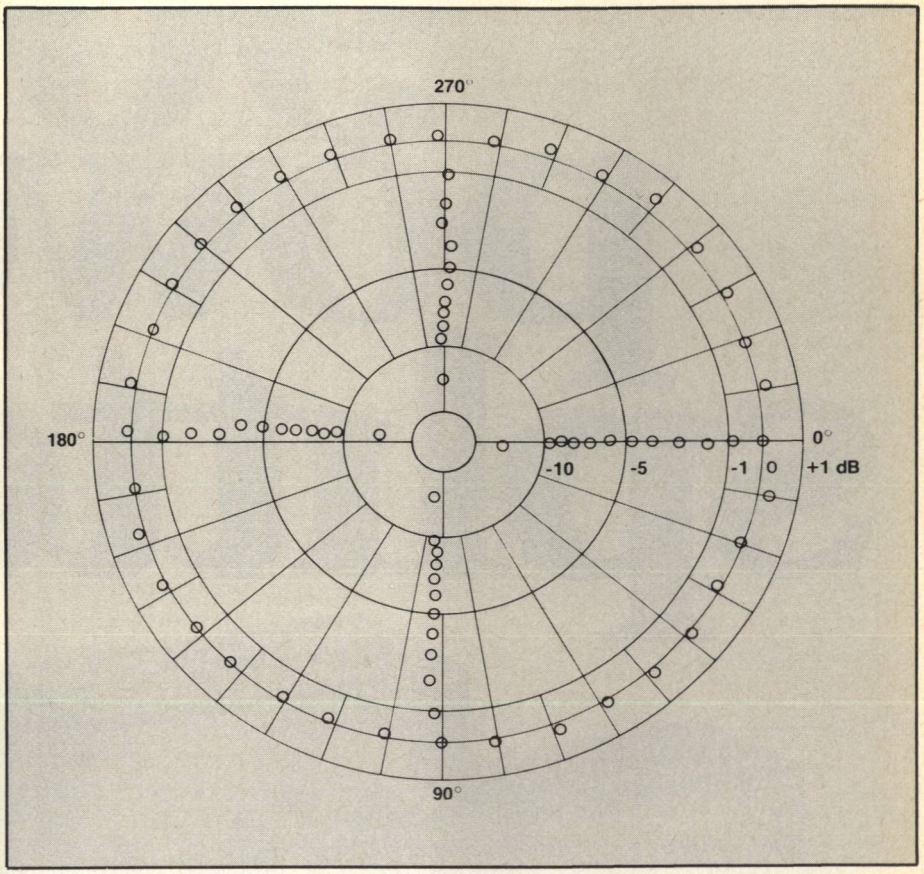

Fig. 17 A typical performance of the AFNU.

$K(\varphi_{ACT})$ = Temperature constant as a function of φ_{ACT} see Figure 16

Summary

An antenna feed network unit with 1 input and 16 outputs has been designed. Each channel can be set from 0° to 360° in steps by 5° and from 0 to 20 dB in steps by 1 dB. The settings are temperature independent for a range of 18-30°C. All channels can be set independent of each other. The AFNU works in the frequency range 8.9-9.1 GHz. Figure 17 shows a typical performance of the AFNU. The total loss per channel is about 20 dB after loss equalization in-

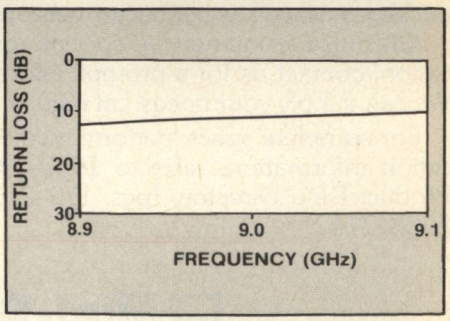

Fig. 18 Return loss at all 16 outputs for the AFNU.

[Continued on page 84]

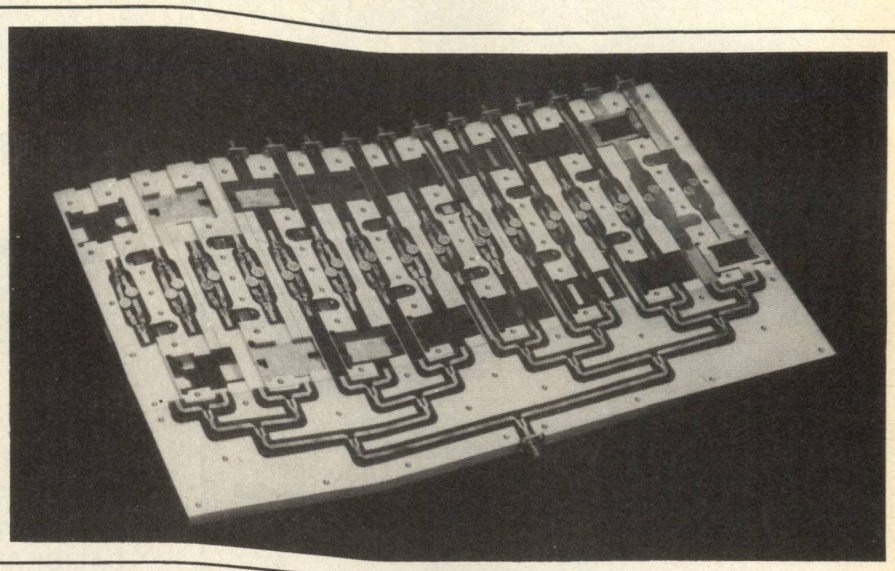

Fig. 19 RF network during assembly.

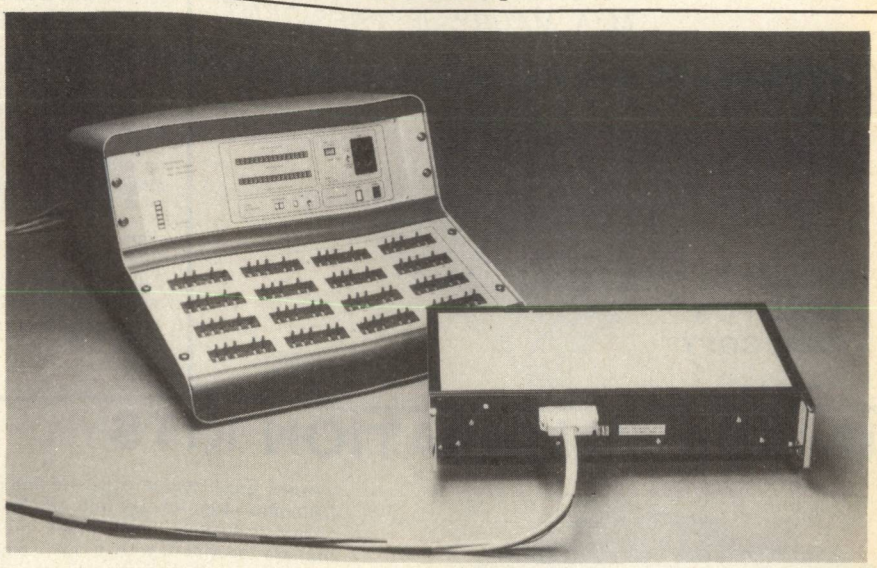

Fig. 20 The AFNU with RF module and operator console. The microcomputer is fitted inside the operator console.

cluding 12 dB originating from the power divider. VSWR at the input is better than 1.5:1. Return loss at the outputs is better than 10 dB for all settings and the entire temperature range, Figure 18. The isolation between the channels is better than 32 dB. Figure 19 shows the RF network during assembly. Figure 20, finally, shows the entire system with RF module, microcomputer and operator console.

Acknowledgments

We wish to thank Professor E. Folke Bolinder for the advice and support he has given us during the work.

We take a great pleasure in thanking Dr. B. Hansson, Dr. S. Rehnmark and Dr. L. Nyström for developing the RF components, B. Ulriksson for his assistance during the calibration procedure and J-O Yxell for the photographs and circuit fabrication. The economical support of the National Defense Research Institute in Sweden is also acknowledged.

REFERENCES

1. Nyström, L, "16-way planar power dividers in improved form", Chalmers University of Technology, Division of Network Theory, Gothenburg, Sweden, Technical Report 8001.
2. Rehnmark, S, "Wideband planar transmission line PIN diode attenuator/modulator", 5th European Microwave Conference, Hamburg, 1975.
3. B. Ingemannsen and A. Olausson, A microprocessor based control system for a 16 channel variable phase and amplitude antenna feed network", to be published. ■

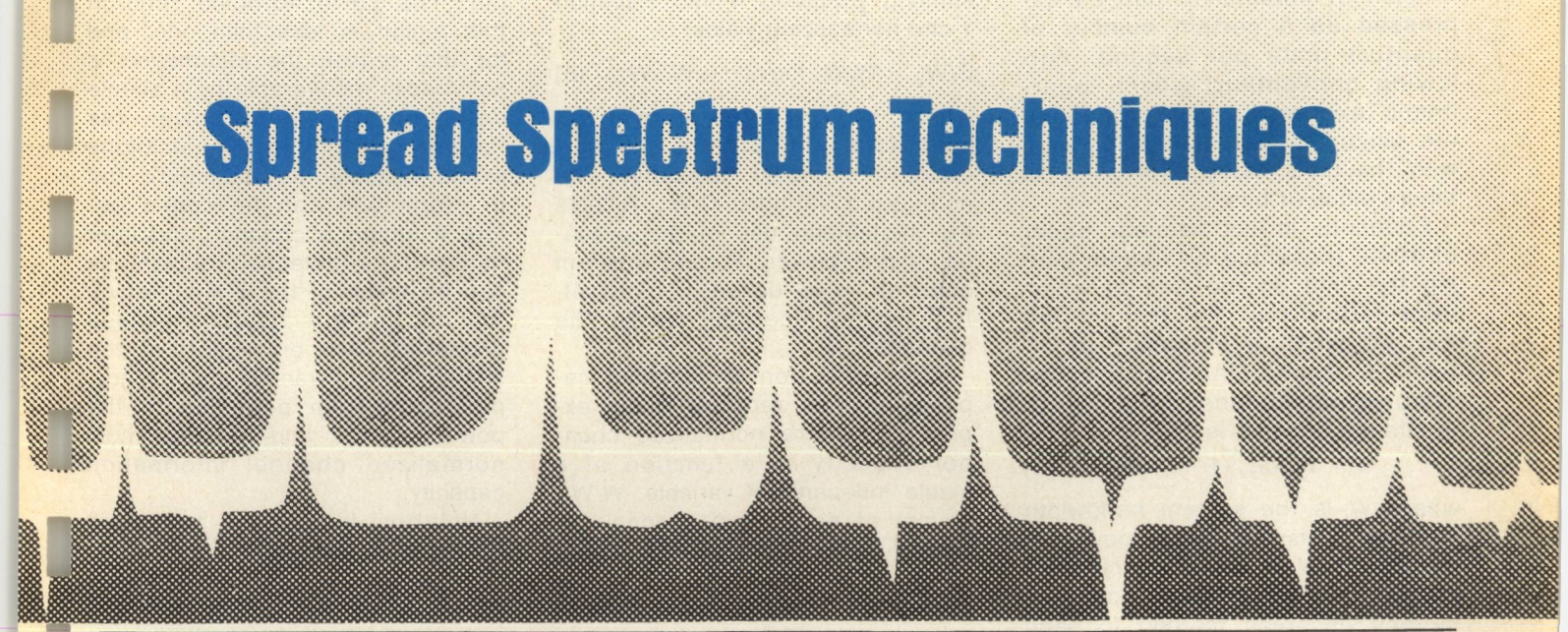

Spread Spectrum Techniques

Robert J. Moser
and
Gerard J. Gross
Locus, Inc.
State College, PA

Introduction and Background

Spread spectrum communications have, until recent years, been of principal interest to designers of special military systems and were often treated only in classified literature. Recently there has been a proliferation of interest in spread spectrum techniques for commercial, as well as military, applications. The following discussion is intended either to introduce the topic to those not already familiar with it, or to provide fresh insights for those who are already familiar with spread spectrum applications.

The following sections will review the theoretical background, as drawn from information theory, in order to identify the advantages of spread spectrum techniques. Then the implementation of a spread spectrum system will be described, followed by a discussion of applications, with special emphasis on one application of particular interest for commercial uses.

Many discussions of spread spectrum techniques begin with a definition of "spread spectrum", followed by a description of the four principal types of spread spectrum signals[1], with answers to the question, "Why spread spectrum?" left implicit. In contrast, the discussion here will begin with a consideration of some basic reasons for choosing spread spectrum techniques.

Traditionally, communication system designers have used frequency as a means to separate one communications channel from another. The art and science of developing frequency-stable sources, bandpass filters, and all the assorted modulation techniques needed to prevent interference of one channel with another is well-documented in the literature. Within a given frequency channel, high-signal power has always been associated with communication reliability. As the user population has increased, designers have sought methods for narrowing transmission bandwidths to accomodate more users within the existing spectrum, while maintaining high signal power for communications reliability. As noted by Costas, "this philosophy of spectrum usage is based on a particular course of development which the radio art happened to take, rather than on any fundamental physical principles."[2] The inherent communication capacity of the spectrum can be exploited in other ways, and spread spectrum represents one method of doing so.

Theory

In any communication system, the information rate is limited by three basic features of the communication channel: the inherent noise density within the channel, N_o (typically in units of watts/Hz), the channel bandwidth W (in Hz), and available signal power, P (in watts). In principle, considering the basic properties of information, it is possible to encode it into either the power or bandwidth intensive domain. Each domain exhibits properties which the communication system designer can

exploit to solve the problem of transferring information from the sender to the receiver with an arbitrarily small error rate.

In the discussion to follow, it is assumed that information content is quantified, and that rate of transmission of information can be expressed as a certain number of quantum units per second. Following convention, where logarithmic expressions of probability are used, the base two is chosen, with the units being expressed as binary digits or bits.

Shannon, in his seminar paper of 1949, presented a theorem stating the limit on the rate at which information can be transmitted with as small a frequency of errors as desired.[3] According to his Theorem 2, channel capacity, C, in bits per second, is given by

$$C = W \log_2 (1 + P/N), \qquad (1)$$

where W is the system bandwidth in hertz, P is the signal power in watts, and N is the channel noise power in watts. It is not possible by any encoding method to send at a higher rate and have an arbitrarily low frequency of errors. This theorem is shown to hold true for the worst case of white thermal noise, for which each amplitude distribution is Gaussian. Since C represents the theoretical limit on channel capacity, one can define an actual channel capacity, C_A, such that the closeness of C_A to C represents the goodness of encoding the signal to fit the channel statistics.

In Equation 1, the channel capacity is a function of three independent variables, W, P, and N. However, by proper normalization, this dependence can be essentially reduced to a single variable. The noise power can be expressed as:

$$N = N_0 W \qquad (2)$$

where N_0 and W were previously defined. The available signal power, P, and the channel noise density can also be used to define a new variable, W_0, such that

$$P = N_0 W_0 \text{ or } W_0 = P/N_0 \qquad (3)$$

where W_0 is the bandwidth which would yield a noise power equivalent to the signal power. Combining Equations 2 and 3, the signal power-to-noise ratio can be expressed as:

$$P/N = \frac{N_0 W_0}{N_0 W} = W_0/W. \qquad (4)$$

Thus, the power-to-noise ratio is equated to a bandwidth ratio. Substituting Equation 4 into Equation 1 and normalizing yields:

$$C/W_0 = W/W_0 \log_2 (1 + W_0/W), \qquad (5)$$

where W/W_0 is the normalized bandwidth, and C/W_0 is the normalized channel capacity. The normalized variable, C/W_0, reflects the systematic use of the available signal power, P, and inherent channel noise density, N_0, to effect communications within the channel.

The expression for channel capacity is now reduced to an expression where normalized channel capacity is a function of a single independent variable, W/W_0. A plot of normalized channel capacity versus normalized bandwidth (Equation 5) is shown in Figure 1. The channel power-to-noise ratio is also plotted on the same graph in order to aid in the interpretation of the expression.

Notice that the normalized channel capacity decreases rapidly as the normalized bandwidth, W/W_0, is reduced below unity. In this region of the graph, shown cross-hatched in Figure 1, the power-to-noise ratio is greater than one, and increases rapidly as normalized bandwidth, W/W_0, decreases. This is the region traditionally used for reliable power domain communications.

However, another region exists, $W/W_0 > 1$ (shown shaded in Figure 1), within which information can also be transmitted within a channel. The power-to-noise ratio in this region is less than one, and for that reason the information is not readily recoverable by a simple detection of signal power (as "power domain" communications would typically be detected). But if information can be coded before it enters a channel, and later decoded for detection, advantage can be taken of the $P/N < 1$ region for information transfer. These properties are protection of the signal from unwanted interference, protection from detection in the power domain, and near-maximum normalized channel information capacity.

Note that in Figure 1, to the left of the $W/W_0 = 1$, $C/W_0 = 1$ point, the curve of C/W_0 is strongly power-sensitive (small changes in W/W_0 relate to large changes in P/N), whereas to the right of this point, the curve is bandwidth-sensitive. The rationale for spread spectrum communications is to coherently convert the signal, before it enters the channel, from the power-intensive domain to the bandwidth-intensive domain to take advantage of the $P/N < 1$ region of Figure 1. At the receiving end, the bandwidth-spread

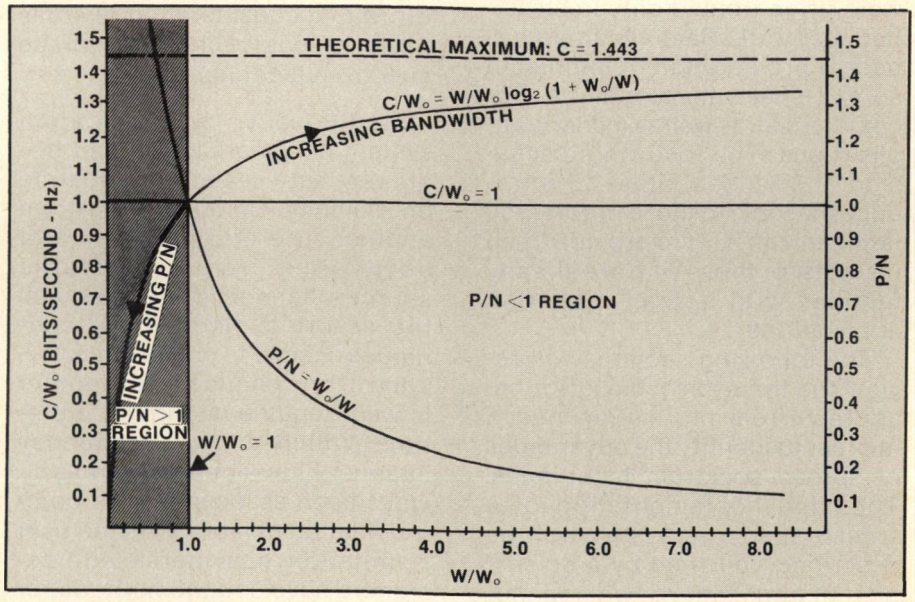

Fig. 1 Normalized channel capacity vs. normalized bandwidth.

signal is converted (correlated) back to the power domain and detected as a standard power domain signal.

From Figure 1, it can be observed that if the average signal power, P, and the noise-power density, N_o, are fixed, but the normalized bandwidth, W/W_o, is increased sufficiently, the normalized channel information capacity, C/W_o, becomes essentially independent of the normalized bandwidth. This constancy of normalized information capacity holds true even though the receiver noise power, N, is increasing (because of increasing bandwidth) and may greatly exceed the signal power. This effect is particularly significant for a system subjected to unwanted interference. The power necessary to interfere with a system designed for a wide-band, "spread spectrum", operation is in direct proportion to the system bandwidth. This concept, then, of spreading the information over a wide bandwidth in which incoherent noise exists, establishes the basis for the implementation of spread spectrum techniques.

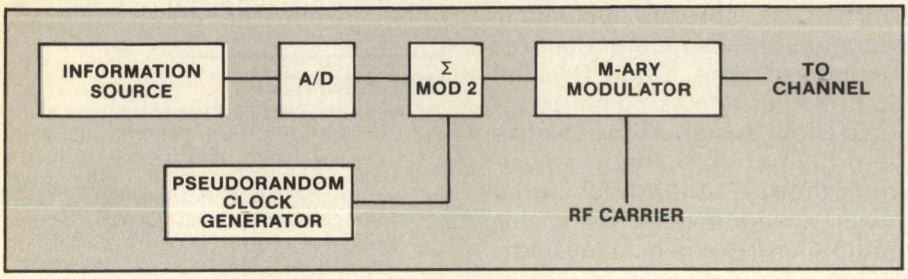

Fig. 2 Spread spectrum modulation system.

Spread Spectrum System Implementation

The term "spread spectrum" implies a technique in which the information is first converted to a digitized data stream. This data stream is then added to another bit stream which is pseudorandom in nature. The combined data is then used to modulate an RF carrier in either an M-ARY Frequency Shift Keyed (FSK) or Phase Shift Keyed (PSK) fashion. A simplified block diagram of the process is shown in Figure 2. The bandwidth of the pseudorandom clock generator is generally much wider than that associated with the data rate from the information source. Thus, the adding of the information data with the pseudorandom sequence greatly increases the signal bandwidth and determines the spectral characteristics of the resultant signal.

In a generic communication system, a low-frequency baseband signal is transferred to a higher frequency channel by a process called modulation. The low frequency information source changes or modifies a parameter of the high-frequency carrier. The three parameters that can be modified within the carrier are amplitude, frequency, or phase. Variations among these three parameters give rise to the many forms of modulation techniques. The three primary forms used for spread spectrum systems are PSK, FSK, and amplitude (pulse), or On-Off keying (OOK). In each of these modulation forms, the carrier is changed in discrete steps in an ordered set of M total states. Hence the term M-ARY modulation.

In spread spectrum communications, the type of modulation and its modification rate determine the type of spread spectrum involved. In the Direct Sequence Type, the carrier phase is usually shifted between the discrete values of 0° or 180° (bi-phase PSK). The shifting is in response to a single bit of the sum of the data stream and the pseudorandom clock generator. The resulting spectrum is shown in Figure 3. Quadraphase and higher-order direct sequence signals can also be generated.

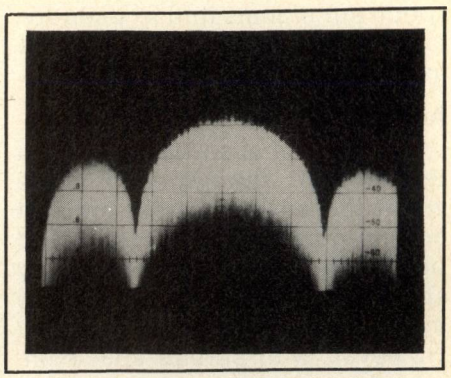

Fig. 3 Direct sequence, biphase PSK signal.

In the frequency hop form of spread spectrum, the sum bit of the data and the pseudorandom generator are assembled into an N-bit pseudorandom word. This N-bit word represents an instantaneous value of a variable between 0 and 2^N. The instantaneous value designates one of the 2^N frequency cells within the carrier frequency range. The resulting spectrum then appears as shown in Figure 4.

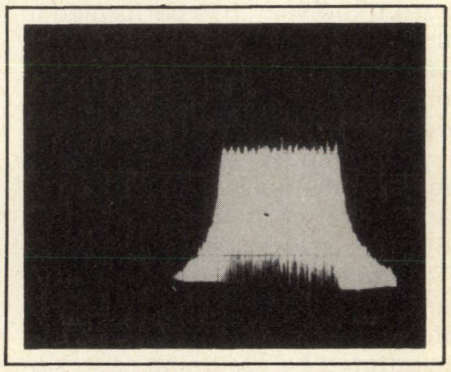

Fig. 4 FSK or frequency hop signal.

On-Off keying is a technique often used with PSK or FSK for hybrid spread spectrum modulation.

One other type of implementation, stacked carrier, is often classified with spread spectrum techniques. In the stacked carrier form of spread spectrum communications, numerous modulated carriers transmit the same information. The primary purpose of this method is transmission reliability. By transmitting the same information at numerous different carrier frequencies, the effects of selective fading, especially on the high frequency bands, are reduced. In the strict sense, stacked carrier signals differ from most spread

spectrum signals in that pseudorandom sequences are usually not used in generating the signals.

Applications and Advantages

The choice of spread spectrum techniques may appear strange when the assumed goal of most communication engineers would be to conserve the frequency spectrum, and certainly not to use many times the needed bandwidth. However, with spread spectrum, signal power requirements (power per unit bandwidth) are converted from the power domain to the frequency domain, and frequency bandwidth is used to perform the same function that signal power has performed in the past. Indeed, in most spread spectrum systems, the signal level within the channel is tens of dB below the channel noise. The detection of a signal on a power basis usually is impossible. Herein lies one of the principal advantages of the spread spectrum technique; that is, the probability of intercept approaches zero if the search is performed in the power domain. Thus, significant application of spread spectrum techniques is for secure communications.

Surprisingly, spread spectrum techniques solve a problem that at first glance they seem to create, that is, spectrum conservation. Traditionally, communication engineers try to keep signals within the radio frequency environment separated by assigning each signal to an allocated frequency slot. However, there are other ways to separate signals, or in the general case, information sources. Consider, for example, the difference between Frequency Division Multiplex (FDM) and Time Division Multiplex (TDM). In the former, each information source is assigned a preselected frequency slot. That source is kept there by carefully designing frequency filters, stable frequency sources, and associated analog frequency-dependent equipment that maintains the integrity of the frequency channel. In the latter, each information source, after being digitized, is assigned a time slot. The bits of the data are maintained in this time slot by carefully designing accurate timing sources (clock), and digital time-dependent circuits that maintain the integrity of the time channel. Note that in both of the above multiplexing techniques, the parameter that maintains the separation of the information source is different (frequency or time). Each of these parameters maintains the separation and integrity of an information source. Each can be considered a different dimension in the world of message space.

As a result of the spread spectrum techniques developed over the past twenty years, a third signal multiplexing technique can be identified, i.e., Code Division Multiplexing. In this technique, both time and frequency are utilized. Each information source is assigned a unique orthogonal code which, when added to the original source data, spreads this data in frequency and pseudorandomizes the data in time. Code Division Multiplexing allows communication system designers to actualize the potential of Shannon's existence theory of trading signal power for bandwidth. Using this multiplexing domain, many information channels can be established in the same frequency channel and, at the same time, without interference between channels. Code Division Multiplexing may be the most promising spread spectrum technique for commercial applications, because it allows implementation of a multiple access system in which many users can share the same channel in an unsynchronized way, with each user being assigned a different pseudorandom code.

The above discussion states several advantages of spread spectrum. In addition to these, the technique allows a processing gain (i.e., collapsing the received signal spectrum back to the original information source spectrum with a gain in signal-to-noise ratio), a high resistance to signal jamming on a power density basis, and an ability to maintain a communication path in the presence of selected fading (as with stacked carrier signals). This latter advantage is of importance in the sometimes fickle high frequency band.

Conclusion

Whereas in the past the high cost of equipment and difficulties in synchronizing pseudorandom codes limited the application of spread spectrum techniques, ongoing technology advances have reduced these limitations. Though processing requirements are complex, the development of inexpensive medium-scale and large-scale integrated circuits has made spread spectrum systems not only feasible, but economically attractive. High-speed digital logic techniques have allowed designers to cope with synchronization problems. Whether or not spread spectrum techniques will bring about a true revolution in communications, it seems certain that the technology will reach maturity and that a wide variety of military and commercial applications will be seen.

REFERENCES

1. See, for example, the Introduction to *Spread Spectrum Techniques*, Ed. Robert C. Dixon, IEEE Press, 1976, pp. 1-14; *Spread Spectrum Techniques Handbook*, W3 Office of Search, National Security Agency, Central Security Service, Report No. W3-057-79, Second Edition, March 1979; and John Oetting, "Spread Spectrum Communications," *Sea Technology*, May 1981, pp. 22-23.
2. Costas, J.P., "Poisson, Shannon, and the Radio Amateur," *Proc. IRE*, Vol. 47, December 1959, pp. 2058-2068.
3. Shannon, Claude E., "Communication in the Presence of Noise," *Proc. IRE*, Vol. 37, January 1949, pp. 10-21.

Gerard Gross, *has a combined background in physics and English, having received his B.S. in physics from Spring Hill College, Mobile, Alabama, in 1962, M.S. in physics from Case Institute of Technology, Cleveland, Ohio, in 1965, and Ph.D. in English from Case Western Reserve University in 1977. From 1965 to 1971 he was employed in the Nuclear Effects Department at The Aerospace Corporation, San Bernardino, California, and from 1974 to 1979 taught technical writing at the Pennsylvania State University. He is at present a Staff Physicist at LOCUS, INC., working on ESM receiver and simulation system development.*

Robert Moser, *received a B.S.E.E. from Gannon College in Erie, Pennsylvania, in 1964 and M.S. from The Pennsylvania State University in 1967. He is a licensed Professional Engineer in the state of Pennsylvania. From 1964 to 1970, he was employed at HRB-Singer, Inc. where he was engaged in advanced telemetry and digital systems. He joined LOCUS, INC. in 1972 and is a Staff Engineer involved in advanced concepts in communication technology.* ■

Broadband Fixture Characterizes any Packaged Microwave Transistor

Richard Q. Lane*
Roger D. Pollard#
Mario A. Maury, Jr.+
James K. Fitzpatrick~

Introduction

This article describes a universal transistor test fixture which has been designed to allow the maximum performance while still providing for the characterization of the greatest possible range of devices.

The fixture fills a need for some common basis on which to interchange high performance transistor data. At present, commercially available transistor test fixtures lack the facility to accomodate a wide range of package types, have limited frequency capability and do not provide the means for calibration to take full advantage of the error correction capabilities of the present generation of automatic network analyzers. Moreover, modern transistors exhibit exceptionally low noise and thus a very low-loss fixture is required in order to be able to measure noise figure accurately.

The present design is derived from a proven scheme[1], various versions of which are now in use in a number of laboratories.

*California Eastern Laboratories, Inc., 3005 Democracy Way, Santa Clara, CA 95050

#Hewlett-Packard Company, Santa Rosa, CA (on leave from the Department of Electrical and Electronic Engineering, The University of Leeds, Leeds LS2 9JT, England)

+Maury Microwave Corporation, 8610 Helms Avenue, Cucamonga, CA 91730

~Hewlett-Packard Company, 1400 Fountain Grove Parkway, Santa Rosa, CA 95404

The vast bulk of the applications of packaged microwave transistors are at frequencies below 18 Ghz. In addition, many of the uses of chip transistors in hybrid microcircuits necessitate the testing of a few chips from each batch; the sample devices being mounted in packages for this purpose. However the wide range of different package styles employed has meant that the majority of those users who wish to characterize their devices have designed their own test fixtures. Such diversity coupled with numerous individual measurement techniques make it difficult to obtain any concensus of the properties of a particular device type.

The major problem associated with the characterization of a transistor in a test fixture is that of extracting the true value of the transistor parameters from the measurement of the circuit in which it is necessarily connected. In most instances the measurement is made with an automatic network analyzer; the problem becomes one of calibration and can be considered as being that of finding a suitable set of known components ("standards") to enable the derivation of the elements of an error model and the correction of subsequent measurements.[2] The accuracy of the final results is directly related to the quality of the calibration devices

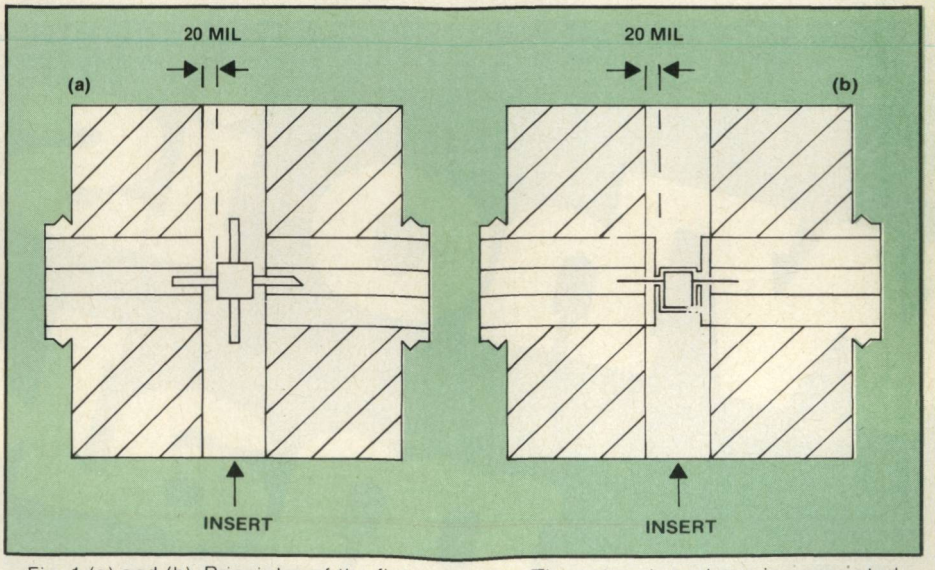

Fig. 1 (a) and (b) Principles of the fixture design. The network analyser is connected by means of 7mm lines. The transistor sits in an insert with the leads in cut-outs in the center conductor.

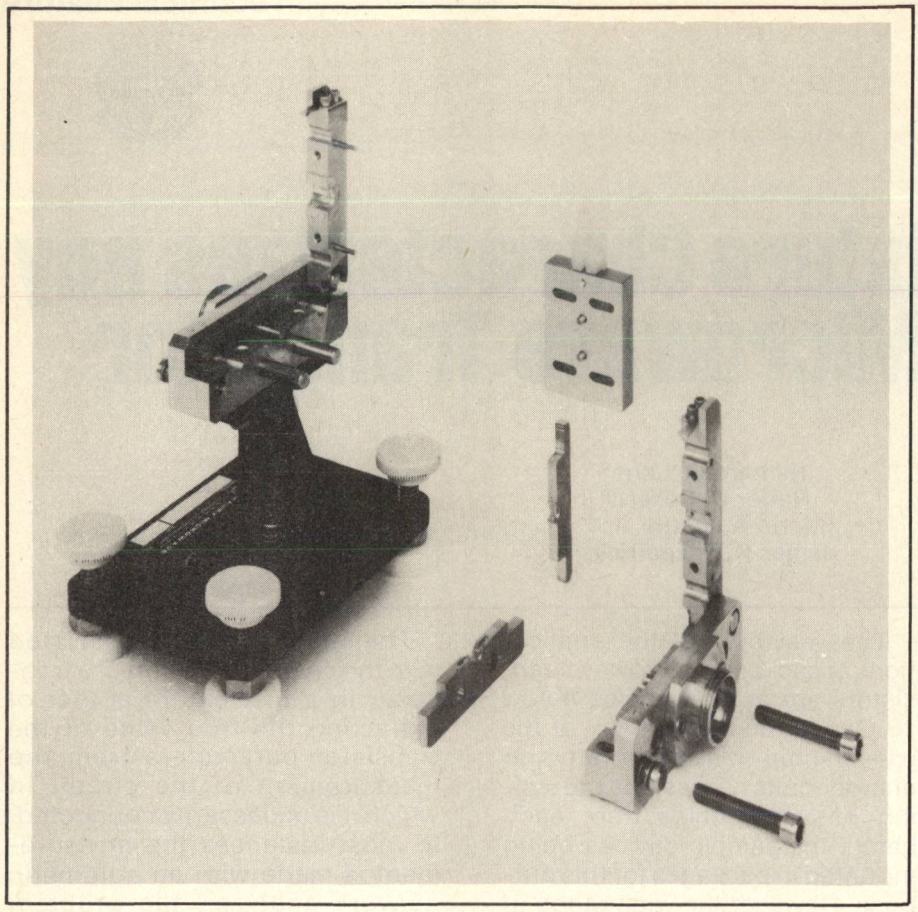

Fig. 2 The fixture dis-assembled to show the components. The insert is located between the two halves of the fixture body with dowel pins. The lid section supplies spring pressure to hold the halves in contact.

and, in general, precision calibration standards are only practicable where the predictability of a high quality connector provides a repeatable interface. The transition from the calibration medium (usually 7mm co-axial line at 50 ohms characteristic impedance) to the region in which the transistor package is located, creates a discontinuity which will render inaccurate any measurements based on a calibration carried out at the automatic network analyzer system reference plane connectors.

The transistor fixture described below employs removeable inserts to customize the structure for different package styles. The inserts are, however, relatively simple and can readily be fabricated to accomodate any transistor package. The major portion of the fixture is device-independent; it is co-axial with 7mm precision connectors and can be calibrated with high quality standards. The discontinuities associated with the presence of the insert are

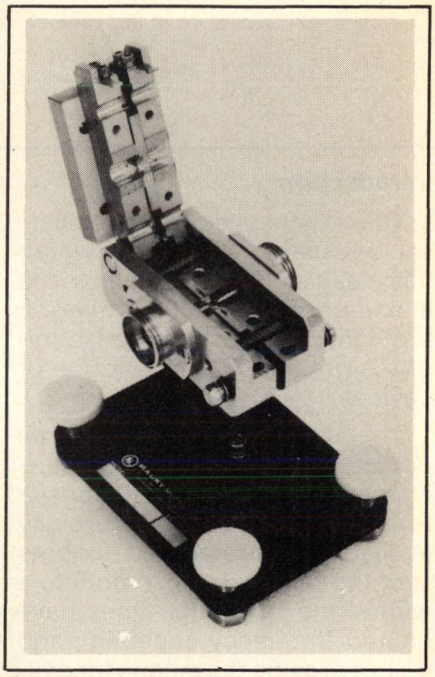

Fig. 3 The fixture assembled on stand with leveling screws to allow alignment with connector on ANA test set.

modelled by the elements of an equivalent circuit. The complete transistor characterization system comprises the fixture, a range of inserts, fixture calibration standards and a program enabling measurements to be made on a Hewlett-Packard 8409B/C automatic network analyzer. The software incorporates the element values characterizing the insert/fixture interface and de-embeds the S-parameters of the transistor itself. With the addition of a further set of calibration pieces, the users can determine for themselves the values for the elements modelling an insert for a particular transistor. In addition, provision is made for checking that the calibration procedure has been correctly carried out and that the de-embedding process is operating with the correct set of element values.

Mechanical Description

The basic principle of the configuration is shown in Figure 1. A 7mm co-axial line with a slot to accomodate the transistor lead is maintained up to the insert and the transistor package itself is located in a small rectangular cutout in a block of metal (the insert). In order to allow the insert to be changed, the fixture is assembled as a sandwich and is also split along the center line to allow insertion of the transistor to be tested. When the fixture is closed, the ground lead(s) from the transistor package, which are located

[Continued on page 101]

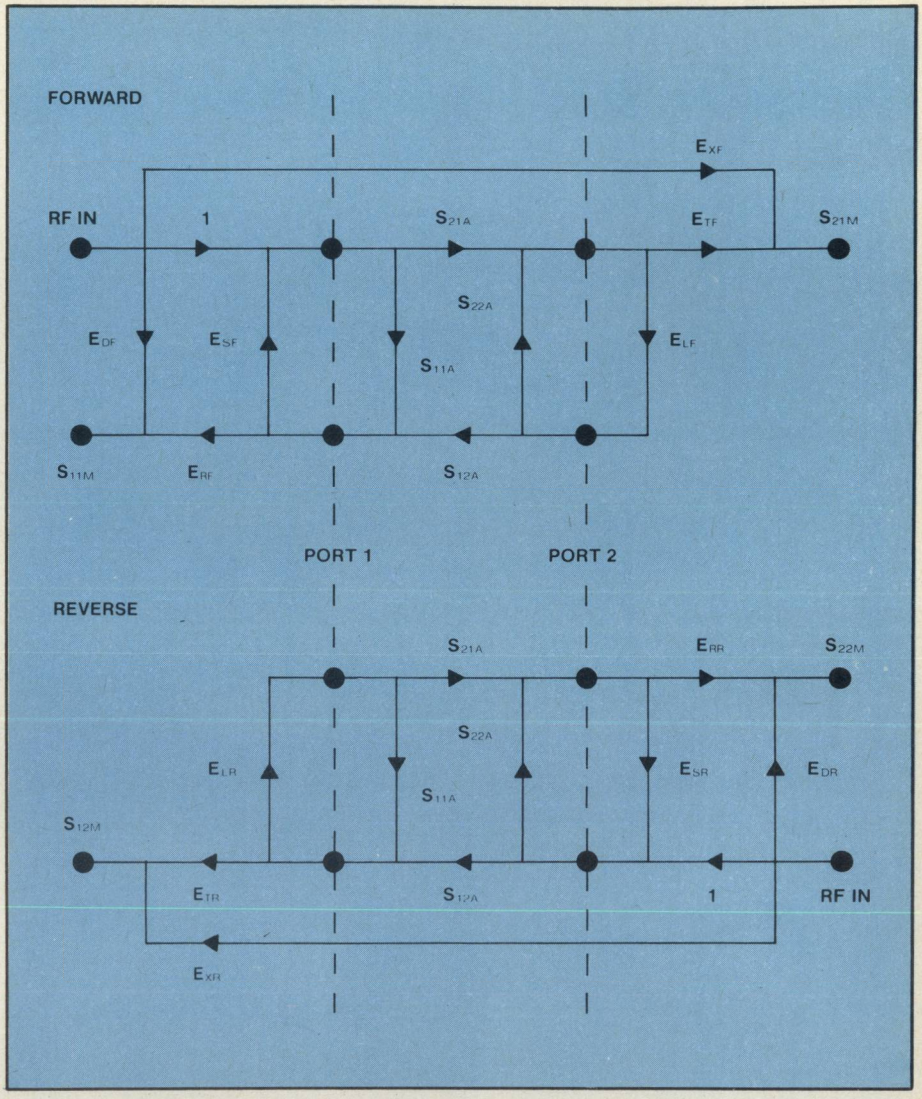

Fig. 4 Twelve term error model used for error correction on automatic network analyser measurements.

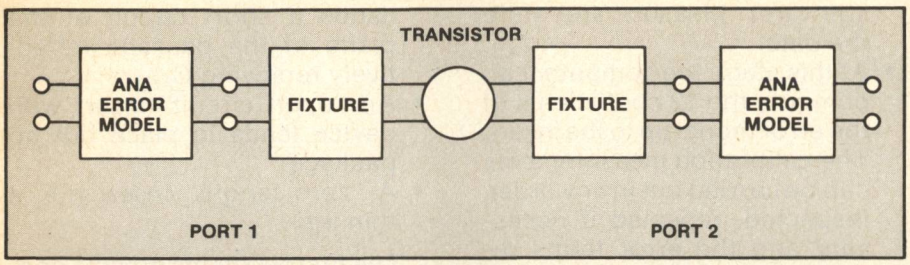

Fig. 5 Overall measurement circuit with transistor test fixture in place. The device to be measured must be de-embedded from two layers of test circuit.

in recesses which provide for repeatable positioning within the package tolerances, are captured between the two halves of the insert and this serves also to clamp the device in place. The device input and output leads are held in slots in the inner conductors of the 7mm lines by means of .04 inch Rexolite rods and a small lip ensures that contact is always made at the extreme front edge of the inner conductor.

Figure 2 is an exploded view of the fixture and indicates how it is assembled; the dowels ensure accurate alignment of the parts. Although constructed from four distinct parts, the fixture nonetheless assembles into a single complete unit with the top section functioning as a hinged lid which it sprung open by pressure on a pair of push buttons.

Figure 3 is a photograph of the complete fixture assembled on a stand equipped with levelling feet.

Calibration and Measurement

The use of a 12-term error model to describe the systematic errors in the measurement of the scattering parameters of a two port network on an automatic network analyzer[3] is now widely accepted by the microwave community. This model is shown in Figure 4 and the calibration of the system (i.e., the determination of the 12 error coefficients) requires that calibration devices be placed at the reference planes. In the case of a transistor fixture, the "device under test" is the transistor itself in spite of the fact that both the fixture and the transistor are connected between the calibrated ports. The measurement circuit is shown in Figure 5, where an additional network is interposed between the reference planes and the device under test. This network is the result of the transition between the co-axial line and the transistor insert and experience has shown that it can be modelled very successfully as the pi network shown in Figure 6. The values of the elements C_1, C_2 and L need to be evaluated for the insert for each different transistor package.

The automatic network analyzer calibration and measurement procedure is then as follows:

- Separate the fixture, remove the insert and connect the two halves to the analyzer using a return cable to link the second port.
- Connect precision 50 ohm loads to both halves (a "double load", constructed similar to an insert, is provided to make this operation easy); measure and store the directivity E_{DF} and E_{DR}.
- Connect a double short circuit between the two halves of the fixture; measure and store the data.
- Connect a double shielded open circuit between the two halves of the fixture; measure and store the data.
- Connect the two halves of the fixture together to establish a thru (a thru insert is provided to ensure repeatability; the electrical length and loss of this insert are accounted for in the

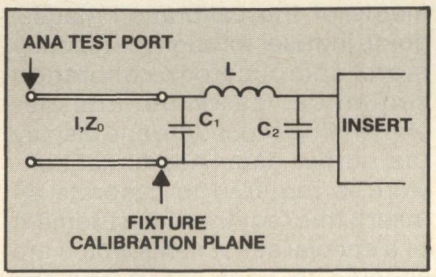

Fig. 6 Circuit model for the transition region between the fixture body and the transistor within the insert. The elements account for the change in dimensions and a short length of transistor lead.

[Continued on page 102]

software). Measure and store the data.

- At this stage the computer can compute the 12 coefficients of the error model up to the insert. The calibration measurements can be carried out in any order, inspected, repeated if necessary and the error terms recomputed.
- Assemble the fixture with the insert in place and notify the controlling program which insert is in use to ensure that the appropriate circuit is used to model the transition.
- Measure transistor packages provided as check devices and confirm that the results correspond to the data provided. If there are substantial differences, check the calibration data and the insert model used, then repeat some part or all of the calibration procedure.
- Open the fixture, drop the transistor into the slots, close the fixture.
- Turn on the bias supply and initiate the measurement. The transistor S-parameters will be de-embedded from the fixture after the data has been error corrected.
- The results may be printed, plotted, etc. as required.

A significant advantage of the calibration scheme is that dummy packages are not employed. It is therefore possible to use transistor packages either empty or containing passive networks as check devices.

The software is an enhanced version of the programs currently used to control the Hewlett-Packard 8409 series of automatic network analyzers with additions to store the individual measurements of the calibration stages, guide the user through the (slightly more complicated) calibration sequence, carry out the de-embedding procedure and display the output data. Additional software is required to calibrate an insert; this requires measurement of a special set of items which are specific to each insert and the calculation of the element values of the transition model. The insert calibration devices comprise:

- A shorting piece which establishes a short circuit at the plane of the package (effectively removing C_2).
- An "open circuit" insert with device leads in place but no package.
- A "zero length" insert (i.e. a thin iris).

The first two items provide one-port data, the third provides two-port data which can be used to derive the three element value for the pi network. The frequency variation of the data provides enough information to check on the validity of the model.

Conclusions

In figure 7, we show some S-parameter data for an NEC NE70083 0.5 micron gate gallium arsenide MESFET. The data appears smooth and well behaved, with S_{21} falling at about 6dB per octave with increasing frequency. The data taken with the fixture has been very consistent and yields good results which are repeatable at different times and locations.

The fixture is also well suited to measurements of noise parameters and load pull. In these applications the fixture model is applied to embed the device in the overall test circuit.

The fixture will be available from Maury Microwave Corporation as model MT950 and Hewlett-Packard expects to have the complete software (for the 8409B and 8409C ANAs only) available as a product in early 1983. In addition, Maury Microwave plans to expand its offering of inserts to cover all the popular transistor package styles.

From the description of the characterization problem and the solution discussed here (especially the calibration process), it becomes apparent that meaningful, repeatable transistor measurements only become practicable when the power of an automatic network analyzer is employed. The entire fixture development program was undertaken with the assumption that ANA error correction routines would be applied.

Acknowledgements

A project of this nature, encompassing a range of disciplines could not be completed without

[Continued on page 104]

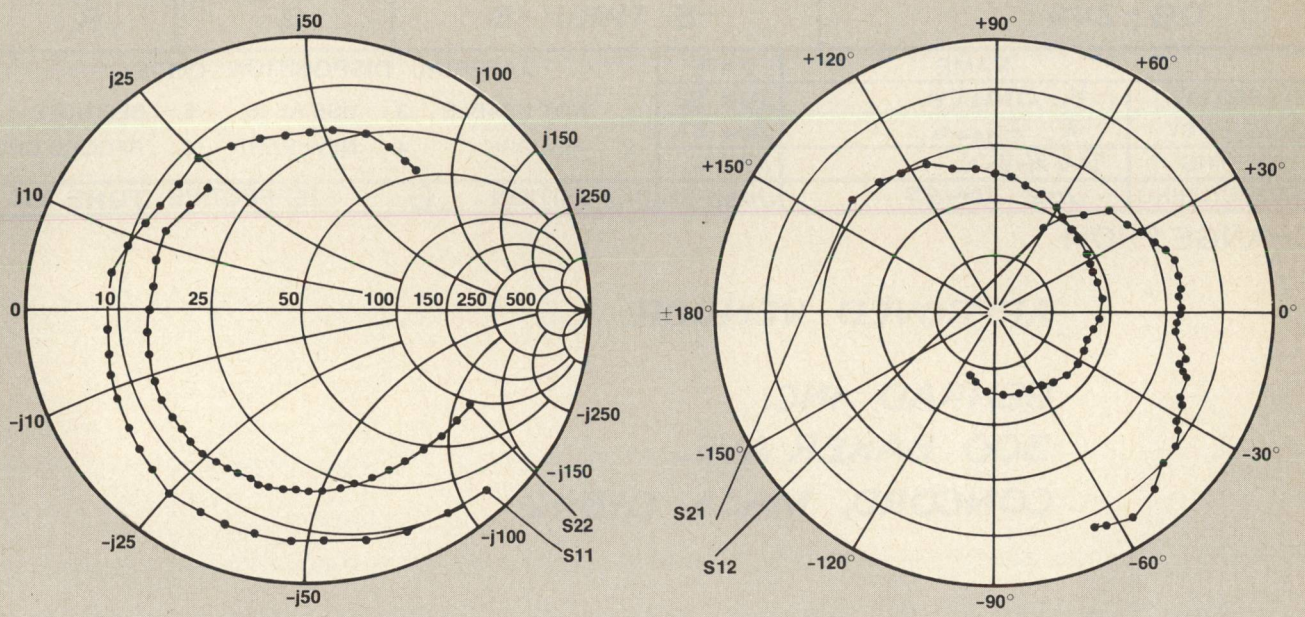

NE 70083 #111 @ 3V 10mA
S21: 5.00 full scale, S12: 0.10 full scale, 2.00 to 18.00 by 0.50 GHz

S-MAGN AND PHASE — Cma=Cms if k less than 1

FREQUENCY (MHz)	S11		S21		S12		S22		k	Gma dB
2000	0.952	-44	3.206	140	0.036	50	0.713	-29	0.23	19.5
2500	0.925	-54	3.110	129	0.043	54	0.705	-36	0.30	18.6
3000	0.908	-64	3.004	122	0.049	47	0.696	-43	0.33	17.9
3500	0.886	-73	2.951	113	0.056	42	0.691	-49	0.35	17.2
4000	0.855	-83	2.731	104	0.058	33	0.678	-56	0.47	16.7
4500	0.850	-91	2.648	96	0.061	29	0.677	-61	0.48	16.4
5000	0.835	-99	2.558	88	0.064	24	0.674	-66	0.51	16.0
5500	0.827	-107	2.520	81	0.066	20	0.674	-72	0.50	15.8
6000	0.813	-114	2.421	75	0.068	16	0.674	-76	0.53	15.5
6500	0.807	-123	2.364	67	0.068	11	0.677	-82	0.54	15.4
7000	0.774	-130	2.261	59	0.068	7	0.673	-86	0.67	15.2
7500	0.753	-137	2.165	54	0.067	5	0.667	-90	0.76	15.1
8000	0.733	-143	2.104	46	0.068	1	0.664	-94	0.85	14.9
8500	0.709	-152	2.070	41	0.067	-1	0.660	-98	0.91	14.9
9000	0.697	-160	2.031	32	0.067	-4	0.658	-102	1.00	14.8
9500	0.675	-166	1.990	27	0.067	-5	0.642	-104	1.11	12.7
10000	0.664	-174	1.976	22	0.067	-6	0.631	-109	1.13	12.5
10500	0.660	178	1.989	16	0.067	-6	0.634	-112	1.09	12.9
11000	0.660	168	2.019	7	0.069	-11	0.628	-117	1.05	13.2
11500	0.633	158	1.940	-3	0.071	-14	0.626	-122	1.15	12.0
12000	0.613	149	1.864	-10	0.069	-15	0.616	-127	1.30	11.0
12500	0.603	141	1.783	-16	0.072	-18	0.601	-132	1.39	10.2
13000	0.611	131	1.803	-22	0.074	-19	0.591	-138	1.30	10.6
13500	0.645	121	1.824	-31	0.075	-25	0.584	-144	1.16	11.4
14000	0.633	110	1.783	-40	0.076	-26	0.569	-151	1.24	10.8
14500	0.634	100	1.700	-48	0.078	-31	0.546	-162	1.33	10.0
15000	0.636	92	1.638	-55	0.080	-33	0.533	-171	1.37	9.5
15500	0.651	85	1.584	-63	0.082	-37	0.511	-179	1.37	9.2
16000	0.670	78	1.572	-71	0.082	-42	0.511	171	1.30	9.5
16500	0.693	68	1.540	-81	0.087	-48	0.524	-160	1.10	10.5
17000	0.684	60	1.464	-92	0.091	-56	0.540	148	1.12	10.0
17500	0.673	54	1.302	-102	0.088	-63	0.531	136	1.41	7.9
18000	0.666	50	1.212	-107	0.087	-65	0.538	124	1.58	7.0

Fig. 7 S-parameters of a GaAs FET measured in the test fixture after de-embedding.

[Continued on page 106]

the contributions of many people. Those who have made substantial contributions to the production model fixture include Julius Botka, Sy Ramsey (H-P), Marc Maury, Carol Fuchs (Maury Microwave), Gary McCollum and Fred Oey (CEL).

APPENDIX

Insert Calibration

In order to derive element values for the pi-network used to model the transition between the fixture body and the insert, it is necessary to employ a set of known devices. In principle, since three unknown quantities are required, three independent measurements are sufficient to determine them. The principles of a technique employing three devices is shown in the diagram with the resulting circuit models. It is assumed that the fixture calibration is carried and that the network analyser is therefore measuring at the plane of the end of the fixture body.

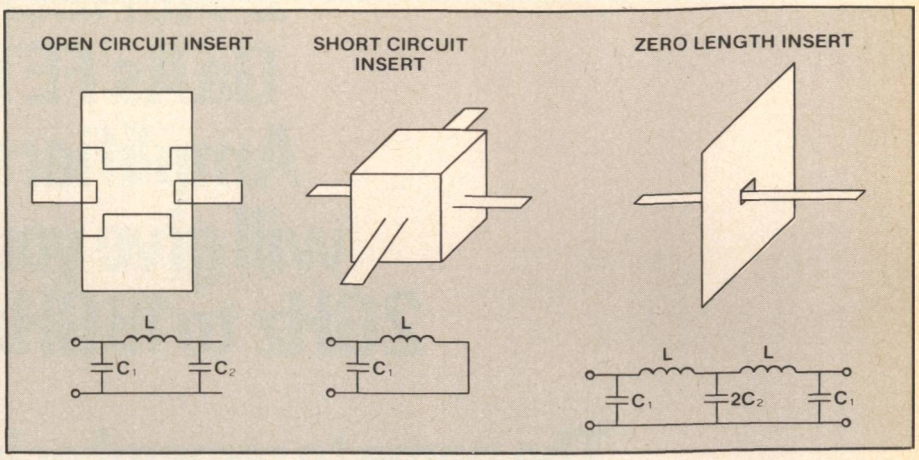

Measurement with the short circuited insert gives an impedance

$$Z_1 = \frac{j\omega L}{1 - \omega^2 L C_1}$$

which exhibits a single shunt resonance at frequency

$$f_1 = \frac{1}{2\pi\sqrt{LC_1}}$$

The open circuited insert yields

$$Z_2 = \frac{1 - \omega^2 L C_2}{j\omega(C_1 + C_2 - \omega^2 L C_1 C_2)}$$

which has a series resonance at frequency

$$f_2 = \frac{1}{2\pi\sqrt{LC_2}}$$

and a shunt resonance when

$$f_3 = \frac{1}{2\pi\sqrt{LC_t}}$$

where $C_t = C_1C_2/(C_1+C_2)$, the series combination of the two capacitors.

These three resonant frequencies, however, are not sufficient to determine the required parameters. Also, the values of L, C_1 and C_2 are small in most circumstances and the resonant frequencies may not be in the measurement band. The measurements as a function of frequency can therefore be used to establish values for the parameters by extrapolation and these values used as starting points for curve fitting to the additional set of data obtained by measurements on the thru connection. The data taken on the thru should exhibit two of the resonances of the simpler arrangements as well as identifiable transmission properties.

The frequency dependence of the circuit can be used both to confirm the validity of the model for the particular insert configuration in use as well as to enhance the accuracy of the parameters obtained from the calculations on the data.

REFERENCES

1. Lane, R.Q. and G.L. McCollum, "A New

[Continued on page 109]

[From page 106] **MICROWAVE TRANSISTOR**

Self-Calibrating Transistor Test Fixture", IEEE MTT-S Symposium Digest, June 1979.

2. Hewlett-Packard Co., "Automating the 8410B Microwave Network Analyser", Application Note 221A, June 1980.
3. Fitzpatrick, J., "Error Models for Systems Measurement", Microwave Journal, May 1978.

Richard Q. Lane, *born in Melbourne, Australia on June 13, 1928, received the Higher National Certificate in electrical engineering from Derby Technical College, Derby, England in 1953. He joined Fairchild Camera and Instrument Corporation in 1960, later transferring to their Research and Development Laboratory. In April, 1975, he joined California Eastern Laboratories where he is Senior Staff Engineer concerned with Microwave Measurement Techniques including CAT and CAD. Mr. Lane has authored and co-authored numerous papers on circuit design and fixturing. He is a member of the Institution of Electrical Engineers [London].*

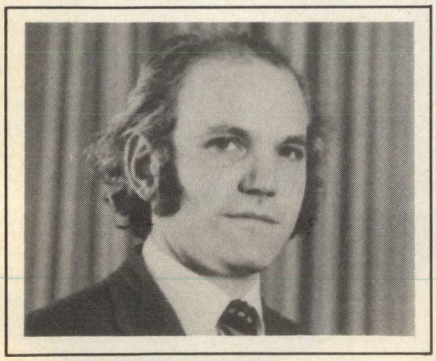

Roger D. Pollard *was born in London, England in 1946. He received his technical education, graduating with the degrees of B.Sc. and Ph.D. in Electrical and Electronic Engineering, at the University of Leeds in England.*

He is currently a Lecturer in the Department of Electrical and Electronic Engineering in the University of Leeds where he has been engaged in research on topics connected with microwave solid-state devices and circuits for some 10 years. Experience has included work on microwave transistor circuits, two-terminal negative resistance devices and the use of automated techniques for the measurement of the parameters of active devices and circuits.

He has acted as consultant to various organizations and is presently working at Hewlett-Packard, Santa Rosa, CA during periods of leave from the University of Leeds. Dr. Pollard is a member of the Institution of Electrical Engineers [U.K.], the Institute of Physics [U.K.] and the I.E.E.E.

Mario A. Maury, Jr. *is President of Maury Microwave Corporation, Cucamonga, California [which is celebrating its 25th anniversary in 1982]. He has been actively engaged in Automated Microwave Measurements for the past 15 years, particularly in the creation of calibration standards for Automatic Network Analyzers. He is currently chairman of the Executive Committee of the Automatic R. F. Techniques Group [ARFTG] and chairman of the Technical Committee on Automatic Measurements [MTT-12] of Microwave Theory and Techniques Society [MTTS].*

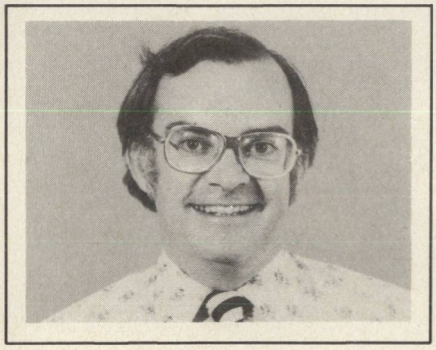

Jim Fitzpatrick, *is product manager for Microwave Network Analyzers in Hewlett Packard's Network Measurement Division in Santa Rosa, CA.*

At HP since 1972, he has been responsible for the marketing and development of the HP 8409 family of network analyzers. He was involved in software design for the HP 8507 systems and the HP 8542B.

From 1969 thru 1972 Jim was Executive Vice President and Engineering Manager of Computer-Metrics, Rochelle Park, NJ, co-founder of this microwave measurement service bureau.

From 1966 thru 1969 he was a Field Engineer/Account Manager for HP in New Jersey.

His first six years after B.E.E. in 1969 from Manhattan College were spent in microwave design at ITT Federal Laboratories in Nutley, N.J., Budelman Electronics in Stamford, Conn., and Western Union's Radio Research Division in New York.

Design accomplishments included the local oscillator/Beacon of INTELSAT III, the first FCC type-accepted GHz solid-state transmitter and other solid-state amplifiers, multipliers and mixers used in both ground and space communications. ■

Transform Receivers for ECM Applications

Daniel Nichols

Senior Engineer
Electronic Warfare Division
Westinghouse Electric Corporation
Baltimore, Maryland

This paper gives an overview of the theory of operation and performance characteristics for compressive and acousto-optical receivers. Included are simplified block diagrams, input/output relationships, processing element technology, data interface, and typical ranges of bandwidth and data rates. Key performance requirements for Radar Warning and ECM are compared showing the features which make these receiver types powerful tools for future systems.

Introduction

The density of the electromagnetic signal environment during postulated hostilities has been increasing rapidly. Emitters with agile characteristics have also become a reality. The result has been a need to improve ESM signal acquisition capabilities. Receivers of wide instantaneous RF bandwidth, coupled to powerful processing algorithms, are required to maintain short-acquisition times in the environment. The wide instantaneous bandwidth receiver also increases the probability of intercept (POI) on emitters which illuminate the platform with low duty cycles. However, as bandwidth increases in such an environment, so also does the probability that two or more signals will exist simultaneously within the receiver. To maintain good acquisition performance on each of these signals, the receiving system should be capable of encoding frequency and time of arrival of all such simultaneous signals.

Driven by these requirements, the trend in ESM receivers for Radar Warning ECM systems of the future is to replace the familiar crystal video, superheterodyne, and IFM receivers of today by receivers which are capable of processing simultaneous signals over wide instantaneous RF bandwidths. Foremost among these are the compressive and acousto-optical receivers.

This paper presents an overview of the operating principles of these receiver types and compares performance with critical ESM requirements to show the applicability of these devices to the Radar Warning and ECM role.

Receiver Requirements

Electronic Support Measures (ESM) is defined as: "The actions to search for, intercept, locate, and immediately identify radiated electromagnetic energy for the

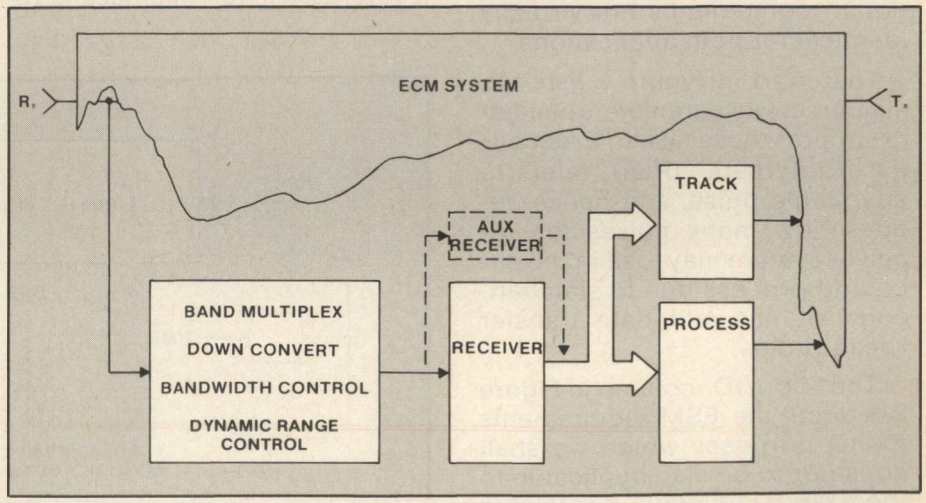

Fig. 1 General ECM block diagram showing receiver functions.

ECM RECEIVING SYSTEM REQUIREMENTS			
	Sort/ID	Analysis	Track
	ESM		
Instantaneous BW	300-3000	300	30 MHz
Freq Resolution	5-10	1-2	1 MHz
TOA Resolution	500	50	50 nsec
Prob of Intercept	90	99	90%

Fig. 2 (U) ECM receiving requirements.

purpose of immediate threat recognition".[1]

This definition is applicable not only to the modern Radar Warning Receiver (RWR), but to that portion of the power management ECM system which is associated with the identification of emitters for jamming purposes.

Figure 1 is a generalized block diagram of a typical power management ECM system. The RF spectrum is divided into bands, which are down converted and time multiplexed into a common Intermediate Frequency (IF) base band. The receiving function is thereafter performed within the base band frequency range.

Often no single receiver can adequately support all of these tasks, and an auxiliary receiver, as shown in Figure 1, must be used to supplement the receiver function. The ECM receiver must support three distinct tasks; signal identification, signal parameter extraction, analysis, and signal tracking. The signal identification function is essentially the same for ECM or Radar Warning systems, and hence the receiver functional requirements are virtually identical for both applications.

The chart in Figure 2 lists the major receiver parameters needed to support these tasks. "Probability of intercept" (POI), refers to any single pulse, and hence defines how many pulses the receiver system may lose in the encoding process due to simultaneous signals and data transfer "dead" times.

The "Sort/ID" column in Figure 2 reflects the ESM requirements for ID purposes which we shall consider to be also applicable to the RWR ID function. It is toward this wideband, coarser resolution application that this paper is primarily directed.

— Time Domain Receivers

There are several types of receivers presently in general use for ESM applications. These include the crystal video, superheterodyne instantaneous frequency measurement (IFM) and channelized receivers. These receivers operate in the time domain, that is, the primary receiver output is a video pulse which is representative of the time-of-arrival of the input pulse. If measured, the signal frequency information is usually a digital word which is time coincident with the video pulse.

— Frequency Domain Receiver

In recent years the development of surface acoustic wave and laser technology have made possible the practical implementation of the frequency domain receiver. As shown in Figure 3, this receiver produces an output much like a spectrum analyzer output, which is essentially the envelope of the Fourier transform of the input signal. These receiver types are the compressive (or microscan) receiver and the acousto-optical (A-O) receiver.

— The Compressive Receiver

It can be shown[6,25] through a rearrangement of the classical Fourier transform, called the chirp transform, that the mathematical Fourier transform F(w) of an input signal F(t) has an exact electrical equivalent.

This electrical implementation requires three operations: First, the input signal is multiplied by a chirp reference signal, i.e., a signal which exhibits a frequency variation that is a linear function of time. Secondly, the resultant product is convolved in a dispersive delay line which, when properly matched to the chirp characteristics, produces an output signal with an envelope that corresponds to the Fourier transform of the input signal. Thirdly, a multiplication by a second chirp signal will remove the phase distortion introduced by the first chirp multiplication.

In spectral analysis applications, such as radar ESM, the second chirp multiplication is usually omitted since the desired information is the envelope of the Fourier transform. Such a receiver mechanization, shown in simplified form in Figure 4, consists of a mixer using a chirp local oscillator signal, a SAW dispersive delay line, appropriate detection circuitry and data interface.

When an input signal at any given frequency within the receiver passband is mixed with the chirp local oscillator, the resultant IF

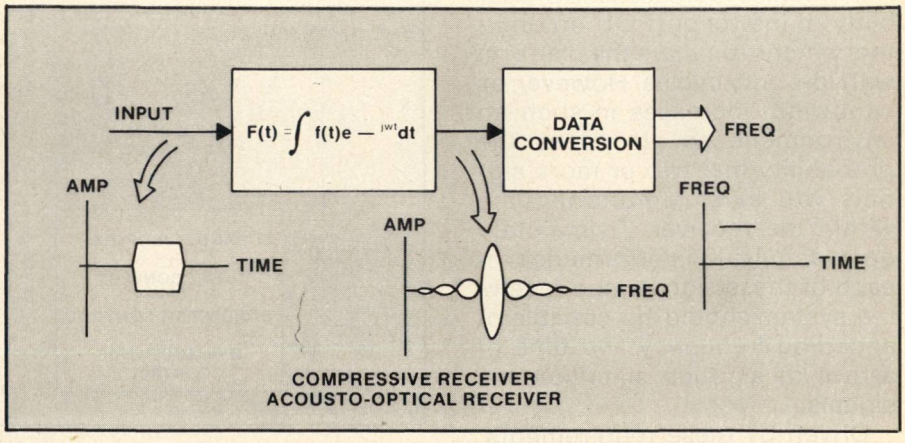

Fig. 3 The transformer receiver. Data is converted into a frequency.

[Continued on page 116]

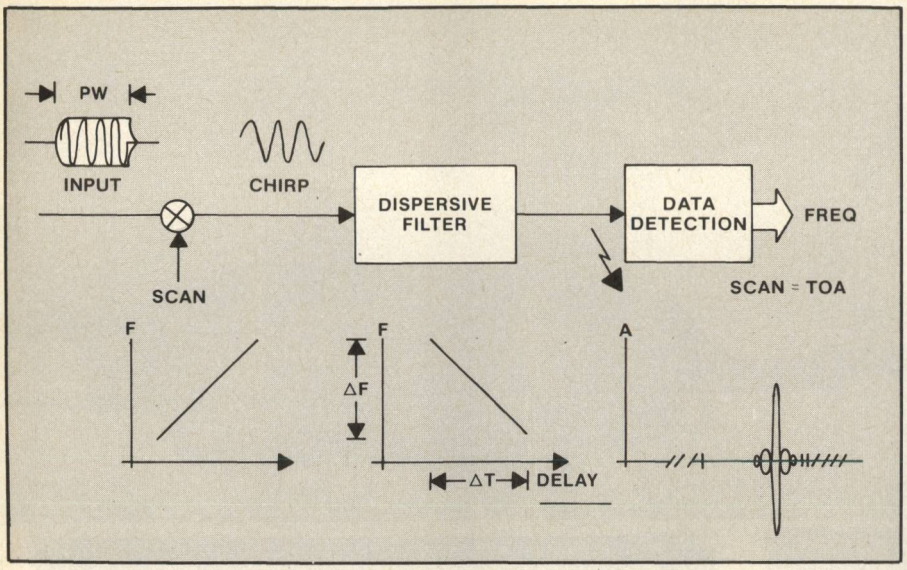

Fig. 4 The compressive receiver block diagram.

signal also has a chirp frequency characteristic.

The dispersive delay line varies with input frequency. This dispersion characteristic, T/F is such that the chirp IF frequency components which enter the delay line first experience a greater time delay within the dispersive filter than do the subsequent input frequency components. The result is that all components of the chirp input signal tend to arrive at the output of the delay line at the same time. For example, a CW would produce an impulse at the output, corresponding to the Fourier transform of a constant signal.

In practical circumstances the chirp scan is limited in time duration and the input is gated to the receiver only during the local oscillator scan time. Thus the output for a CW input corresponds to the Fourier transform of a gated pulse of duration equal to the scan.

The local oscillator scan is often derived by applying an input pulse to a second matched delay line to produce chirp scan by inverse Fourier transformation. In this way, a chirp of correct characteristics can be easily implemented within the close tolerances associated with the lithographic processes of SAW fabrication.

The compressive receiver displays excellent spurious signal rejection. Because the output is of frequency-versus-time format, out-of-band signals, which may enter the receiver on the edge of the input filter selectivity response, appear at the output separated in time from the desired signals. These spurious, appearing in the "slash"-marked areas of Figure 4 may be effectively rejected by time gating. Mixer image rejection is also excellent since these inputs are inversely chirped at the delay line input and are thus spread instead of being compressed.

— Delay Line Technology

Dispersive delay lines are usually compared on a basis of their time-bandwidth product, that is, the total linear time dispersion times the RF bandwidth. Receiver performance, however, must trade-off between these parameters, with large dispersion time giving better frequency resolution, and large bandwidth being required to obtain wide receiver bandwidth.

For wide band pulse applications, the current practical limit on receiver bandwidth is currently set by limitations in digital output circuitry and not available delay line bandwidth[11].

Delay lines for compressive receivers of wide instantaneous bandwidth are summarized in Figure 5. Usually, dispersive delay lines employ SAW propagation. Dispersive characteristics are obtained either by design of the interdigital transducers (IDT) or by reflective array compressor (RAC) design[6 7]. Recently, delay lines have been fabricated using Magnetostatic surface wave (MSW) propagation.

The IDT delay line obtains dispersion through the geometric arrangement of the input and output transducers on the substrate. This technique produces delay lines of wide bandwidth and short time dispersion.

IDT delay lines depend upon lithographic reproduction of transducer patterns on the substrate; whereas RAC delay lines employ etching processes to generate the dispersion characteristics. For this reason, IDT delay lines usually display better production uniformity (than RAC devices), necessary for matching delay line characteristics.

Experimental delay lines have been fabricated using magnetostatic surface wave propagation on substrates of Yttrium-iron garnet (YIG) material[4 5]. Devices using this mechanism can operate at higher frequencies and hence are capable of larger instantaneous bandwidth. With short time dispersion, they may potentially increase the bandwidth of pulse receivers for spectral (ESM) analysis.

— Compression Receiver Operation

Figure 6 depicts a typical compressive receiver. In such a mechanization the local oscillator would scan over a frequency range equal to one-half the delay line bandwidth (F/2). If the input bandwidth (BW) is also limited to one-half the delay line bandwidth, all input signals will produce chirp IF signals within the delay line passband, F. The local oscillator scanning at a rate F/T would therefore require T/2 (microseconds) to scan.

Usually the local oscillator scan is operated at a 50 percent duty cycle. This allows for sufficient time for data processing, scan flyback etc. Time gating the input and local oscillator usually accompanies such operation.

In Figure 6, the operational sequence is shown in some detail. Two input signals, F_1 and F_2 exist simultaneously at the input within the receiver bandwidth (BW) during the scan time, t. Signals at the

[Continued on page 118]

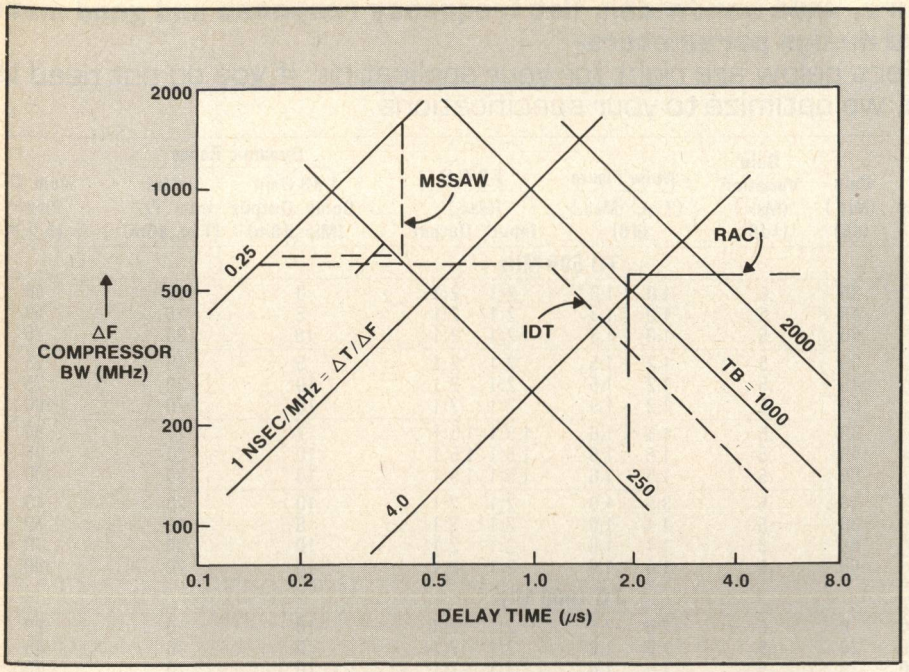

Fig. 5 Dispersive delay line technology.

input are time-gated into the receiver during the scan. The compressed signals appear at the dispersive filter output with the (different) time delay associated with each input frequency.

The receiver in Figure 6, working at 50% duty cycle will have a 100% POI for signals of pulse width greater than 2t (scan time (t) plus the processing dead time). For pulses shorter than t, the POI equals the duty cycle (50%). In order to achieve a receiver of 100% POI for very narrow pulses, dual receiver channels are mechanized. In the dual channel compressive receiver a second identical channel will scan the environment during the recycle time for the first, thus even short pulses will be intercepted.

For input signals of pulse width (PW) less than the receiver gate time, the compressed (sin x)/x pulse will be 1/PW (hertz) wide; corresponding to the Fourier transform of the input pulse[8]. Multiplication by the dispersion characteristic, T/F yields the time duration of the output pulse.

CW or long pulse signals are gated by the receiver scan gate t, and thus appear at the filter input as pulse of width t, and chirp equal to the receiver bandwidth (BW). At the output, the compressed pulse will have a (sin x)/x response with 3 dB bandwidth of 1/t, and a time duration of 1/BW.

The (sin x)/x response of a square pulse has first order sidelobes which are 13.5 dB down and which fall off at 20 dB per decade. In the compressive receiver the sidelobes are often suppressed using Taylor amplitude weighting techniques to enhance separation and detection of signals which are close together in frequency. These techniques allow detection dynamic ranges of 35 dB for closely spaced signals to be achieved, increasing ultimately to 50 dB as signal separation increases. Such weighting techniques do however, increase the width of the compressed pulse by a ratio of approximately 1.5:1[9].

Compressed pulse (3 dB BW) — 1.5/PW (1)

Compressed pulse (time duration) — (1.5/PW) X (T/F) (2)

— Frequency Resolution

The minimum compressed pulse width will occur for the longest pulse processed. Since the input gating limits processed pulse width to the scan time for CW or long pulses, the minimum bandwidth of the compressed pulse by equation 1 would be approximately 1.5/scan time. Equation 2 determines the duration of this pulse as (1.5/scan) x (T/F). For pulses shorter than the scan time, the compressed pulse is of longer time duration.

— Compression Gain

The input exeriences a compression gain within the dispersive delay line due to the effective integration of the pulse energy. The gain is equal to the integration time (PW) times the chirp frequency change (PW x (PW (F/T)).

Compression gain =
$10 \log [PW^2(F/T)]$ (3)

Signals of equal amplitude but which have different pulse widths at the input, will generate compressed output pulses which differ in amplitude by the square of the ratio of the pulse widths. If the

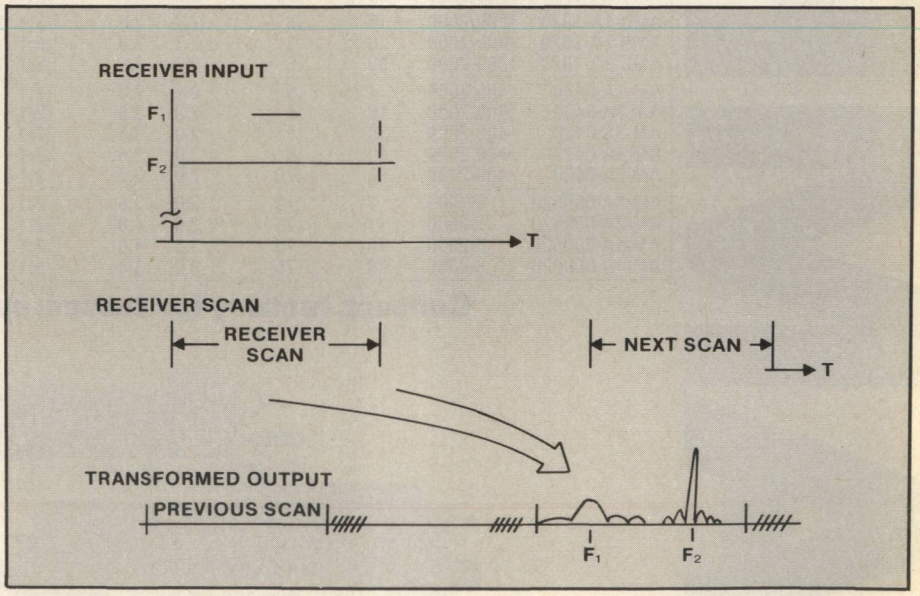

Fig. 6 Example compressive receiver operation.

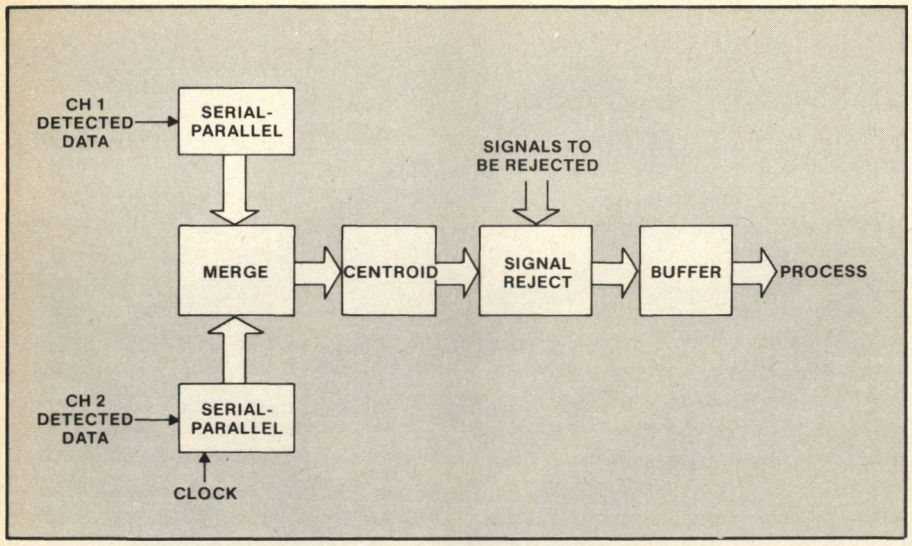

Fig. 7 Dual compressive receiver interface.

minimum expected pulse width (MINPW) is less than the maximum pulse width set by the scan time gate, the output dynamic range will be greater than the input dynamic range.

Output Dynamic Range = Input Dynamic Range + 20 log (MINPW/SCAN) (4)

From the equation 4, it follows that, for compressive receivers intended for short pulse detection the compressive receiver scan should be kept short. This requirement, in turn demands a trade-off of dynamic range and data thruput (TOA resolution) versus frequency resolution.

Since thermal noise does not undergo coherent compression in the delay line, the effective peak signal-to-noise ratio is enhanced by the compression gain.

— Digital Interface

The compressed output from the dispersive delay line (Figure 6) is a frequency-versus-time sweep similar to that of a spectrum analyzer scan. In compressive receivers for pulse applications this scan will be of 0.1 to 1.0 microsecond duration. Threshold detection and conversion to a serial digital data format implies a sampling process at a high rate. Using, as an example, the receiver described in Figure 6 and a scan of 150 nanoseconds, with a dispersion characteristic F/T of 2.2 MHz/nsec, the minimum pulse width (equation 3) is only 4.5 nanoseconds duration. Therefore, the sampling period cannot be less than 4.5 nsec, and, to ensure good probability of detection, should be increased somewhat to about 3 nsec(330 MHz), about the limit of current emitter coupled logic (ECL) devices.

In wideband pulse applications, the high data rate precludes the recovery of quantitative amplitude information from the compressive module.

Figure 7 is a typical digital interface for a dual channel (100% POI) compressive receiver. ECL devices are used to sample the detected, compressed signal pulses and to convert the data streams to parallel format for further processing. Data from both channels may be merged by delaying data from one channel by the scan time. The centroid operation locates the center of the (sin x)/x response for short pulses where the width of the compressed pulse may create detections lasting several sample periods.

Because the raw data contain several million scans of the RF environment every second preprocessing must delete redundant data from the processor input. In the example here, emitter stripping[9] is used to delete signals already identified.

— Design Trade-Offs

In implementing a compressive receiver channel optimized for short pulse (radar ESM) applications (operating at 50% duty cycle), one must trade-off between receiver frequency resolution and relative response to short pulses. The scan time must be shortened to obtain short pulse response. Note how this corresponds to the trade-off in the channelized receiver (time domain) where channel bandwidth must be sufficient to obtain short pulse responses. In each case the trade-off results in a loss of frequency resolution.

— Typical Capabilities

Figure 8 summarizes the present capabilities[7,11,12] of compressive receiver modules for short pulse (0.1 μsec) ESM applications, where trade-off between frequency resolution and TOA resolution has been made to be consistent with the requirements of Figure 2.

The compessive receiver mechanization is well adapted to the ESM requirements with the critical capability of detecting simultaneous signals. The instantaneous bandwidth is on the low end of our requirements. However, the simplicity of the RF design, reproducibility of delay line characteristics, and development of custom digital interface circuits facilitate the mechanization of additional receiver modules which can increase the overall reception bandwidth. Such modules may work either in parallel or independently.

Figure 9 is an example of a dual compressive receiver assembly. The 10 cubic inch RF assembly contains two channels for 100 percent POI over 375 MHz bandwidth, with a resolution of 6.8 MHz. The digital interface requires similar volume.

— Development Trends

Currently, compressive receivers employing SAW and ECL

[Continued on page 120]

COMPRESSIVE RECEIVER TYPICAL CAPABILITIES

RF Bandwidth*	200 - 400 MHz
Frequency Resolution	3-15 MHz
Dynamic Range	≥50 dB
Noise Bandwidth	2.5 - 5 MHz
Complexity	RF - Low Digital - High

*RF BW = 1/2 Compressor BW

Fig. 8 Compressive receiver typical capabilities.

[From page 119] **ECM APPLICATIONS**

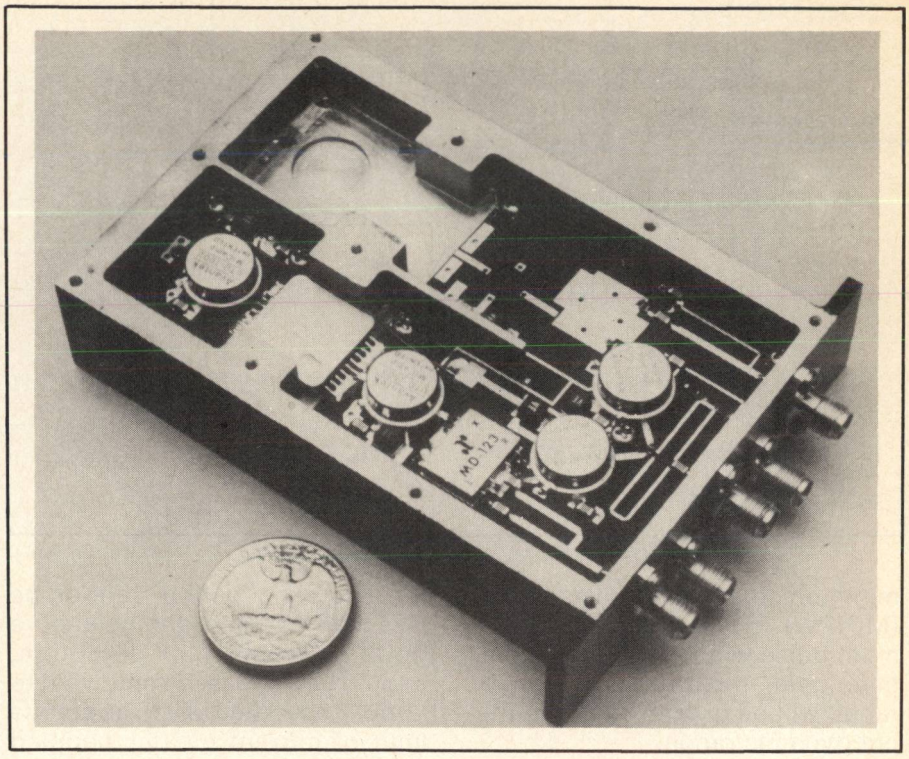

Fig. 9 A dual compressive receiver (BW=375 MHz, resolution 6.8 MHz.)

devices have a mature technology base. Receivers to meet radar ESM requirements may be readily fabricated. Present technology employing 2 to 3 parallel receiver modules can be fabricated in a volume highly competitive with IFM technology.[12] In the near term, efforts to reduce size and complexity apear to be centered on the development of custom integrated interface circuits[18]. The developmental device technologies such as, GaAs logic devices, VHSIC preprocessing circuits, and MSW dispersive delay lines may in the future make a 1 GHz compressive receiver module practical.

The Acousto-Optical Receiver

The acousto-optical (A-O) receiver operates on interaction of a

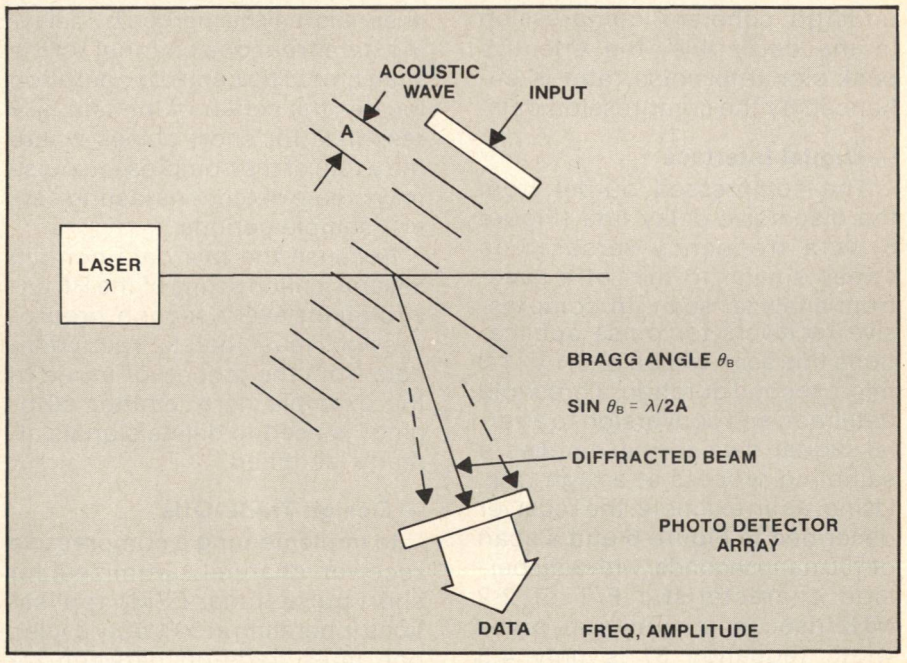

Fig. 10 The acousto-optical receiver operating principal.

beam of light and the periodic variation of the index of refraction associated with an acoustic wave[13,14,15]

Figure 10 depicts the operating principle of the A-O receiver. The laser produces a coherent light beam which is focused upon an acoustic wave propagating within, or on, a transparent medium. The acoustic wave causes periodic variations in the index of refraction which result in diffraction of the light beam. At a certain critical angle of incidence, the Bragg angle, the energy in the first order diffraction is maximized. Fixing the geometry of the two incident beams and the wavelength of the light source produces diffraction at an angle proportional to the wavelength of the acoustic signal. Thus the Bragg interaction converts acoustic frequency to spatial displacement.

A lens is then employed to focus the diffracted signal onto a photo detector array located at the lens focal point. It is an established optical principal[6,14] that a lens will produce the Fourier transformation. Thus the diffracted beam will be focused to a single spot on the detector array. The position of the spot on the array is proportional to the angle of the incident beam, and hence, to the frequency of the input signal. Amplitude of the optical signal is proportional to the strength of the RF input signal.

Thus, the A-O receiver is a device capable of receiving many simultaneous signals at a high POI and of encoding each with a sensitivity commensurate with the narrow RF bandwidth of a single photosensor element.

— The Bulk A-O Receiver

The bulk acousto-optical receiver is shown in Figure 11. The acoustic Bragg cell contains a microwave transducer fabricated onto the surface of the acoustic medium, (eg. lithium-niobate). When properly driven, this transducer causes acoustic waves to propagate within the bulk crystal. Center frequencies of up to three GHz may be used for the bulk acoustic wave, thus allowing transducer bandwidths of up to 1 GHz. In the bulk A-O receiver the laser, lens systems, and detector

[Continued on page 122]

[From page 121] **ECM APPLICATIONS**

array are separate devices. Until recently, the very rigid mechanical mounting requirements needed to maintain stable operation over vibration and temperature variations posed serious fabrication difficulties in th Bulk A-O Receiver. Presently receivers of this type are available for military applications with compression factors of up to 1000; for instance, 1 GHz bandwidth with 1 MHz resolution[17, 13, 18, 2].

Diffraction with bulk acoustic waves is a relatively low efficiency process. As a result substantial laser power is required to achieve diffracted signals within the dynamic range of the photo detectors[4].

To date, the development of A-O receivers has trended toward signal analysis rather than spectrum analysis. Photosensors are often charge-coupled device (CCD) arrays which integrate received signal energy over an interval of, at least, a few microseconds[17, 18, 19]. By converting the analog amplitude of each detector cell using an Analog-to-Digital (A/D) converter, the Fourier transform of signals are converted into discrete transform points for analysis by digital processing.

This procedure recovers the amplitude as well as the frequency characteristics of the signal, but requires considerable data readout and much conversion time. Since the TOA resolution is limited to the several microseconds required for the output procedure, currently, TOA resolution is inadequate for ESM using time based sorting algorithms for identification.

— Dynamic Range and Frequency Resolution

The detection of two signals of different amplitudes is a function of the frequency spacing between the signals. Spurious spreading of a larger signal may mask a second smaller signal if the signals are close in frequency. Using a modified gaussian density distribution profile on the optic beam suppresses the spurious sidebands close to the signal frequency to about 35 dB below the carrier, setting the dynamic range at this level. Dynamic range of 50 dB may be achieved for simultaneous signals with considerable frequency separation[17]

Frequency Resolution is determined by the focal length of the transform lens and upon the angular separation of successive photo sensors. For reception of short pulse signals, whose (sin x)/x energy distribution excites many photosensors, fine frequency resolution requires considerable data processing or preprocessing to find the centroid of the signal energy distribution.

— The Integrated Acousto-Optic (IA-O) Receiver

Considerable development effort[20,21,22,23,25] is currently being directed toward the IA-O receiver (Figure 12) incorporating the Bragg cell transducer and optic lens on a common substrate. A separate semiconductor laser light source and photosensor array using CCD's or photodiodes complete the receiver. Heat sink requirements and differences in device manufacturing processes require that the semiconductor

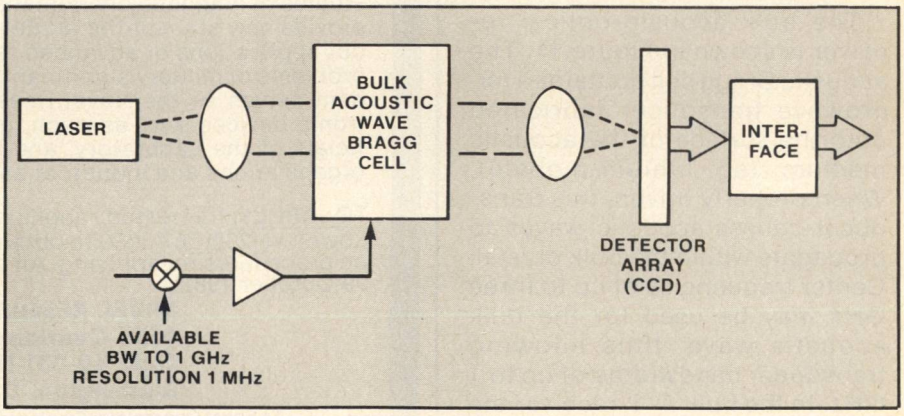

Fig. 11 The bulk A-O receiver.

laser be fabricated as a separate device which is bonded to the end of the substrate.

In the IA-O receiver, the laser light beam is confined to the surface of the substrate and the signal propagates as a surface acoustic wave (SAW). This produces a Bragg intersection of higher efficiency than that using bulk waves and is compatible with lenses fabricated into the surface of substrates.

Lens fabrication is accomplished by matching a hole into the substrate surface with considerable precision. The lens effect then is produced by the difference in index of refraction between the substrate and lens (air) media.

The substrate is usually fabricated of lithium-niobate. During fabrication of the substrate, the surface is treated by the introduction of a metal film which, thru subsequent diffusion, creates an optical channel (waveguide) just below the surface of the substrate. This channel then confines the laser energy to the surface region of the substrate where interaction with the surface acoustic wave takes place[20].

Performance of the IA-O Receiver

Presently IA-O receivers have RF bandwidth associated with SAW propagation of up to 500 MHz.

In the IA-O receiver, frequency resolution is determined by several parameters, including: detector element spacing (dimension), lens focal length, lens aberration, and size and distribution (weighting) of the optic beam which intercepts the acoustic wave[23,20]. In the IA-O receiver using LiNb03, limited substrate size requires the use of small f-number lenses. The resolution is then limited by the spacing of the photosensor array elements, usually a few microns[19].

To date, frequency resolution of 4 to 6 MHZ[21,22] has been achieved.

Using current laser diodes, dynamic range of 25 to 30 dB has been achieved. This should improve as detector dynamic range, lens fabrication, laser power, and laser/substrate coupling improve.

Figure 13 shows a developmental model of an IA-O receiver. This unit has a 400 MHz bandwidth with 4 MHz resolution. Utilizing a unique high speed photo detector diode array, eight bits of amplitude data can be processed from each of the 100 detectors every 2 microseconds.

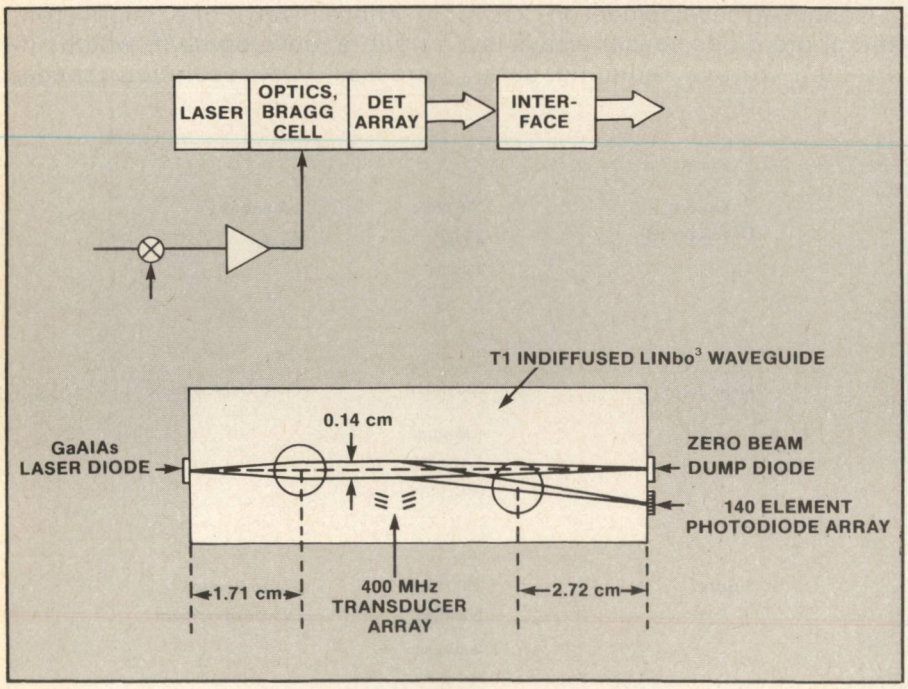

Fig. 12 The integrated acousto-optical (IA-O) receiver.

[Continued on page 124]

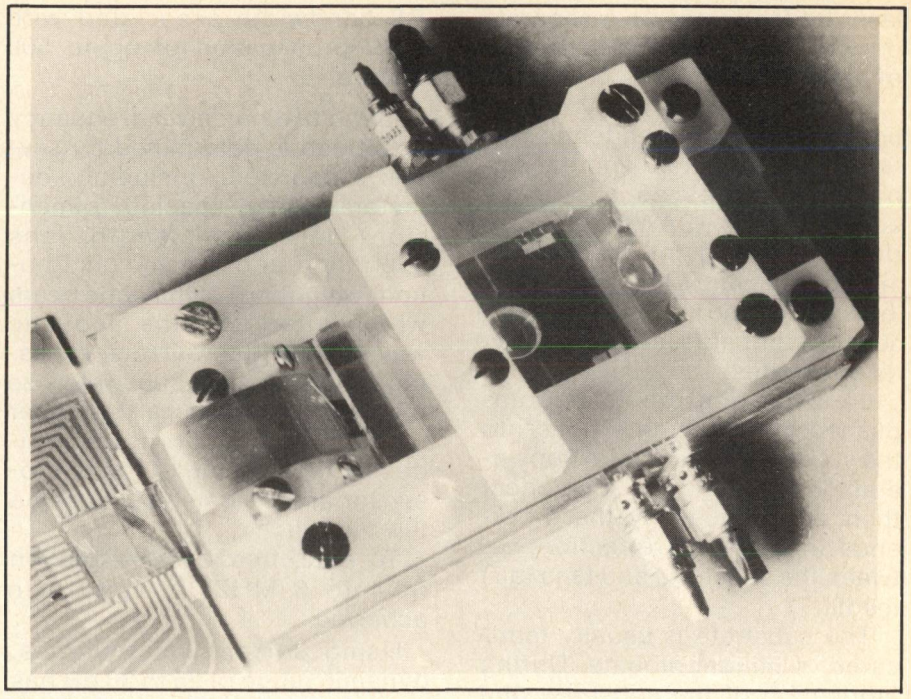

Fig. 13 A development model IA-O receiver.

Acousto-Optical Receiver Development Trends

Current Bulk A-O receivers, having access times of several microseconds, provide bandwidths up to 1 GHz with 1 MHz resolution. Development of AOA processing capability is continuing[24] and may possibly lead to the fielding of this capability within a few years.

Continued development on CCD and photo diode sensor arrays is directed toward reducing data acquisition and throughput times. However, consider that to achieve the desired 0.5 microsecond TOA resolution (Figure 2) in a receiver of 1 GHz and 1 MHz resolution, 1000 A/D conversion must be made every 0.5 microseconds. This might be achieved using 1000 parallel, 0.5 microsecond A/D converters, but would incur considerable complexity.

Alternatively, one might consider a development which increases TOA resolution (speed)

Current Development	500 MHz 4 MHz 2 μsec	Laboratory 50 IN^3
Near Term	500 MHz 1 Module 5-10 MHz 0.25 usec	Field Deployment
Future	1000 MHz 1-2 MHz 0.1 usec	Photo Sensor I/O Development

Fig. 14 Integrated A-O receiver development.

[Continued on page 126]

[From page 124] **ECM APPLICATIONS**

	CVR	IFM	Chan	Comp	IAO
BW (1 GHz)	√	√	√	3*	2*
Resolution	None	√	√	√	√
Multisignal	Poor	Poor	√	√	√
Complexity	Low	Med	High	Med	Low
Maturity	√	√	√	√	Low

*No. Parallel Modules

Fig. 15 Summary ESM capabilities for various wideband receiver types.

by trading amplitude and/or frequency resolution[17]. For spectral analysis, a one bit A/D conversion; (i.e., simple detection) would do quite well for most applications. In the few instances where amplitude is required, an auxiliary amplitude detection (log amp) can be used, as is done with IFM or compressive receivers. Also, for pulse ESM applications, frequency resolution can be relaxed (Figure 2) to 5 to 10 MHz. These measures would reduce the photosensor array to 100 to 200 detectors with 100-200 bits of output data every 0.5 microseconds. For example; 8-16 bit words, at 62 nsec per word, from a 128 element detector array could service an A-O receiver of 1 GHz bandwidth, 7.8 MHz frequency resolution, and 0.5 microsecond TOA resolution. Fabrication of such detector arrays should not pose any significant development problems and would enable the deployment of A-O receivers for ESM applications forthwith.

Figure 14 depicts the current and near term prospects for the integrated A-O receiver. Current development effort is expected to continue with the near term goal of increased dynamic range. Coupled with a photosensor optimized for TOA resolution, one could expect realization of an IA-O receiver for ESM applications as shown.

Summary

The relative performance of the various wideband receiver types is shown by capabilities versus the requirements of Figure 2. Figure 15 shows the comparison for a nominal 1 GHz bandwidth ESM receiver mechanization. The compressive receiver, mechanized in three or more parallel subbands, is a viable alternative to the channelized receiver where simultaneous signal capability is required. Also highlighted is the very promising potential of the acousto-optical receiver.

In summary, no receiver offers all the four important characteristics of wide bandwidth, multiple signal capability, fine frequency measurement and good TOA resolution. One can expect to tradeoff at least one parameter. For example, the IFM is a wide band, time domain device which produces fine frequency resolution by real time video processing and has only limited multiple signal capabilities.

The frequency domain receivers offer another alternative. High POI, wide bandwidth, and multiple signal capability are inherent in the compressive and A-O receivers. In applications requiring fine TOA resolution, bandwidth and/or fre-

quency resolution may be sacrificed.

Conclusion

For ESM applications the compressive receiver is a viable alternative to the IFM and channelized time domain receivers. A single module provides performance comparable to the typical channelized receiver with reduced size and complexity. Parallel modules can achieve the overall bandwidth of the IFM and provide multiple, simultaneous signal capability.

The Acousto-Optical receiver has the potential for becoming the ESM receiver of the future. Its desirable features and natural simplicity offer an exciting promise. For ESM applications, a new direction in photosensor array development should be undertaken which could considerably shorten the time for widespread application.

Acknowledgements

The author would like to thank Mr. C. Nothnick and Dr. D. Mergerian of Westinghouse Electric Corp. for their suggestions and for contribution of photographs for this paper.

Mr. Nichols, *joined Westinghouse Defense and Space Center in 1963. For 10 years he was involved in the design of radar receiver and tracking circuits. Since 1973 he has been employed as a systems engineer in the Electronic Warfare Department, where his responsibilities have included work on RF memory loop systems, digital communications, and system design on the ALQ-119, ALQ-131, and ASPJ ECM systems.*

Mr. Nichols is currently engineering Manager of the Comprehensive Power Management Subsystem of the Advanced Self-Protection Jammer [ASPJ] program.

BIBLIOGRAPHY

1. Vanbrudt, L.; Applied ECM; EW Engineering Inc. 1978, Lib. Congress 78-50538.
2. Drogin, E. M.; Frequency Encoding Essential for Overlapping Pulses: MSN July 1979, pg. 50-61.
3. Huber, Lane, et. al.; A Low Sidelobe SAW Contiguous Filterbank Using MDC $LiTaO_3$; Proc. IEEE Ultrasonics Symposium 1977, pg. 568-572.
4. Daniel, M. R., Adam, J. D., Okeeffe, T. W.; A Linearly Dispersive Magnetostatic Delay LIne at X Band; IEEE Trans. Mag, MAG-15 Nov 1979, pg. 1735-37.
5. Adam, J. D., Collins, J. H.; Microwave Magnetostatic Delay Devices Based on Epitaxial Yttrium Iron Garnet; Proc. IEEE Vol. 64 May 1976, pg. 794-800.
6. Jac, M. A., Grant, P. M., Collins, J. H.; The Theory, Design, and Applications of Surface Acoustic Wave Fourier-Transform Processors; Proc. IEEE, Vol. 68, No. 4, April 1980, pg. 450-468.
7. Crufut, W.; SAW's Citical to Avionics; MSN Nov. 1980, pg. 56-64.
8. Crufut, W.; 2500 Filters In One; R. F. Design Sept./Oct. 1979, pg. 20-23.
9. Cook, C.; Bernfeld, M. Radar Signals; Academic Press, New York and London 1967, pg. 198-206.
10. RAppolt, F.; Receivers Tools Improve Difficult RF Signal Acquisition; MSN April 1981, pg. 62-86.
11. Collins, J. H., Grant, P. M.; Signal Processing Pivotal to Next Generation ESM Receivers; MSN April 1981, pg. 102-107.
12. Moule, G. L., Bale, R. A., Browing, T. I.; A 1 GHz Bandwidth Compressive Receiver; Proc. 1980 IEEE Ultrasonics Symposium, pg. 216-219.
13. Hoffman, C. B., Baron, A. R.; Wideband ESM Receiving Systems, Part I; Microwave Journal Sept. 1980, pg. 23-33.
14. Berg, Lee, Casseday, and Udelson; Surface Wave Delay Line Acoustooptic Devices for Signal Processing; Applied Optics Vol. 18 No. 16, 15 Aug. 1979, pg. 2767-74.
15. Poon, T. C., Korpel, A.; Optical Transfer Function of an Acousto-optic Heterodyning Image Processor; Optic Letters Vol. 4 No. 10 Oct 1979, pg. 317-319.
16. Mertz, L.; Transforms in Optics; Wiley, New York 1965.
17. Elson, B.; Signal Processing Technology Advances; Aviation Week and Space Technology, 15 Dec. 1980.
18. Harper, T.; Receivers Evolve to Era of Computer-Controlled 'Hybridization'; MSN Aug. 1979, pg. 112-120.
19. Boyd, J. T., Ramey, D. A.; Optical Channel Waveguide Arrays Coupled To Integrated Charge-Coupled Devices and Their Applications; Proc. soc. of Photo-optical Instrumentation Engineers (SPIE) Symposium on Guided Wave Optical Systems and Devices II: Vol. 176 1979, pg. 141-146.
20. Chen, B. Barnoski, M. K.; Integrated Optic (Bragg) Spectrum Analyzer; Proc. SPIE Symposium on guided Optical Systems and Devices II; Vol. 176 1979, pg. 56-61.
21. The Real Revolution Waits for Optical I C's; (Staff); Microwaves Aug. 1981, pg. 100.
22. Optics Integrated for Processing; (Staff); MSN May 1981, pg. 92-94.
23. Giallorenzi, T. G., Hamilton, M. C. RF; Spectrum Analysis Using Optical Waveguides; Proc. IEEE MTT International Microwave Symposium, May 1979.
24. G.T.E. Inc. Optical Data Processing Brochure; G.T.E. Products Corp, 1981.
25. Gerard, H. M., Otto, O. W.; Chirp Transforms Open New Processing Possibilities; MSN October 1977, pg. 815-90. ■

Amplifier Application Notes

Anzac Div. Adams Russell
Burlington, MA

Introduction

Broadband radio frequency amplifiers designed for operation below microwave frequencies generally use high-gain bipolar transistors in combination with negative feedback circuitry. This note presents a discussion of feedback with emphasis on circuits having fundamental advantages in noise figure and dynamic range performance. Also included are basic amplifier definitions and information useful for predicting the noise figure and intermodulation performance of amplifier cascades.

Feedback Amplifiers

The bipolar and field effect transistors, which are the basic gain producing devices used in virtually all RF receiving amplifiers, are not particularly attractive for that use from a design stand point. They are characterized by frequency dependent gain, poor impedance match, and non-linear operation. Negative feedback circuits are designed to overcome these effects; and it is the designer's task to provide amplifiers having flat gain, good impedance match, and distortion reduced for acceptable systems operation.

Most such amplifiers are designed using a technique commonly known as resistive feedback, shown in Figure 1. One feedback resistor connects between collector and base; a second connects between emitter and the ground of the common emitter transistor. Selection of these two resistors controls the gain and terminal impedances as given by the approximate equations in Figure 1. These feedback resistors are inherent noise producers and power dissipators. As feedback is increased in order to decrease gain and distortion, these resistors add more noise and dissipate more output power. With feedback sufficient to reduce gain to 10 dB, the noise figure will have increased by about 3 dB and the available output power will have decreased by about 3 dB compared to the performance of the same transistor operating without feedback.

To avoid this degradation of performance, a negative feedback structure based on ferrite transformers is used. This patented technique, known as "lossless feedback," provides lower noise figure and higher linear output than can be achieved using resistive feedback with the same transistors. Figure 2 shows a block diagram of a transformer feedback circuit in which a directional coupler is the feedback network. The coupling ratio between ports D and C determines the magnitude of the feedback, and hence, the gain. The feedback is negative due to the in-phase coupling between ports D and C and the inversion of the active device.

There are no shortcuts to producing a sophisticated EW system that demands high performance and trusted reliability. Only good design executed with quality components will suffice.

Each Avantek component is a singular example of the levels of systems performance now achievable. From one end of the system to the other, no one else can offer such a comprehensive selection of solid-state components—from low-noise octave-bandwidth preamplifiers, limiting and loop amplifiers, to mixers, switches, oscillators, filters, and modular IF and power amplifiers. All with high performance, high reliability, and available in volume production. Avantek quality microwave components are the first choice of designers and program managers throughout the EW industry.

RF Amplifiers

An electronic defense receiver can use all the detection range it can get. Avantek pushes the edge with a complete series of octave-bandwidth, low-noise preamplifiers featuring guaranteed noise figures of less than 4.0 dB at X-band. These include production amplifiers from 18 to 26.5 GHz, and 26 to 40 GHz devices to be available soon.

Typical Noise Figure vs. Frequency

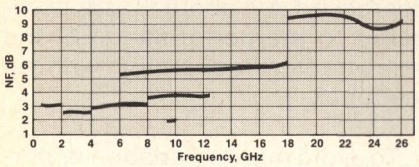

For IFM and other signal processing applications, Avantek output-limited amplifiers provide exceptionally flat power output over a wide input dynamic range.

Typical Limiting Amp Performance

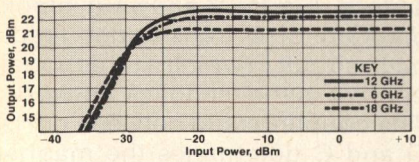

Medium power amplifiers, rugged enough to take severe military operating conditions, are available with up to two watts output over a 2 to 18 GHz frequency range.

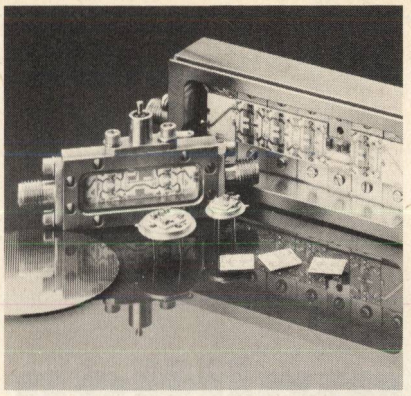

Typical Power Output, (1 dB GCP)

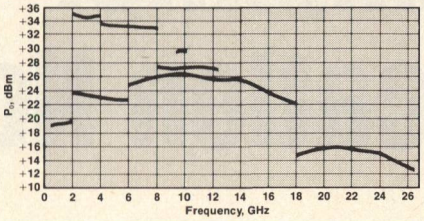

Avantek is also experienced in designing and manufacturing frequency memory loop and other specialized RF amplifiers for advanced signal processing applications.

IF Amplifiers and Microwave Mixers

Avantek's innovative leadership in IF amplifiers means ever-increasing design flexibility. You get lower noise figures, low current drain, higher output power, and very high dynamic range over a wide choice of intermediate frequencies.

Typical Gain vs. Frequency

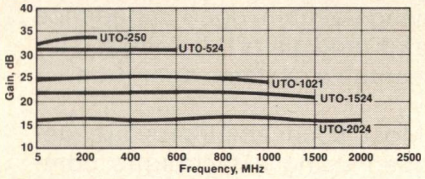

Avantek IF amplifiers are available in convenient TO-8 packages, or up to three hybrid modules can be cascaded in the Avanpak™, a unique miniature flat package. All are hermetically sealed, with circuits protected against moisture and corrosion by an inert gas to withstand the harshest military environments.

Avantek double-balanced mixers offer an unmatched combination of performance features, with LO bandwidths as wide as 2 to 26 GHz, and input intercept point options from +15 dBm to +32 dBm.

DBX-18212M Conversion Loss

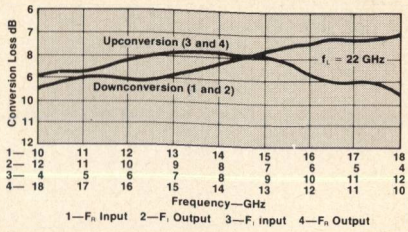

Oscillators and Tracking Filters

With Avantek fundamental-output YIG-tuned transistor oscillators, the designer can cover the full 2 to 26 GHz range with just three units, while always being assured of tuning linearity and power output stability over the full band.

Guaranteed Power Output

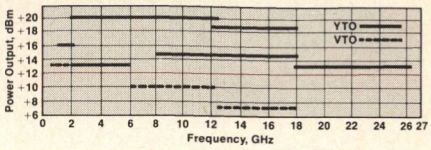

Tracking YIG filters complete the team for predictable system performance. And for extremely fast tuning speeds, varactor-tuned oscillators or switched fixed frequency oscillators fit many electronic defense applications.

Advanced Solid-State Microwave Technology

Avantek's entire product line promotes system operating and packaging efficiency for superior performance and absolute reliability. This is only possible because each component is manufactured in facilities dedicated to the most modern processing methods. The implementation of such techniques as laser drilling and resistor trimming, ion implantation, automatic wire bonding, and all-gold metalization illustrate Avantek's forward-looking philosophy.

Call or write today for more details. Avantek is the single best source for your EW microwave component requirements.

Avantek

3175 Bowers Avenue
Santa Clara, California 95051
Sales: (408) 496-6710

CIRCLE 91 ON READER SERVICE CARD

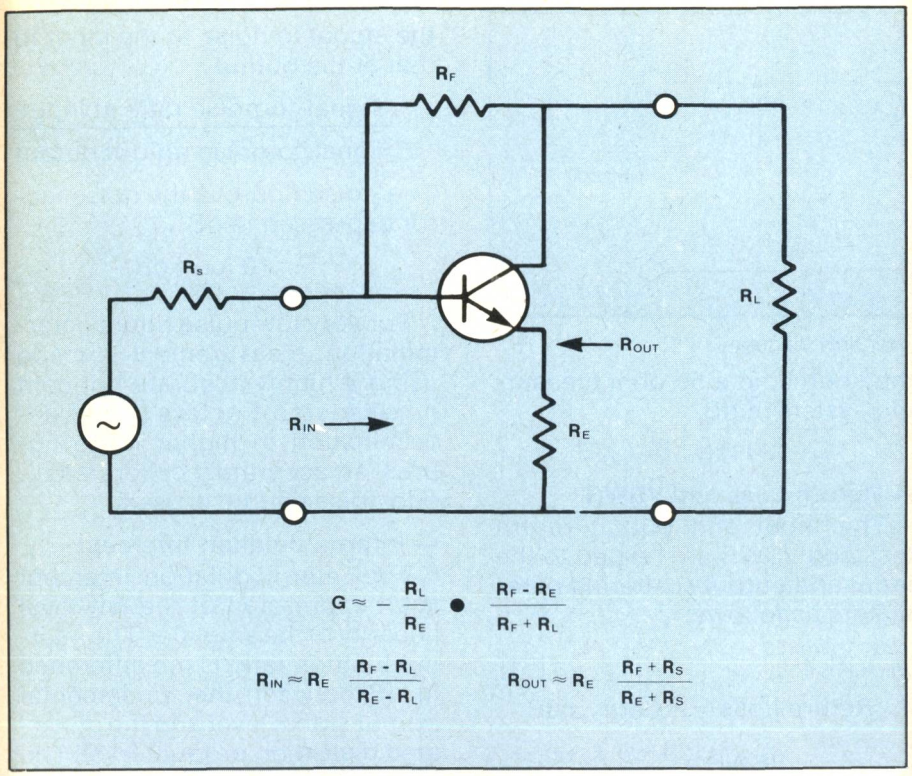

Fig. 1 Resistive feedback amplifier.

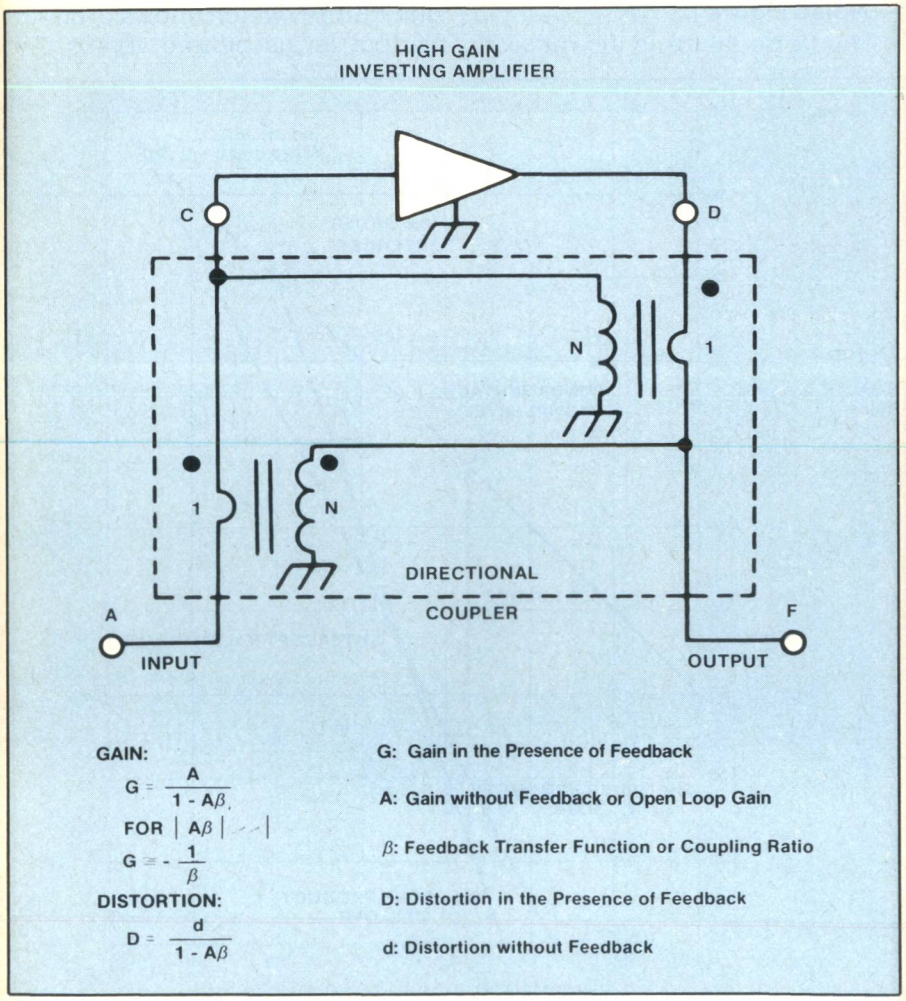

Fig. 2 Block diagram of transformer feedback circuit.

[Continued on page 132]

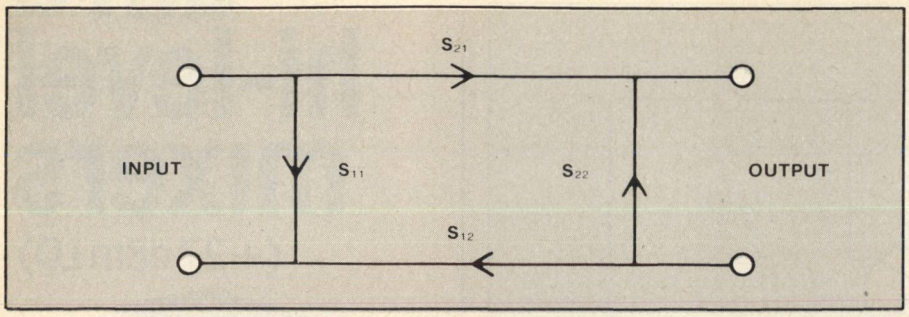

Fig. 3 Scattering parameter flow diagram.

The isolation of the coupler prevents output power from the active element applied to port D from appearing at the input port A; therefore, impedance match can be maintained in the presence of feedback. Finally, the signal transfer properties of the coupler are such that all of the input signal at A is added to the transistor output signal at D to yield a total output signal at B which is greater than the active device output; this is in contrast to the resistive feedback configuration in which the output power is less than that delivered by the active device. The only noise figure degradation is that produced by the very small incidental losses in the coupler.

The directional coupler feedback circuit gives great flexibility in application. The gain can be varied over a wide range by changing the transformer turns ratio and therefore the coupling ratio. Taps are regularly added to the transformers allowing the source and load impedances presented to the transistor to be changed. This allows noise figure and output linearity characteristics to be optimized. The couplers are very broadband devices allowing wide bandwidths, limited only by the active device, to be achieved.

A more detailed discussion of these circuits is contained in reference (1).

Definition and Measurement of Amplifier Parameters

— Gain

A network analyzer is used to measure the two-port scattering parameters of the amplifier as shown in the accompanying flow graph (Figure 3). The small signal insertion gain is defined as the ratio of the power delivered to the load to the power available from the source, in a 50 ohm measuring system in dB,

$$G = 20 \log_{10} |S_{21}| \text{ dB}$$

— Return Loss and VSWR

The input and output return loss and VSWR are related to the input and output scattering parameters as follows:

$$\rho_{in} = |S_{11}| \qquad \rho_{out} = |S_{22}|$$

$$\text{Return Loss} = 20 \log_{10} \rho \text{ dB}$$

$$\text{VSWR} = \frac{1 + \rho}{1 - \rho}$$

— Noise Figure

The noise factor is the ratio of the signal to noise at the input to that at the output.

$$f = \frac{\text{Signal-to-noise ratio at input}}{\text{Signal-to-noise ratio at output}}$$

The noise figure is the noise factor expressed in dB

$$F = 10 \log f \text{ dB}$$

For very low noise figure determination, measurement is made using a highly accurate hot-cold noise source. For less critical determination of higher noise figures, an accurately calibrated diode noise source is used.

— Intermodulation Intercept

The intermodulation intercept is an expression of the low level linearity of the amplifier. The intermodulation ratio is the difference in dB between the fundamental output signal level and the generated distortion product level. The relationship between intercept and intermodulation ratio is illustrated in Figure 4, which shows product output levels plotted versus the

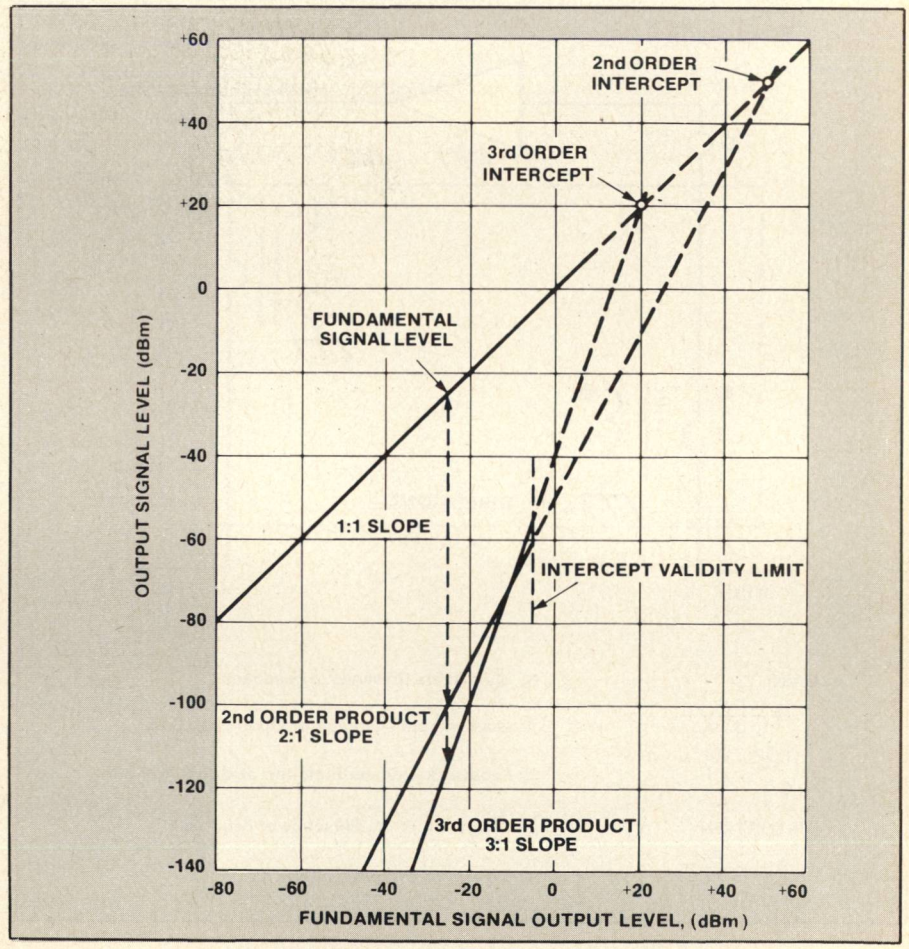

Fig. 4 Intercept diagram.

level of the fundamental output for two equal strength output signals at different frequencies. The upper line shows the fundamental output plotted against itself with a 1 dB to 1 dB slope. The second and third order products lie below the fundamentals and exhibit a 2:1 and 3:1 slope respectively. The intercept point for either product is the intersection of the extensions of the product curve with the fundamental output.

The intercept point is determined by measuring the intermodulation ratio at a single output level and projecting along the appropriate product slope to the point of intersection with the fundamental. When the intercept point is known the intermodulation ratio can be determined by the reverse process. The second order IMR is equal to the difference in dB between the second order intercept and the fundamental output level. The third order IMR is equal to twice the difference between the third order intercept and the fundamental output level. These are expressed:

$$IP_2 = P_{out} + IMR_2$$
$$IP_3 = P_{out} + 1/2\ IMR_3$$

where P_{out} is the power level in dBm of each of a pair of equal level fundamental output signals, IP_2 and IP_3 are the second and third order output intercepts in dBm, and IMR_2 and IMR_3 are the second and third order intermodulation ratios in dB.

The intermodulation intercept is a valid indicator of intermodulation performance only in the small signal operating range of the amplifier. Above some output level which is below the 1 dB compression point the active device moves into large signal operation which is attended by signal strength dependent bias level shifts. At this point the intermodulation products no longer follow the straight line output slopes, and the intercept description is no longer valid.

The intermodulation ratios are determined by measurement using a conventional spectrum analyzer. The measurement dynamic range is enhanced using appropriate cancellation techniques when required to accomodate high dynamic range amplifiers.

— Compression

The 1 dB compression point is the output level at which the amplifier gain drops 1 dB below its small signal value. It is an indication of the signal level at which small signal conditions no longer apply. At this level, the intermodulation intercepts no longer adequately predict the amplifier distortion behavior.

The measurement of the compression level is made using a frequency discriminating detector in order to detect the gain decrease at the fundamental frequency. This is preferable to using a total power detection measurement, since it is the fundamental frequency which is probably of most interest to the user.

— Maximum Signal

The maximum signal level is the largest CW or pulsed RF signal which may be safely applied to the amplifier. Larger signals will exceed the emitter base breakdown voltage of the transistor and will result in permanent degradation of noise figure and, for large enough signals, reduction of gain and increase in distortion.

The specified level is determined by applying successively larger CW signals and measuring the noise figure until 0.5 dB degradation is observed. The maximum signal level is specified 3 dB below the level which causes the 0.5 dB degradation.

— Stability

Broadband feedback amplifiers, in general, may not be unconditionally stable at all frequencies, particularly outside of their specified operating bandwidth. When lossless feedback techniques are employed, stability margins tend to be smaller than when resistive methods are used. Indeed, it has been observed that when completely lossless feedback networks are utilized, for the purpose of achieving the lowest possible noise figures and highest dynamic range, it may not also be possible to achieve unconditional stability simultaneously. Unconditional stability may well be a trade-off against the noise figure require-

[Continued on page 134]

[From page 133] **AMPLIFIER NOTE**

ment in particular.

For this reason, the analysis capability of automatic network analyzers are used in order to calculate the stability conditions for amplifiers from their measured S-parameters. Using equations from reference (2) it is possible to compute the K factor and the stability circle locations directly from the S-parameters at all frequencies of measurement. If the K factor is greater than unity, the amplifier is unconditionally stable at that frequency. If K is less than unity, then the stability circles, which are the boundaries between the stable and the potentially unstable load regions, may be calculated and plotted on the source and load plane Smith charts. This information, along with the system designer's knowledge of the source and load impedances in which the amplifier will be embedded, make it possible to utilize, with confidence, amplifiers whose desirable characteristics outweigh their lack of unconditional stability.

— Survivability

Recent published work (3) has been done on the topic of amplifier survivability and protection against strong RF signal inputs. It was found that the most probable overload failure mechanism is breakdown of the emitter base junction when the applied signal negative peaks drive the base beyond the BV_{EBO} rating of the transistor. Amplifiers which utilize transistors with breakdown voltages in excess of 3 volts can withstand signals up to +20 dBm. High frequency amplifiers using very high f_t devices with 1.5 volt breakdown voltages are susceptible to damage with signals in the vicinity of +13 dBm.

The problem is related to peak voltages rather than average power and is therefore as severe for low duty cycle pulses as for CW signals. Indeed, it may be more sev-

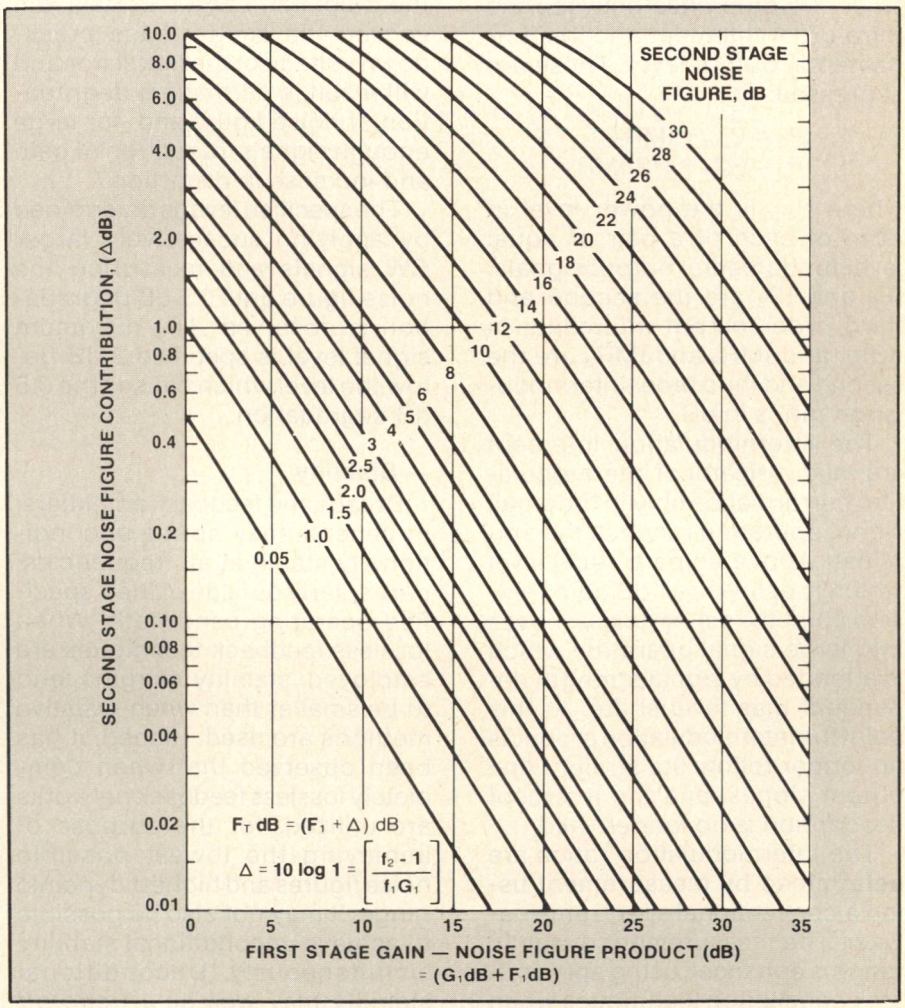

Fig. 5 Graphical solution for cascaded noise figure.

ere for repetitive pulses if the transient response of the input biasing circuitry is not well controlled.

Special protection against overdrive have been developed and can be incorporated in special designs as required. The most effective protection has been obtained by placing a low resistance Schottky diode directly across the emitter-base junction in the reverse bias direction. This diode has no effect on the small signal operation of the amplifier; specifically, it does not degrade noise figure or intermodulation intercept. When overloading signals are applied, however, the diode conducts on the negative peaks and limits the emitter-base voltage below the level of breakdown. By proper application of this technique, including the design of the bias circuitry, it is possible to protect very low noise amplifiers against overloading signals in excess of one watt.

Cascading Amplifiers

Two graphs are presented here which are useful in designing cascades of amplifiers or other components. The first graph is an easily used presentation of the added noise figure due to the second stage in a cascade of two units. The standard formula for the total noise figure, f_{29} in terms of the first and second stage noise figures and the first stage gain is:

$$f_t = f_t + \frac{f_2 - 1}{g_1}$$

Since noise figure is normally given in dB rather than in power terms, it is useful to reformulate the above to:

$F_t = F_1 \Delta$ in dB, where Δ is given by

$$\Delta = 10 \log \quad 1 + \frac{f_2 - 1}{f_1 g_1}$$

Figure 5 allows Δ to be read directly on the ordinate in dB at the crossing of the abscissa, which represents the sum of the first stage gain and noise figure in dB, and the diagonal, which represents the second stage noise figure.

The second graph shows the effect on the intermodulation intercept caused by the cascading of two stages. It can be shown that the total cascade intercept, I_T, is related to that of the second stage, I_2 by:

$$I_T = I_2 - \Delta$$

where I_T and I_2 are in dBm and Δ is in dB, where

$$\Delta = 20 \log 1 + \frac{1}{g_2} \frac{i_2^2}{i_1^2} \quad \text{for second order}$$

$$\text{and } \Delta = 10 \log 1 + \frac{1}{g_2} \frac{i_2^3}{i_1^3} \quad \text{for third order}$$

Here i_1, i_2, and g_2 are the first stage intercept, the second stage intercept, and the second stage gain, respectively, expressed as powers and power ratio. The superscipts 2 and 3 identify the product order. Δ is seen to represent the reduction in the cascade intercept from that of the second stage alone. [Continued on page 136]

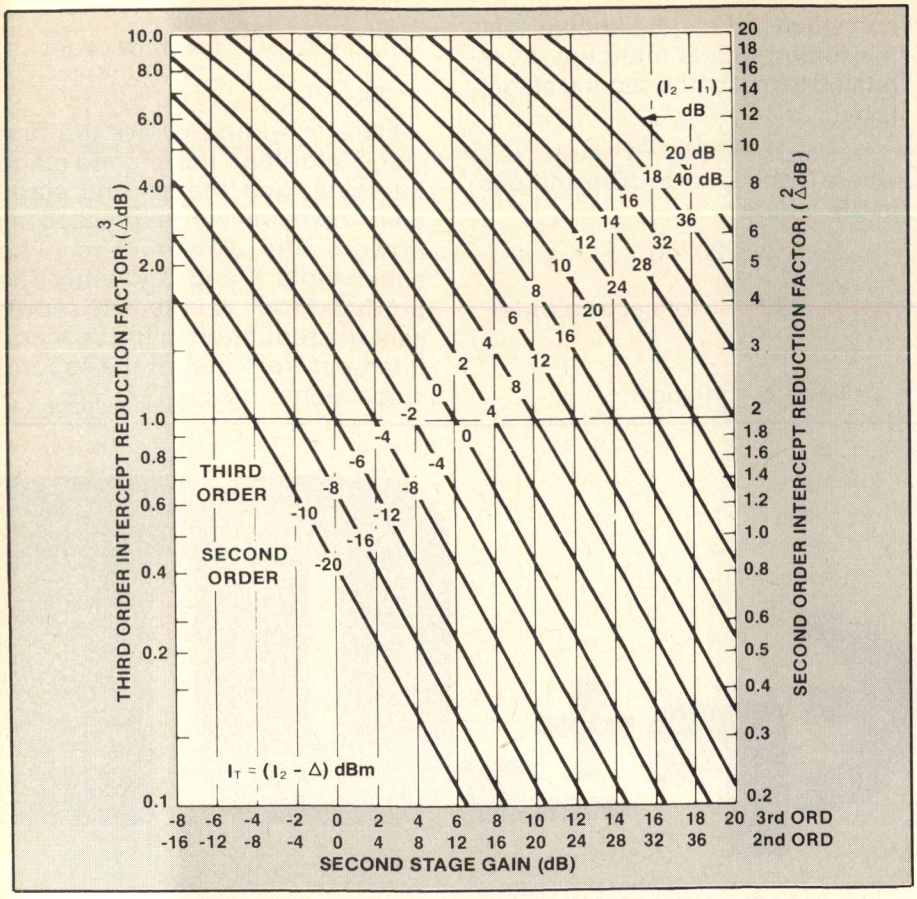

Fig. 6 Graphical solution for cascaded intercept.

Figure 6 allows Δ to be read directly in dB at the intersection of the abscissa which represents the second stage gain and the diagonals which represent the difference between the third and second stage intercept in dB. Both second and third order products are represented. The underlined scales are used for second order intercepts while the scales without underlines are used for third orders.

Conclusion

Low noise amplifiers utilizing various negative feedback techniques are available. Understanding the advantages of coupler feedback allows the system designer to achieve improved system performance and when necessary the ultimate possible amplifier performance.

REFERENCES

1 Norton, D. E., High Dynamic Range Transistor Amplifier Using Lossless Feedback, Microwave Journal, May, 1976, pp. 53-57.
2. Hewlett Packard application note 154.
3. Norton, D. E., Strong Signal Survivability Design for Lossless Feedback Amplifiers, Proceedings, Eleventh Annual European Microwave Conference. ■

The Series Connection in Stripline

I. Galin
Aerojet ElectroSystems Company

Introduction

The introduction of printed circuit technology into the microwave field served an important role to open gates for many technological ventures. Its importance merits consideration of a related problem about which little has been said. Printed distributed elements lend themselves easily to parallel and cascade connections in microwave circuits, Figures 1A and 1B, but connecting the same elements in series, Figure 1C, is complicated. This article reviews the progress made in stripline vis-a-vis the problem, and presents additional explanation to an essential ingredient of the solution.

Difficulties in realizing a series connection are typical for distributed circuit elements that support a dominant TEM mode coaxial line as well as printed lines in stripline and in microstripline. For this reason the more mature coaxial-line technology is used in this review as a reference.

Series Connection in Coaxial Lines

Coupled-line structures were developed in conjunction with the coaxial-line technology. These structures — with electrical equivalents containing circuit elements connected in series — in effect bypassed the problem. However, the direct realization of distributed elements connected in series proved to be crucial in the development of wideband components such as 3-dB hybrid couplers[1] bandpass filters[2] and diplexers[3].

At the heart of these significant achievements is a structure connecting coaxial lines in series[4]. Conductor A, Figure 2, is a center conductor in the coaxial line with characteristic impedance (Z_{01}) consisting of conductors A and B. The hollow conductor B is the center conductor in coaxial line, with characteristic impedance (Z_{02}) consisting of conductor B and C. The potential of conductor B is floating between that of conductors A and D, thus yielding an electrical series connection between Z_{01} and Z_{02} conductors A and C through B.

Series Connection in Stripline

To a large degree the progress in realizing stripline components, employing distributed elements connected in series, follows in the footsteps of similar progress in coaxial components. Coupled-line arrays with circuit elements connected in series contained in their electrical equivalents were implemented successfully. Indeed, many common microwave filters (side-coupled, interdigital) employ this concept, as do other microwave components such as couplers and multiplexers.

However, exactly as in the case of coaxial lines, a direct realization of stripline elements connected in series proved to be important (a) for the development of wideband components such as hybrid couplers[5], where the concept of a "reentrant coupled section"[1] was applied to a printed circuit configuration, as well as (b) for the development of wideband filters[6] and compact diplexers[7]. These achievements were made possible by establishing a successful method for realizing a series connection in stripline.

Unlike coaxial lines, printed lines consist of very thin conductors, a fact that called for modifications in the method described above, Figure 2 for realizing series connections. Instead of a hollow conductor, two broadside-coupled lines[8] (Figure 4A) are being used. The coupled lines provide the electrical shielding for conductor A (Figure 4A) and maintain a floating potential above ground. The stripline conductor A will excite the coupled lines symmetrically (in the even mode). Figure 4A illustrates two broadside-coupled lines centered between ground planes, which are separated by a distance B; the width of the coupled lines is W_o and the distance between them is B_o.

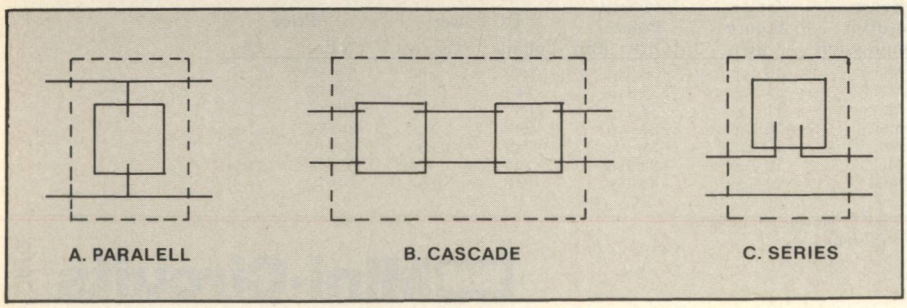

Fig. 1 Electrical circuit connections.

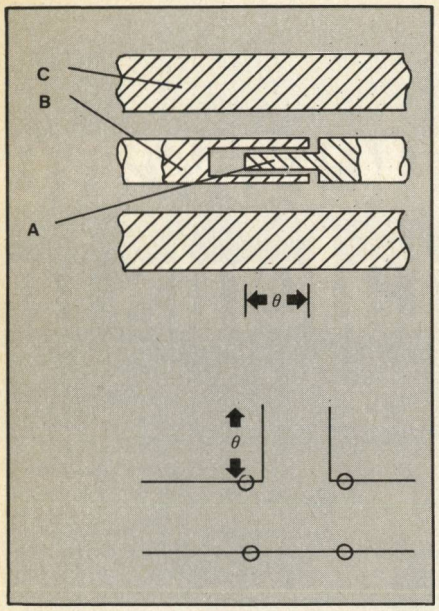

Fig. 2 Series connection configuration in coax.

Schematics and equivalent circuits are shown (taken from Reference 9) for coupled lines terminated with shorts (Figure 3A) and for the open case (Figure 3B). The equivalent circuit for the symmetrical case ($Z_{oo} = 0$) is easily reduced to a stub to ground (shorted or open) where the input impedance of this stub is given as follows. For the shorted case,

$$Z_{il} = jZ_{01} \tan\theta$$

For the open case,

$$Z_{il} = -jZ_{01} \cot\theta$$

and

$$Z_{01} = 1/2Z_{0E}$$

Z_{0E} is the even-mode (symmetrical) characteristic impedance of the broadside-coupled lines. This analysis supplements the somewhat intuitive argument of References 6 and 7 for justifying the method of realizing this ingredient of the series connection in stripline.

A transmission line with Z_{01} and Z_{02} (Figure 4A) yields an "L" network. To ensure a series connection

$$W_o > W_1 + 2B_o$$

The L section has been extended (Refs 6 and 7, respectively) to realize a two-way "T" section (Figure 4B) and a three-way "Y" section (Figure 4C). In these cases, ensuring series connections requires:

$$W_o > \Sigma W_i + \Sigma S_{i,i+1} + 2B_o$$

and

$$S_{i,i+1} > B_o$$

The W and S terms, which are omitted in Figures 4B and 4C, respectively, represent the widths of the corresponding studs and the distances separating them. This set of relations ensures no coupled-line modes between the series-connected lines and establishes a practical limit on the number of different channels emerging from a junction.

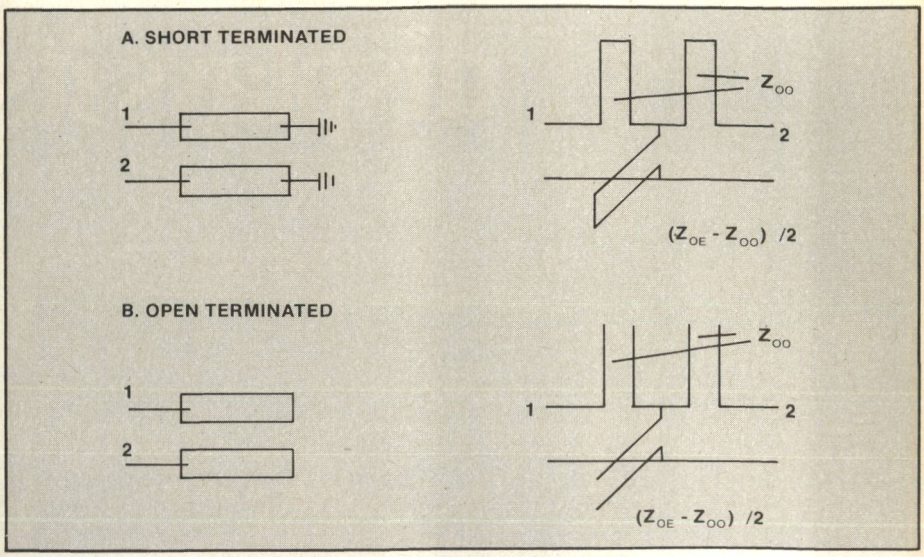

Fig. 3 Coupled sections.

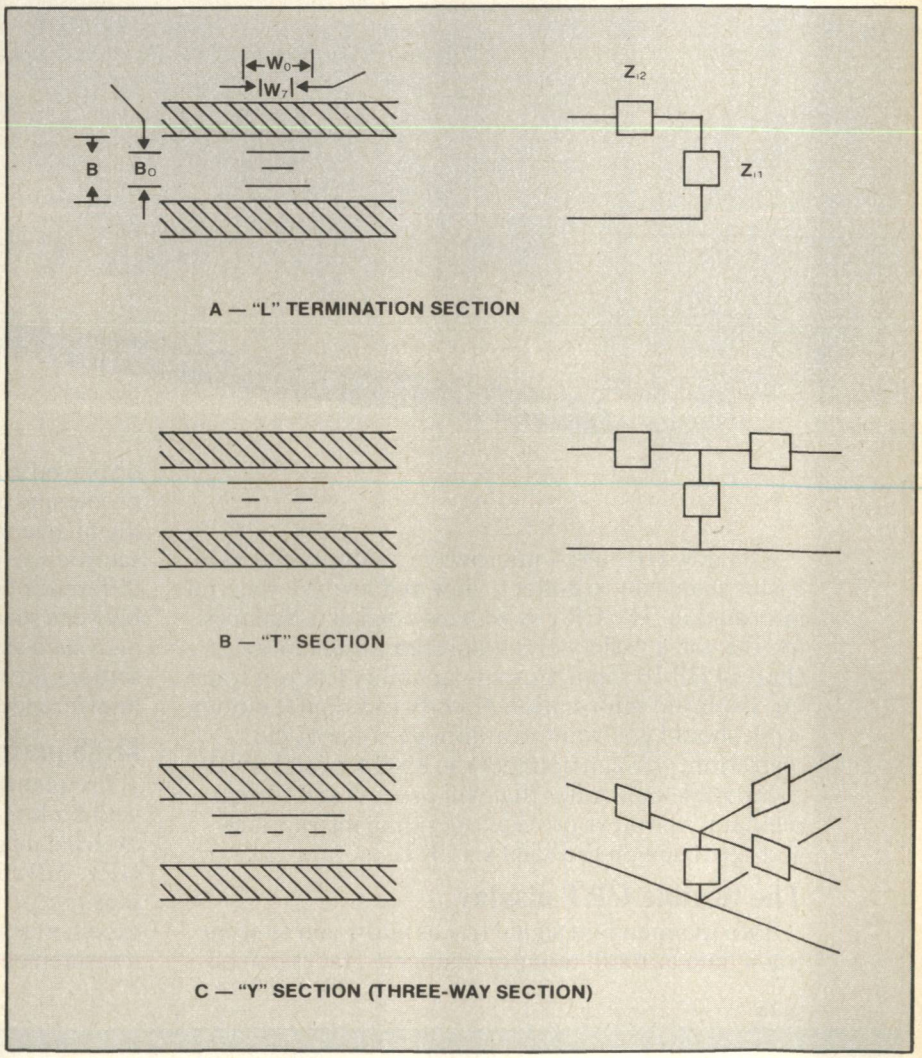

Fig. 4 Series connection configurations in stripline.

[Continued on page 142]

Summary

The method established for realizing series connections in stripline calls for a multi-dielectric layer, which adds unfavorably to the complexity. In addition, the vertically positioned printed lines, if not assembled symmetrically, may excite undesirable orthogonal modes. The number of these modes increases with the number of the conductors yielding the series connection.

However, this method yields the following important benefits:

- The spectrum of options available in the stripline game has been broadened.
- Components employing the method proved to yield expanded bandwidths.
- Compactness is a built-in feature of this method. The more efficient use of the vertical dimension of the stripline structure leads to savings in the area occupied by a component.
- Employing stubs connected in series and reducing the reliance on coupled-line arrays appears to help in accurate realization of microwave components. It can be argued that, for stripline components, controlling the width and length of a stub is simpler than controlling two line widths, the spacing between them, and the length simultaneously, as is the case for two coupled lines.
- The junction between different lines connected in series is realized in a vertical structure; in this case an undistorted reference plane, is maintained at the junction. It appears that in this case fewer parasitics are incorporated in the junction as compared to junctions between printed lines connected in cascade or in parallel (Ref. 10). There is support for this belief in the very wideband components that have been realized without providing compensation for parasitic-element problems.

Overall connecting circuit elements in series in stripline, has many significant benefits and is suggested as a viable option for microwave component designers.

References

1. Seymour, B. Cohn, "The Re-Entrant Cross Section and Wide-Band 3-dB Hybrid Couplers", IEEE Trans. MTT-11, July 1963.
2. R.J. Wenzel, "Exact Theory of Interdigital Bandpass Filters and Related Coupled Structures", IEEE Trans. MTT-13, September 1965.
3. R.J. Wenzel, "Wideband High-Selectivity Diplexers Utilizing Digital Elliptic Filters", IEEE Trans., MTT-15, December 1967.
4. George L. Ragan, "Microwave Transmission Circuits", McGraw-Hill, p.408,1948.
5. Samuel Hopfer, "Hybrid Coupler for Microstrip Configuration", IEEE MTT-S Digest, 1979.
6. I. Galin, A.I. Grayzel, "A New Type of a Compact Wideband Stripline Filter", European Microwave Conf., Brussels, 1973.
7. I. Galin, "A New Diplexer - Realized in Stripline", IEEE MTT-S Digest, 1981.
8. S.B. Cohn, Characteristic, Impedances of Broadside-Coupled Strip Transmission Lines", IRE Trans. MTT-8, November 1960.
9. G.L. Matthaei, L. Young, E.M.T. Jones, "Microwave Filters, Impedance Matching Networks, and Coupling Structures", McGraw-Hill, New York, 1964.
10. I.J. Bahl, R. Garg, "A Designer's Guide to Stripline Circuits", Microwaves, January 1978. ■